RÉPUBLIQUE ALGÉRIENNE DÉMOCRATIQUE ET POPULAIRE
MINISTÈRE D'ENSEIGNEMENT SUPÉRIEUR ET DE RECHERCHE SCIENTIFIQUE
UNIVERSITÉ MOHAMED BOUDIAF - M'SILA
FACULTÉ DE MATHÉMATIQUES ET DE L'INFORMATIQUE
DÉPARTEMENT DE MATHÉMATIQUES

N° d'ordre: .....

T H È S E

Présenté pour l'obtention du diplôme
de Doctorat troisième cycle

Spécialité:

Mathématiques

Option:

Mathématiques appliquées

Par:

Souad Bounouiga

Thème

Etude de quelques systèmes dynamique différentiels liés à la propagation d'épidémies

---

Soutenu publiquement le : 07/05/2025, devant le jury :

Gasmi Abdelkader	Prof.	Université Mohamed Boudiaf - M'sila	Président
Benhamidouche Noureddine	Prof.	Université Mohamed Boudiaf - M'sila	Rapporteur
Basti Bilal	M.C.A.	Université Mohamed Boudiaf - M'sila	Co-Rapporteur
Mohammed-Salah Abdelouahab	Prof.	Centre Universitaire de Mila	Examinateur
Arioua Yacine	Prof.	Université Mohamed Boudiaf - M'sila	Examinateur

Année académique 2024/2025.

PEOPLE'S DEMOCRATIC REPUBLIC OF ALGERIA
MINISTRY OF HIGHER EDUCATION AND SCIENTIFIC RESEARCH
UNIVERSITY OF MOUHAMED BOUDIAF / M'SILA
FACULTY OF MATHEMATICS AND COMPUTER SCIENCES
DEPARTMENT OF MATHEMATICS

N° d'ordre: .....

THESIS

Presented for obtaining the diploma
of doctoral degree 3rd cycle LMD

Speciality:

Mathematics

Option:

Applied Mathematics

By:

SOUAD BOUNOUIGA

Theme

Study of Some Differential Dynamic Systems Linked to the Spread of Epidemics

Thesis defended publicly on : 07/05/ 2025, before a jury composed of:

Gasmi Abdelkader	Prof.,	University of M'sila	Chair
Noureddine benhamidouche	Prof.,	University of M'sila	Supervisor
Bilal Basti	M.C.A,	University of M'sila	Co-supervisor
Mohammed-Salah Abdelouahab	Prof.,	University Center of Mila	Examiner
Arioua Yacine	Prof.,	University of M'sila	Examiner

University Year: 2024/2025

Acknowledgments

Above all, my praise and gratitude is due to Allah the almighty who granted me strength and patience to complete this thesis. I would like to express my sincere gratitude to everyone who has been part of this journey. First and foremost, I am indebted to my supervisor *Prof.* BENHAMIDOUCHE NOUREDDINE for his patience, valuable advice and guidance and consistent encouragement that he provided throughout this research. I am also deeply grateful to *Dr.* BASTI BILAL who introduced me to this field. Furthermore, I would like to extend my thanks and appreciation to the panel of examiners, *Prof.* MOHAMMED-SALAH ABDELOUAHAB, *Prof.* ARIOUA YACINE, and president of the committee *Prof.* GASMI ABDELKADER My journey has been made more endurable with the help and thoughtful encouragement I have received from my family and friends, and so my greatest thanks go to them.

Notation

$\mathbb{N}$	Natural numbers $\{0, 1, 2, 3, \ldots\}$.
$\mathbb{N}^*$	Nonzero natural numbers $\{1, 2, 3, \ldots\}$.
$\mathbb{R}$	Real numbers $(-\infty, \infty)$.
$\mathbb{R}_+$	Positive real numbers $(0, \infty)$.
$C(\Omega)$	The BANACH space of all continuous functions φ on Ω, for which $\|\varphi\|_\infty = \sup_{0 \le \eta \le \ell} \|\varphi(\eta)\|$.
$\Gamma(\cdot)$	EULER gamma function.
$\mathcal{I}_{0^+}^{\alpha} \varphi$	RIEMANN-LIOUVILLE fractional integral of order α.
${}^{C}\mathcal{D}_{0^+}^{\alpha} \varphi$	CAPUTO fractional derivative of order α.

Contents

Introduction **1**

1 Fundamentals of Mathematical Epidemic Modeling: Concepts and Definitions **7**

1.1 Introduction to Dynamical Systems 7

1.2 Continuous dynamical systems 8

1.3 Equilibria, linearization, and stability analysis 9

1.3.1 Linearization 9

1.3.2 Routh-Hurwitz criterion 10

1.4 Fundamental Concepts in Epidemic Modeling 11

1.5 The Basic Reproduction Number $\mathfrak{Rb}$ 12

1.6 Introduction to Basic Epidemic Models 14

1.6.1 SI model 14

1.6.2 SIR Model 16

1.6.3 SIRS Model 19

1.6.4 SEIR Model 22

1.6.5 SEIRS Model with Vital Dynamic 24

1.7 The Fundamental Concepts in Fractional Calculus 26

2 Malaria Transmission Dynamics Using Fractional Models **27**

2.1 Introduction 27

2.2 Dynamic Analysis of the Feasible Region 30

2.2.1 Positivity and Boundedness of the Model 30

2.2.2 Existence Results of Solutions for the Normalized Model 32

2.2.3 Ulam-Hyers Stability for the Normalized Model 37

2.3 Analysis for the Fractional SIP(N)–SI(M) Model 39

2.3.1 Basic Reproduction Number and Equilibrium Points 39

2.3.2 Stability Study of Disease-Free Equilibrium Point 42

2.3.3 Stability Study of Endemic Equilibrium Point 43

2.4 Data Fitting Analysis through Numerical Simulation 46
2.4.1 Numerical Scheme for the Fractional SIP(N)–SI(M) Model 46
2.4.2 Fitted Data Analysis of Malaria in Algeria 49
2.4.3 Significance and Closing Remarks on Numerical Simulation 54

3 Dengue Fever Dynamics Using Advanced Mathematical Approaches 56
3.1 Introduction 56
3.2 Dynamic Analysis of the Feasible Region 59
3.2.1 Positivity and Boundedness of the Model 59
3.2.2 Existence Results of Solutions for the Normalized Model 61
3.2.3 Ulam-Hyers Stability for the Normalized Model 63
3.3 Analysis for the SIHR(N)–SEI(M) Model 65
3.3.1 Basic Reproduction Number and Equilibrium Points 65
3.3.2 Stability Study of Disease-Free Equilibrium Point 68
3.3.3 Stability Study of Endemic Equilibrium Point 69
3.4 Data Fitting Analysis through Numerical Simulation 74
3.4.1 Evaluating Dengue Control in Low $\mathfrak{Rb}$ Countries 74
3.4.2 Assessing Dengue Challenges in High $\mathfrak{Rb}$ Countries 82

4 Mathematical Insights into Cutaneous Leishmaniasis Dynamics 90
4.1 Introduction 90
4.2 Dynamic Analysis of the Feasible Region 93
4.2.1 Positivity and Boundedness of the Model 93
4.2.2 Existence Results of Solutions for the Normalized Model 95
4.2.3 Ulam-Hyers Stability for the Normalized Model 97
4.3 Analysis for the SEIAR(N)–SI(M) Model 99
4.3.1 Basic Reproduction Number and Equilibrium Points 99
4.3.2 Stability Study of Disease-Free Equilibrium Point 102
4.3.3 Stability Study of Endemic Equilibrium Point 104
4.4 Data Fitting Analysis through Numerical Simulation 108
4.4.1 Fitted Data Analysis of Cutaneous Leishmaniasis in Algeria 109
4.4.2 Fitted Data Analysis of Cutaneous Leishmaniasis in M'Sila 114
4.5 Significance and Closing Remarks on Numerical Simulation 117

Conclusion 118

References **119**

Introduction

Infectious diseases are among the oldest challenges that have shaped human history and continue to be a major global concern. These diseases, caused by various pathogens such as viruses, bacteria, fungi, and parasites, can spread rapidly and widely, resulting in epidemics and pandemics that claim millions of lives. Historical records show that infectious diseases like the plague, smallpox, and influenza have devastated populations, and recent epidemics, such as Ebola, SARS, and COVID-19, illustrate that infectious diseases remain a prominent threat to global health[1, 2, 3].

Modern advances in science and technology have improved our understanding of infectious diseases, leading to the development of vaccines, treatments, and diagnostic tools. However, factors such as globalization, increased travel, urbanization, and climate change have heightened the risk of emerging and re-emerging infectious diseases. These conditions facilitate the spread of pathogens across borders, making effective disease control and prevention a priority. Therefore, studying the dynamics of disease transmission and understanding how infections spread is crucial in order to protect public health and prepare for future outbreaks.

The transmission of infectious diseases varies depending on the type of pathogen and mode of spread. Diseases can be spread through direct contact, such as handshakes or touching, which is common for pathogens like influenza and COVID-19 that are transmitted through respiratory droplets. Airborne transmission is another mode where pathogens remain suspended in the air for longer periods, increasing the risk of infection in crowded and enclosed spaces.

Some diseases are transmitted indirectly through contact with contaminated objects or surfaces, such as door handles or personal items [4, 5]. Foodborne and waterborne pathogens also pose significant risks, as they can lead to outbreaks through contaminated food supplies or inadequate sanitation, as seen in diseases like cholera and typhoid.

In contrast to these direct and indirect modes, vector-borne diseases rely on biological carriers, known as vectors, to transfer the pathogen from one host to another. The role of vectors, such as mosquitoes and sandflies, is particularly important in the spread of certain diseases in specific regions, often where climate and ecological conditions favor the life cycles of these vectors. Understanding the various mechanisms of transmission is essential for designing targeted interventions and minimizing the spread of infections in diverse populations.

Vector-borne diseases represent a unique and complex category of infectious diseases with significant global health implications. These diseases rely on intermediate hosts, typically arthropods like mosquitoes, ticks, and flies, to transfer pathogens to humans. The transmission process is influenced by factors like climate, environmental conditions, and human activities, making vector-borne diseases particularly challenging to control in regions with ideal vector breeding conditions, such as tropical and subtropical zones.

Examples of vector-borne diseases include malaria, which is transmitted by Anopheles mosquitoes; dengue fever, spread by Aedes mosquitoes; and leishmaniasis, caused by sand fly bites. Malaria alone causes hundreds of thousands of deaths annually, with the highest burden in sub-Saharan Africa. Dengue fever is prevalent in urban areas across Asia and Latin America, leading to severe health complications and high economic costs. Leishmaniasis affects millions of people worldwide, causing skin and internal damage, with cutaneous leishmaniasis being one of the most widespread forms.

The economic and social impact of these diseases is profound, especially in low- and middle-income countries where healthcare resources are limited. Vector control efforts, such as insecticide-treated bed nets, spraying programs, and environmental management, play a crucial role in reducing transmission. However, these interventions alone are often insufficient, highlighting the need for integrated strategies and continuous monitoring. Mathematical modeling offers a valuable approach to simulate disease transmission dynamics and assess the effectiveness of vector control strategies [6, 7, 8, 9, 10].

Mathematical modeling has become a cornerstone in epidemiological research, providing a framework for analyzing and predicting disease transmission patterns [11, 12, 13, 14, 15, 16, 17]. Through mathematical equations and simulations, models can represent complex biological processes and capture the behavior of diseases within a population. Traditional epidemiological models, such as the SIR (Susceptible-Infected-Recovered) model, have been widely used to estimate infection rates and evaluate control strategie [18, 19, 20, 21]. The SIR model divides the population into compartments, representing the

susceptible, infected, and recovered individuals, and uses differential equations to describe transitions between these compartments over time.

Advanced models expand upon the basic SIR structure to include additional factors such as birth and death rates, seasonal variations, and vaccination coverage. These extensions make it possible to simulate more realistic scenarios and predict the spread of diseases under different intervention strategies. Mathematical models are particularly valuable in informing public health decision-making by providing insights into critical parameters, such as the basic reproduction number ($\mathfrak{Rb}$), which measures how many individuals, on average, an infected person will infect. When $\mathfrak{Rb}$ is below 1, the disease is expected to die out; when it is above 1, the disease may continue to spread.

In the context of vector-borne diseases, modeling helps researchers understand how environmental factors, such as temperature and humidity, affect vector populations and transmission rates. Models can also explore potential outcomes of vector control measures, enabling policymakers to develop and implement data-driven interventions that effectively reduce disease burden.

Fractional modeling, which employs fractional derivatives rather than traditional integer-order derivatives, has gained attention in recent years as a sophisticated approach in mathematical modeling. Fractional calculus introduces the concept of memory and hereditary effects, allowing for a more nuanced analysis of systems that exhibit complex temporal dependencies. In biological systems, these memory effects are significant because the current state of an organism or population may be influenced by past exposures or interactions[22, 23, 24, 25, 26, 27, 28].

Fractional differential equations are particularly useful in modeling infectious diseases where memory effects play a role in disease progression and transmission. For example, the fractional order can represent the extent to which past infections impact susceptibility to future infections, capturing long-term dependencies and cumulative effects. This capability makes fractional models well-suited for studying diseases with prolonged infection cycles, delayed immune responses, or cumulative environmental impacts on vector populations[27, 28, 29, 30, 31].

By incorporating fractional derivatives, researchers can create models that are more flexible and accurate in simulating real-world disease transmission patterns. Fractional modeling is especially valuable for studying vector-borne diseases, as it provides insights into how historical environmental conditions and population dynamics influence present-day transmission[32, 33, 34, 35, 36, 37, 38, 39, 40, 41, 42, 43, 44]. These models can contribute

to more effective and targeted public health interventions by offering precise estimates and identifying key factors in disease spread.

In this thesis, we focused on studying the dynamics of epidemic disease transmission using mathematical models to analyze the behavior of three major diseases: malaria, dengue fever, and cutaneous leishmaniasis. In each chapter, we presented a comprehensive study of a specific dynamic system that reflects disease transmission, aiming to provide insights into the development of effective prevention and control strategies.

In the first chapter, we concentrated on the theoretical foundations of mathematical modeling for epidemics, including an explanation of dynamic systems based on differential equations. We discussed the basic concepts related to the mathematical systems used to study disease transmission, such as the SIR model (susceptible, infected, recovered), with an emphasis on how these models are constructed and applied.

In the second chapter, we studied a dynamic system to analyze malaria transmission between humans and mosquitoes. The model in this chapter is based on fractional differential equations that account for the effects of memory and time on disease spread. We presented the mathematical equations representing malaria transmission, with a focus on the influence of environmental factors and preventive interventions. The model was analyzed using real data from Algeria.

Based on the work presented above, for $0 \leq t \leq \ell < \infty$, and $0 < \alpha \leq 1$, we have:

$$\begin{cases} {}^{C}\mathcal{D}_{0^+}^{\alpha} S_N(t) &= \Lambda N(t) + \delta P_N(t) - \left(\dfrac{\beta I_M(t)}{M(t)} + \mu\right) S_N(t), \\ {}^{C}\mathcal{D}_{0^+}^{\alpha} I_N(t) &= \dfrac{\beta I_M(t)}{M(t)} S_N(t) - (\kappa + \mu) I_N(t), \\ {}^{C}\mathcal{D}_{0^+}^{\alpha} P_N(t) &= \kappa I_N(t) - (\delta + \mu) P_N(t), \\ {}^{C}\mathcal{D}_{0^+}^{\alpha} S_M(t) &= \lambda M(t) - \left(\dfrac{\gamma I_N(t)}{H(t)} + \upsilon\right) S_M(t), \\ {}^{C}\mathcal{D}_{0^+}^{\alpha} I_M(t) &= \dfrac{\gamma I_N(t)}{N(t)} S_M(t) - \upsilon I_M(t), \end{cases}$$

Here, $N(t) = S_N(t) + I_N(t) + P_N(t)$ represents the total human population, where:

- S_N: Susceptible human.
- I_N: Infected human.
- P_N: Partially Immune human.

Similarly, $M(t) = S_M(t) + I_M(t)$ represents the total mosquito population, where:

- S_M: Susceptible mosquitoes.
- I_M: Infected mosquitoes.

In the third chapter, we studied a traditional mathematical model using ordinary differential equations to examine dengue fever transmission between humans and mosquitoes. We analyzed how environmental variables such as temperature and humidity affect mosquito life cycles and disease transmission. Additionally, we discussed the potential effects of various interventions such as insecticide spraying and the use of protective nets.

Based on the works mentioned above, we proposed the following system of ordinary differential equations for $0 \leq t \leq \ell < \infty$:

$$\begin{cases} \frac{dS_N(t)}{dt} &= \Lambda N(t) + \kappa R_N(t) - \left(\frac{\beta I_M(t)}{M(t)} + \mu\right) S_N(t) \\ \frac{dI_N(t)}{dt} &= \frac{\beta I_M(t)}{M(t)} S_H(t) - (p+q+\theta+\mu) I_N(t) \\ \frac{dH_N(t)}{dt} &= pI_N(t) - (\tau+\mu) H_N(t) \\ \frac{dR_N(t)}{dt} &= qI_N(t) + \tau H_N(t) - (\kappa+\mu) R_N(t) \\ \frac{dS_M(t)}{dt} &= \lambda M(t) - \left(\frac{\gamma I_N(t)}{N(t)} + \upsilon\right) S_M(t) \\ \frac{dE_M(t)}{dt} &= \frac{\gamma I_N(t)}{N} S_M(t) - (\delta+\upsilon) E_M(t) \\ \frac{dI_M(t)}{dt} &= \delta E_M(t) - \upsilon I_M(t). \end{cases}$$

Here, $N(t) = S_N(t) + I_N(t) + H_N(t) + R_N(t)$ represents the total human population, where:

- S_N: Susceptible individuals.
- I_H: Infected individuals.
- H_N: Hospitalized individuals.
- R_N: Recovered individuals.

Similarly, $M(t) = S_M(t) + E_M(t) + I_M(t)$ represents the total mosquito population, where:

- S_M: Susceptible mosquitoes.
- E_M: Exposed mosquitoes.
- I_M: Infected mosquitoes.

Finally, in the fourth chapter, we focused on a traditional mathematical model to study the transmission of cutaneous leishmaniasis between humans and infected mosquitoes. We presented mathematical equations describing disease transmission across different groups, focusing on factors affecting disease development, such as preventive measures, environmental conditions, and climate change.

Based on the works presented above, we proposed the following system of ordinary differential equations for $0 \leq t \leq \ell < \infty$:

$$\begin{cases} \frac{dS_N(t)}{dt} &= \Lambda N(t) + \kappa R_N(t) - \left(\frac{\beta I_M(t)}{M(t)} + \mu\right) S_N(t) \\ \frac{dE_N(t)}{dt} &= \frac{\beta I_M(t)}{M(t)} S_N(t) - (\delta + \mu) E_N(t) \\ \frac{dI_N(t)}{dt} &= \theta\delta E_N(t) - (p + \mu) I_N(t) \\ \frac{dA_N(t)}{dt} &= (1-\theta)\delta E_N(t) - (q + \mu) A_N(t) \\ \frac{dR_N(t)}{dt} &= pI_N(t) + qA_N(t) - (\kappa + \mu) R_N(t) \\ \frac{dS_M(t)}{dt} &= \lambda M(t) - \left(\frac{\gamma(I_N(t) + A_N(t))}{N(t)} + \upsilon\right) S_M(t) \\ \frac{dI_M(t)}{dt}) &= \frac{\gamma(I_N(t) + A_N(t))}{N(t)} S_M(t) - \upsilon I_M(t). \end{cases}$$

Here, $N(t) = S_N(t) + E_N(t) + I_N(t) + A_N(t) + R_N(t)$ represents the total human population, where:

- S_N: Susceptible individuals.
- E_N: Exposed individuals.
- I_N: Symptomatic infectious individuals.
- A_N:Asymptomatic infectious individuals.
- R_N: Recovered individuals. Similarly, $M(t) = S_M(t) + I_M(t)$ represents the total sandfly population, where:
- S_M: Susceptible sandflies.
- I_M: Infected sandflies.

The parameters $\Lambda, \lambda, \beta, \gamma, \delta, \kappa, \upsilon, p, q, \theta, \tau$, and μ will be defined later in the thesis.

The objective of this thesis was to provide a deep understanding of the dynamics of epidemic disease transmission using various mathematical tools. We also aimed to provide recommendations based on mathematical analysis and numerical results to develop more effective strategies for disease prevention and control.

CHAPTER 1

FUNDAMENTALS OF MATHEMATICAL EPIDEMIC MODELING: CONCEPTS AND DEFINITIONS

This chapter introduces the fundamental principles of mathematical epidemiology, focusing on dynamic systems like the SIR model used to describe disease transmission within a population.

1.1 Introduction to Dynamical Systems

A dynamical system is a mathematical model used to describe how a system evolves over time. It is characterized by its dependence on the current state to determine future states, often displaying patterns of repetition or predictable ,behavior. These systems are widely used in various fields, including physics, biology economics, and engineering, to analyze and predict the behavior of complex phenomena.

In general, any system that undergoes changes over time can be classified as a dynamical system. From a mathematical perspective, a dynamical system consists of two fundamental components:

► **State Vector**:Represents the precise condition of the system at a given moment. It encapsulates all relevant variables necessary to describe the systems current status.

► **Evolution Rule**: Defines the mechanism governing how the system progresses from one state to another over time. This rule can be expressed through differential equations, difference equations, or iterative mappings, depending on whether the system is continuous or discrete (Scheinerman, 2013 [45]).

Main Types of Dynamical Systems:

• **Discrete-Time Systems**:

- Time is represented as discrete intervals (e. g. , $t \in \mathbb{Z}$ or $t \in \mathbb{N}$).
- These systems are modeled using difference equations or iterative applications.

• **Continuous-Time Systems**:

- Time is represented as a continuous variable (e. g. , $t \in \mathbb{R}$).
- These systems are governed by differential equations.

Some examples of dynamic systems are:

Exponential Growth Model:

This model describes the growth of living organisms and is governed by the equation:

$$\dot{x} = rx$$

Where x represents the population size, and $r > 0$ is the growth rate.

Pendulum Motion Model:

This model describes the dynamics of a swinging pendulum and is expressed by the equation:

$$\ddot{x} + \frac{g}{L}\sin(x) = 0$$

Where x is the pendulums angular displacement, g is the acceleration due to gravity, and L is the length of the pendulum.

1.2 Continuous dynamical systems

The mathematical formulation of a continuous-time dynamical system can be expressed as Layek (2015):

$$\frac{dx}{dt} = \dot{x} = \psi(x,t), \tag{1.1}$$

where $\psi(x,t)$ is a smooth function defied on a subset $U \subset \mathbb{R} \times \mathbb{R}$. Here, $x = x(t) \in \mathbb{R}^n$ represents the state vector, and $t \in I \subseteq \mathbb{R}$ typically denotes time.

► A system is termed autonomous if the function $\psi(x,t)$ does not explicitly depend on t. In this case, the systems trajectories remain unchanged over time.

► A system is considered nonautonomous if $\psi(x,t)$ explicitly depends on t.

To convert an n-dimensional nonautonomous system into an autonomous one, an additional variable x_{n+1} is introduced, where $x_{n+1} = t$. To achieve this, we need to develop autonomous systems

1.3 Equilibria, linearization, and stability analysis

Definition 1.1. *A point $x^* \in \mathbb{R}^n$ is called an equilibirium point of the system*

$$\dot{x} = \psi\left(x\left(t\right)\right), \tag{1.2}$$

if and only if

$$\psi\left(x^*\right) = 0.$$

Definition 1.2 (Lyapunov Stability [46])**.** *The equilibirium point x^* is said to be stable in the sense of Lyapunov if and only if :*

$$\forall \varepsilon > 0, \exists \delta > 0 : \left\|x_0 - x^*\right\|_{\mathbb{R}^n} \leq \delta \Rightarrow \left\|x\left(t\right) - x^*\right\|_{\mathbb{R}^n} \leq \varepsilon, \forall t > 0.$$

Definition 1.3 (Asymptotic Stability [46])**.** *The equilibirium point x^* is said to be locally asymptotically stable if and only if :*

$$\exists \delta > 0 : \left\|x_0 - x^*\right\|_{\mathbb{R}^n} \leq \delta \Rightarrow \lim_{t \to +\infty} x\left(t\right) = x^*.$$

1.3.1 Linearization

Linearization is a fundamental analytical tool used to study the behavior of nonlinear dynamical systems near equilibrium points. This technique involves approximating the original system with a linear system obtained from the first-order Taylor expansion around a given equilibrium point. By doing so, it simplifies the analysis of system stability and provides insights into the local dynamics using linear differential equations, which are more tractable compared to the original nonlinear system.

Definition 1.4 ([46])**.** *Consider the system (1.2) with $\psi \in C^1\left(\mathbb{R}^n, \mathbb{R}^n\right)$ and $x^* \in \mathbb{R}^n$. The system linearized at x^* is given by the differential equation system:*

$$\dot{x}\left(t\right) = \psi\left(x^*\right) + \left(x - x^*\right) D\psi\left(x^*\right).$$

This is the system of linear differential equations obtained by replacing $\psi\left(x\right)$ with its first-order Taylor expansion at x^*, where $D\psi\left(x^*\right)$ is the Jacobian matrix of ψ at x^*, defined as:

$$D\psi\left(x^*\right) = \begin{pmatrix} \frac{d\psi_1}{dx_1} & \cdots & \frac{d\psi_1}{dx_n} \\ \vdots & \ddots & \vdots \\ \frac{d\psi_n}{dx_1} & \cdots & \frac{d\psi_n}{dx_n} \end{pmatrix}$$

Since $\psi\left(x^*\right) = 0$, the linearized system simplifies to:

$$\dot{x}\left(t\right) = \left(x - x^*\right) D\psi\left(x^*\right).$$

Theorem 1.1 ([47]). *Let x^* be an equilibirium point of system (1.2). Suppose that the function ψ is of class C^1 in a neighborhood of x^*, and that all the eigenvalues of the Jacobian $D\psi(x^*)$ have strictly negative real parts. Then, x^* is locally asymptotically stable.*

Theorem 1.2 (protect[48]). *Let x^* be an equilibirium point of system (1.2). Suppose that the function ψ is of class C^1 in a neighborhood of x^*, and that all the Jacobian $D\psi(x^*)$ has (at least) one eigenvalue with a strictly positive real part. Then, x^* is unstable.*

1.3.2 Routh-Hurwitz criterion

To establish the asymptotic stability of an equilibrium point, it is generally required to calculate the n eigenvalues λ_i of the matrix A and check that the real part of each eigenvalue is negative, i.e., $Re(\lambda_i) < 0$ for all i. An algebraic method, developed by Routh and Hurwitz, simplifis this process by using specifi determinants known as the Routh-Hurwitz determinants Wiggins (2003)[47]. Consider the system:

$$\dot{x} = \psi(x),$$

Its linearization is written as:

$$\dot{x} = Ax,$$

The eigenvalues of A are the roots of the characteristic equation:

$$P(\lambda) = \det(A - \lambda I) = 0 \Leftrightarrow \lambda_n + a_1\lambda_{n-1} + a_2\lambda_{n-2} + \cdots + a_{n-1}\lambda + a_n = 0$$

The Routh-Hurwitz determinants are defied as follows:

$$H_1 = \begin{vmatrix} a_1 \end{vmatrix}$$

$$H_2 = \begin{vmatrix} a_1 & 1 \\ a_3 & a_2 \end{vmatrix}$$

$$H_3 = \begin{vmatrix} a_1 & 1 & 0 \\ a_3 & a_2 & a_1 \\ a_5 & a_4 & a_3 \end{vmatrix}$$

$$H_i = \begin{vmatrix} a_1 & 1 & 0 & \cdots & 0 \\ a_3 & a_1 & 1 & \cdots & 0 \\ a_5 & a_3 & a_1 & \cdots & 0 \\ \vdots & \vdots & \vdots & \ddots & \vdots \\ a_{2n-1} & a_{2n-3} & a_{2n-5} & \cdots & a_1 \end{vmatrix}$$

Proposition 1.1 ([49]). *The equilibrium point is asymptotically stable if:*

$$\forall i,\ \mathrm{Re}\,(\lambda_i) < 0 \Leftrightarrow \mathrm{Re}\,(H_i) > 0.$$

Theorem 1.3 (Routh-Hurwitz Criterion [49]). *Let $P(\lambda)$ be a polynomial with $a_0 > 0$. For P to exhibit uniform asymptotic stability (u.a.s.), it is required that all the leading principal minors of the Hurwitz matrix be strictly positive.*

1.4 Fundamental Concepts in Epidemic Modeling

Epidemic models are used to understand the dynamics of infectious disease transmission within populations. These models rely on a set of fundamental concepts that describe how diseases spread, the conditions under which outbreaks occur, and the factors influencing their stability or expansion [50, 51]. In this section, we review key epidemiological terms that form the basis for understanding and analyzing the mathematical models used in epidemic studies.

Epidemic: A rapid increase in the incidence of a pathology. Although often used in the context of infectious diseases, this term can be used for general biological phenomena (smallpox, avian fl, HIV, coronavirus, etc.).

Epidemic threshold: A theoretical threshold in mathematical models above which an epidemic will (or may) occur.

Pandemic: Caused by an emerging infectious disease that takes on continental or even global proportions.

Endemic: The usual and stable presence of a disease in a population.

Patient zero: The fist recognized case of an infectious pathology that is the source of all other recorded cases.

Infectious agents (pathogens): Infectious agents are the pathogens responsible for infectious diseases. They can be of different types: bacteria, viruses, parasites, fungi, or prions.

Infectious diseases: Infectious diseases are transmissible diseases caused by a specifi infectious agent or its toxins. They can be transmitted either directly from one person to another, as in the case of inflenza, measles, or diphtheria, among others; through a vector like mosquitoes for chikungunya or malaria; or through the environment, such as through food or water for salmonellosis or cholera.

Vertical transmission: The transmission of a disease is said to be vertical when it occurs from parents to offspring. This is the case, for example, with mother-to-child transmission.

Horizontal transmission: The transmission of a disease is said to be horizontal when it occurs after birth through contact with an infected individual.

Incubation period: The time between when one is infected and when symptoms appear. Latency period: The time between the initial contact and the moment one becomes contagious.

1.5 The Basic Reproduction Number $\mathfrak{Rb}$

The basic reproduction number represents the average number of new cases caused by a single infected individual in a population where everyone is susceptible during the infectious period.

In reality:

• When $\mathfrak{Rb} < 1$: The disease-free equilibrium point is locally and asymptotically stable, indicating that the infection will eventually disappear.

• When $\mathfrak{Rb} > 1$: The disease-free equilibrium point is unstable, meaning that the disease can persist and spread within the population.

Determination of:

$\mathfrak{Rb}$ is determined as the spectral radius of the "next generation operator." This operator is derived by separating the population into two categories: the infected and the uninfected compartments.

For an epidemiological model with n homogeneous compartments, the system's state is represented by the vector x, where x_j denotes the number or concentraction of individuals in compartment j. The compartments are ordered in such a way that the last ones are infected (latent, infectious, etc...). The first k compartments are the individuals free of infection (Susceptible...).

We notice:

• $F_i(x)$: tthe speed of appearance of new infected in the horizontal compartment "i" (from one individual to another), or vertical (from mother to baby).

• $V_i^+(x)$: the speed of what comes from the other compartments by all causes (displacement, aging, healing).

• $V_i^-(x)$: the speed of leaving the compartment (movement, mortality, change of status...) in such a way:

We note X_s the state without disease $X_s = x/x_{p+1} = x_p = ... = x_n = 0$.

The following assumptions are made:

1. $x \geq 0$ et $F_i(x) \geq 0$, $V_i^+(x) \geq 0$, $V_i^-(x) \geq 0$.
2. if $x_i = 0$ so $V_i^+(x) = 0$, If there is nothing in a compartment, nothing can come out. This is the essential property of a compartmental model.
3. if $i \geq p$ so $F_i(x) = 0$. Compartments with an index lower than p are uninfected.

   By defiition, infected cannot appear in these compartments.
4. if $x \in X_s$ or $\dot{x}_i = F_i(x) + V_i^+(x) - V_i^-(x)$, so $F_i = 0$ and for $i \geq p$, we have $V_i^-(x) = 0$. If there are no carriers of germs in the population, there can be no new infected.

The linear system is rewritten:

$$\dot{x}(t) = F_i(x) + V_i^+(x) - V_i^-(x).$$

The Jacobian matrix around the point of equilibrium without disease x0 of the linear system is written:

$$J(x_0) = DF(x_0) + D\left(V^+ - V^-\right)(x_0).$$

Or:

$$DF(x_0) = \begin{pmatrix} g & 0 \\ 0 & 0 \end{pmatrix} \quad \text{and} \quad D\left(V^+ - V^-\right)(x_0) = \begin{pmatrix} \upsilon & 0 \\ J_1 & J_2 \end{pmatrix}$$

with: $\upsilon = \dfrac{dV_i}{dt}_{1<i,j<m}$ and $g = \dfrac{dF_i}{dt}_{1<i,j<m}$

Or: $g \geq 0$ is a positive matrix and υ is an invertible Metzler matrix.

Definition 1.5. ***Metzler matrix****: We call Metzler matrix or quasi-positive matrix or non-negative matrix, the matrix which has positive off-diagonal elements.*

$A = (a_{ij})$, $a_{ij} \geq 0$, $i \neq j$, if A is a Metzler matrix then the following properties are equivalent:

- *A is asymptotically stable.*
- *A is invertible $(\det(A) \neq 0)$ and A^{-1} is positive defiite.*

Definition 1.6. *We call spectral radius of a matrix A, the maximum value of the modulus of the eigenvalues of A : $\rho(A) = \max_{\lambda \in sp(A)} |\lambda|$.*

Definition 1.7. *We defie $\mathfrak{Rb}$ by: $\mathfrak{Rb} = \rho(g\upsilon^{-1})$ such that ρ is the spectral radius of the matrix $g\upsilon^{-1}$.*

1.6 Introduction to Basic Epidemic Models

1.6.1 SI model

Mathematical models play a crucial role in understanding the spread of infectious diseases, and the SI model serves as a foundational step in this domain. Developed by W.H. Hamer in 1906, it is one of the simplest models used to study the dynamics of diseases, offering a basic yet insightful representation of infection transmission within a closed population.

The SI model divides the population into two compartments:

- $S(t)$: The number of susceptible individuals at time .
- $I(t)$ The number of infected individuals at time .

The total population size remains constant and is given by:

$$N(t) = S(t) + I(t).$$

The model assumes homogeneous mixing of the population, meaning every individual has an equal probability of coming into contact with others. The system of equations governing the dynamics of the SI model is:

$$\begin{cases} \dot{S} &= -\beta \frac{SI}{N}, \\ \dot{I} &= \beta \frac{SI}{N}, \end{cases}$$

β: The transmission rate, representing the likelihood of disease spread per contact.

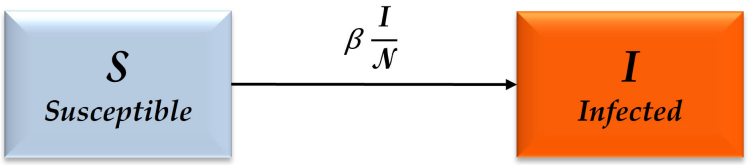

Figure 1.1: Flowchart of SI.

The SI model is based on the following assumptions:

1. Constant Population Size: The total population remains unchanged, i.e., there are no births or deaths during the study period.
2. No Immunity: Individuals are born susceptible and remain so until they become infected.

3. No Recovery: Infected individuals remain in the infected state permanently.

4. Homogeneous Mixing: All individuals have an equal probability of interacting, ignoring geographical or social structures.

Since the population size is constant, the model can be reduced by substituting:

$$\dot{I} = \beta \frac{(N - I)I}{N}.$$

The equilibrium points are determined by solving:

Disease-Free Equilibrium (DFE): where the population is entirely susceptible.

Endemic Equilibrium (EE): where the entire population is infected.

we assume

$$\psi'(I) = \beta - \frac{2\beta I}{N}.$$

- $\psi'(0) = \beta > 0 \quad \Rightarrow \quad$ DFE is unstable.
- $\psi'(N) = -\beta < 0 \quad \Rightarrow \quad$ EE is asymptotically stable.

At the onset of an epidemic, the infection spreads rapidly due to the large number of susceptibles.

Over time, the population transitions to an endemic state where all individuals are infected, and the dynamics stabilize.

The Simulation:

The simulation results are shown in Figure 1.2 The susceptible population decreases over time as individuals become infected, and the infected population rises until it stabilizes.

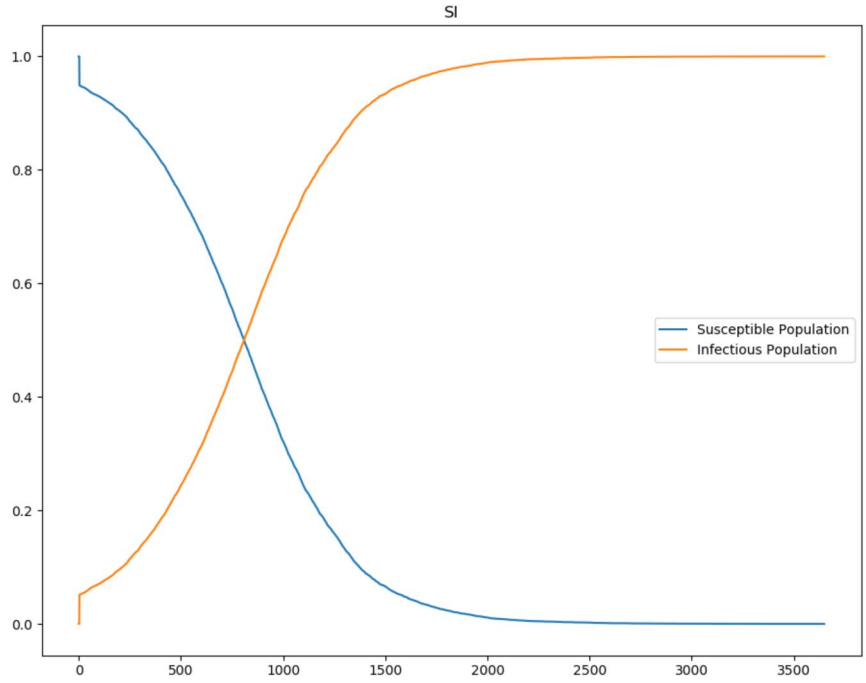

Figure 1.2: Numerical simulation of the SI model with: $\beta = 0.5$ and the initial conditions: $S(0) = 999$ and $I(0) = 1$.

Applications and Limitations:

The SI model is suitable for studying diseases with no recovery phase, such as HIV or certain chronic infections. It provides insights into the long-term dynamics of such diseases.

It ignores recovery or immunity.

It assumes homogeneous mixing, which may not reflect real-world population structures.

It oversimplifies disease dynamics by excluding births, deaths, or interventions like vaccination.

1.6.2 SIR Model

The SIR model is a natural extension of the SI model, introduced by Kermack and McKendrick in 1927, which added the concept of recovery or immunity. This model is a fundamental tool for studying infectious diseases where individuals move from the infected stage to recovery or immunity. It is particularly useful for diseases with acute transmission, such as influenza, measles, and chickenpox.

The SIR model divides the population into three categories:

- $S(t)$ The number of susceptible individuals at time .
- $I(t)$ The number of infected individuals capable of transmitting the disease at time .
- $R(t)$ The number of individuals who have recovered or become immune to the disease at this time.

The total population size is constant and given by the equation:

$$N(t) = S(t) + I(t) + R(t).$$

The SIR model relies on the following assumptions:

1. Constant population size: No births or deaths occur during the period of study.
2. Instantaneous infection: Susceptible individuals become infected as soon as they interact with an infected individual.
3. Permanent immunity: Individuals who recover from the disease are immune and cannot be re-infected.
4. Homogeneous mixing: All individuals are equally likely to interact with one another.

The following differential equations describe the dynamics of the SIR model:

$$\begin{cases} \dot{S} &= -\beta \frac{SI}{N}, \\ \dot{I} &= \beta \frac{SI}{N} - \gamma I, \\ \dot{R} &= \gamma I, \end{cases}$$

Figure 1.3: Flowchart of SIR.

- β: The rate of transmission of the disease.
- γ: The rate of recovery, where represents the average duration of the infection.

Basic Reproduction Number:

The basic reproduction number, $\mathfrak{Rb}$, is a critical threshold in the SIR model and is given by the equation:

$$\mathfrak{Rb} = \frac{\beta}{\gamma}.$$

Equilibrium points occur when, $\dot{S} = 0, \dot{I} = 0$, and $\dot{R} = 0$:

1. Disease-free equilibrium (DFE): $I = 0$ and $R = 1$, where all individuals are susceptible $(S = 0)$.

2. Endemic equilibrium (EE): A state where a fixed number of individuals remain infected, and there is a significant number of immune individuals.

   The Endemic equilibrium is obtained when the system reaches a stable state where the number of infected individuals remains constant. At the endemic equilibrium, the system of equations becomes:

$$\dot{S} = -\beta\frac{SI}{N} = 0,\ \dot{I} = \beta\frac{SI}{N} - \gamma I = 0,\ \dot{R} = \gamma I = 0.$$

Solving for the values of S, I, and R at the endemic equilibrium gives:

$$(S^*, I^*, R^*) = \left(\frac{\gamma}{\beta}N, \frac{\beta N}{\gamma}, N - S^* - I^*\right)$$

At this point, the system reaches a state configuration where the infection continues circulating in the population.

• If $\mathfrak{Rb} > 1$ the disease will persist in the population at the endemic equilibrium. If $\mathfrak{Rb} \leq 1$, the disease willeventully die out.

Dynamics of the Model:

- Initially, the number of susceptible individuals is large, leading to rapid disease spread.

- Over time, the number of susceptible individuals decreases as they become infected or immune, causing the infection to slow down and eventually cease.

Numerical Simulation:

To illustrate the SIR model, we assume the following initial conditions:

The simulation results Figure 1.4 show that the number of susceptible individuals gradually decreases as they transition into the infected category, while the number of infected individuals peaks and then declines as more individuals recover.

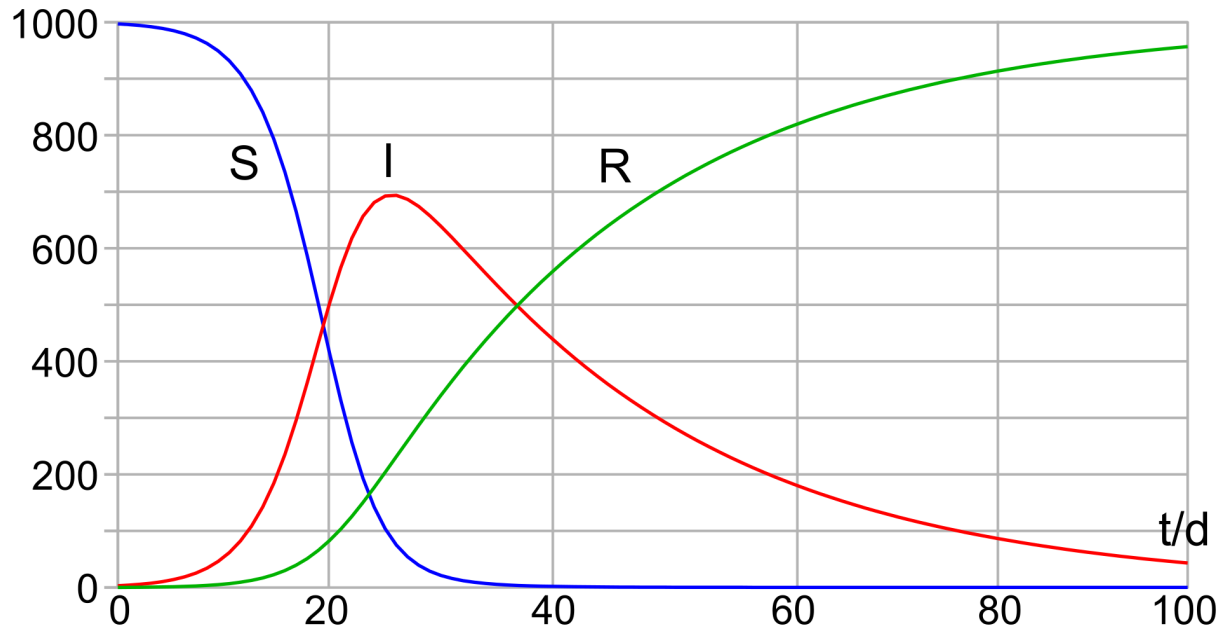

Figure 1.4: Numerical simulation of the SIR model with: $\beta = 0.4$, $\gamma = 0.04$ and the initial conditions: $S(0) = 997$, $I(0) = 3$, and $R(0) = 0$.

Applications and Limitations:

The SIR model is used to study diseases that provide lifelong immunity after recovery, such as measles and smallpox. It can help estimate the number of infected individuals over time and assess the impact of interventions like vaccination.

It does not account for births or deaths.

It assumes permanent immunity after recovery, which is not the case for diseases that do not confer lifelong immunity.

It assumes homogeneous mixing, which may not accurately reflect real-world interactions.

1.6.3 SIRS Model

The SIRS model is an extension of the SIR model, considering that individuals may lose their immunity over time and thus become susceptible to infection again. This model is useful for studying diseases that lead to the loss of immunity over time, such as influenza and other respiratory diseases.

The SIRS model divides the population into four categories:

- $S\,(t)$: The number of susceptible individuals at time .
- $I\,(t)$: The number of infected individuals capable of transmitting the disease at time .

• $R(t)$: The number of individuals who have recovered or become immune to the disease at time .

The system of equations describing the dynamics of the SIRS model is as follows:

$$\begin{cases} \dot{S} &= -\beta\frac{SI}{N} + \delta R, \\ \dot{I} &= \beta\frac{SI}{N} - \gamma I, \\ \dot{R} &= \gamma I - \delta R, \end{cases}$$

where:

• β: The rate of disease transmission.

• γ: The recovery rate (or rate of cure).

• δ: The rate of immunity loss (i.e., individuals transition from the immune class R to the susceptible class S over time).

• $N(t)$: The total population size, which remains constant, where .

$$N(t) = S(t) + I(t) + R(t).$$

The SIRS model relies on the following assumptions:

1. Constant population size: No births or deaths occur during the study period.
2. Instantaneous infection: Susceptible individuals become infected immediately upon interaction with infected individuals.
3. Immunity loss: Individuals who recover from the disease can lose immunity over time and become susceptible again.
4. Homogeneous mixing: All individuals are equally likely to interact with one another.

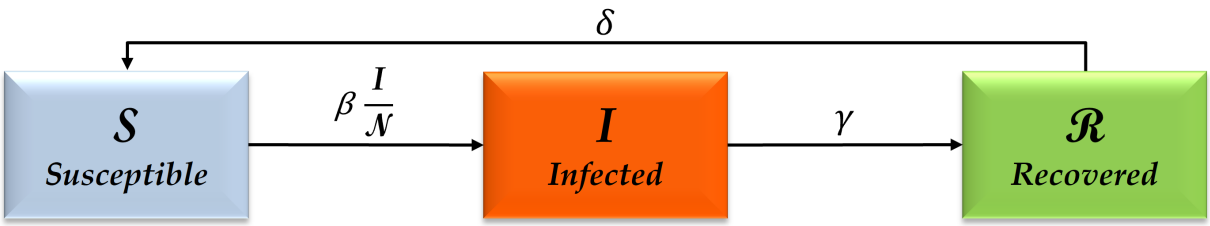

Figure 1.5: Flowchart of SIRS.

Basic Reproduction Number:

The basic reproduction number in the SIRS model is defined as:

$$\mathfrak{Rb} = \frac{\beta}{\gamma + \delta}.$$

Equilibrium points occur when the rates of change for all categories are zero, i.e., when:

$$\dot{S} = \dot{I} = \dot{R} = 0.$$

Solving these equations gives the steady-state values for the system:

• Disease-free equilibrium (DFE): where all individuals are susceptible and there are no infected or immune individuals.

• Endemic equilibrium (EE): A state where a fixed number of individuals remain infected, and there is a significant number of immune individuals who lose immunity and return to the susceptible group.

Endemic equilibrium point: The endemic equilibrium is reached when the system stabilizes, and the equations become:

$$\dot{S} = -\beta\frac{SI}{N} + \delta R = 0, \quad \dot{I} = \beta\frac{SI}{N} - \gamma I = 0, \quad \dot{R} = \gamma I - \delta R = 0.$$

Solving these equations, we obtain:

$$(S^*, I^*, R^*) = \left(\frac{\gamma}{\beta + \delta}N, \frac{\beta N}{\gamma}, N - S^* - I^*\right)$$

If $\mathfrak{Rb} > 1$, the disease will persist in the population at the endemic equilibrium. If $\mathfrak{Rb} \leq 1$, the disease will eventually die out.

Dynamics of the Model:

• Initially, the number of susceptible individuals is large, leading to rapid disease spread.

• Over time, the number of susceptible individuals decreases as they become infected or immune, causing the disease to slow down.

• Eventually, the disease ceases to spread when a balance is reached between infected individuals and immune individuals who lose immunity.

Applications and Limitations:

The SIRS model is used to study diseases for which recovery does not confer lifelong immunity, and individuals can lose immunity over time, such as influenza.

The model does not account for births or deaths.

It assumes that immunity loss occurs at a constant rate.

It does not incorporate factors such as migration or social distancing.

1.6.4 SEIR Model

The SEIR model is an extension of the SIR model that includes an additional class of individuals, E, for exposed individuals. These individuals are infected but not yet infectious. This model is especially useful for diseases where there is an incubation period before individuals become infectious, such as COVID-19 and many viral diseases.

The SEIR model divides the population into four categories:

• $S(t)$: The number of susceptible individuals at time .

• $E(t)$: The number of exposed individuals at time t who have been infected but are not yet infectious.

• $I(t)$: The number of infected individuals at time t who are capable of transmitting the disease.

• $R(t)$: The number of individuals who have recovered or become immune to the disease at time .

The total population size is constant and given by the equation:

$$N(t) = S(t) + E(t) + I(t) + R(t).$$

The SEIR model relies on the following assumptions:

1. Constant population size: No births or deaths occur during the study period.

2. Exposure period: Individuals are exposed to the disease for a certain period before they become infectious. This is modeled by the E class.

3. Instantaneous infection and recovery: Susceptible individuals become infected when they interact with infected individuals, and they either recover or become immune after a certain period.

4. Homogeneous mixing: All individuals are equally likely to interact with one another.

$$\begin{cases} \dot{S} &= -\beta\frac{SI}{N}, \\ \dot{E} &= \beta\frac{SI}{N} - \sigma E, \\ \dot{I} &= \sigma E - \gamma I, \\ \dot{R} &= \gamma I, \end{cases}$$

With:

• β: The rate of disease transmission.

• σ: The rate at which exposed individuals become infectious (the inverse of the incubation period).

• γ: The recovery rate (or rate of cure).

• $N(t)$: The total population size, which remains constant.

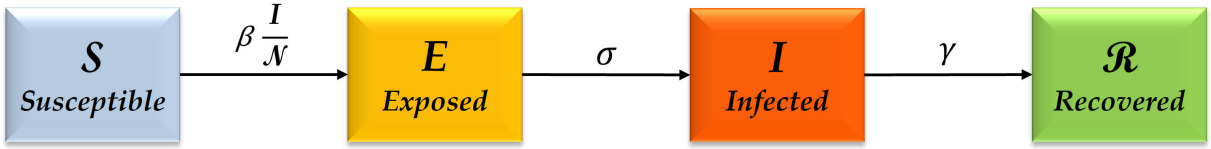

Figure 1.6: Flowchart of SEIR.

Basic Reproduction Number:

The basic reproduction number in the SEIR model is defined as:

$$\mathfrak{Rb} = \frac{\beta}{\gamma + \sigma}.$$

Equilibrium points occur when the rates of change for all classes are zero:

$$\dot{S} = \dot{E} = \dot{I} = \dot{R} = 0.$$

• Disease-free equilibrium (DFE): This occurs when are no infected or exposed individuals in the population, and the system stabilizes at:

$$(S^*, E^*, I^*, R^*) = (N, 0, 0, 0)$$

• Endemic equilibrium (EE): In the endemic equilibrium, a fixed proportion of the population remains in each category, and the disease persists in the population.

These values depend on the parameters of the model and the basic reproduction numbre $\mathfrak{Rb}$. The condition $\mathfrak{Rb} > 1$ indicates the diease persists, leading to an endemic state.

Dynamics of the Model:

Initially, the number of susceptible individuals is large, leading to a rapid spread of the disease. As more individuals are exposed and become infectious, the number of exposed individuals decreases, and the number of infected individuals increases. Eventually, the disease will slow down and may be eradicated once the number of susceptible individuals decreases significantly or enough individuals gain immunity.

Applications and Limitations:

The SEIR model is used to study diseases with an incubation period, such as COVID-19, SARS, and many other viral infections. It is particularly useful for understanding the dynamics of diseases that spread before individuals show symptoms.

It assumes constant rates of transmission, exposure, and recovery, which may not be realistic in all cases.

The model does not account for births, deaths, or other demographic factors that could influence disease dynamics.

It assumes homogeneous mixing, which may not reflect real-world interactions.

1.6.5 SEIRS Model with Vital Dynamic

The SEIRS model is an extension of the SEIR model, incorporting reinfection and immunity loss dynamics. It divides the population into four compartments: Susceptible S, Exposed E, Infected I, and Recovered R. This model considers that recovered individuals may lose immunity and become susceptible again. It is useful for studying diseases where immunity is not permanent, such as certain viral infections with waning immunity.

$$\begin{cases} \dfrac{dS}{dt} = \Lambda N + \delta R - \left(\beta \dfrac{I}{N} + \upsilon + \mu\right) S, \\ \dfrac{dE}{dt} = \beta \dfrac{I}{N} S - (\sigma + \mu)\, E, \\ \dfrac{dI}{dt} = \sigma E - (\gamma + \mu)\, I, \\ \dfrac{dR}{dt} = \upsilon S + \gamma I - (\delta + \mu)\, R. \end{cases}$$

With

- Λ: Birth rate.
- β: Infection transmission rate.
- υ: represent the vaccination rate
- σ: Transition rate from E to I.
- γ: Recovery rate.
- δ: Immunity loss rate.
- μ: Death rate.

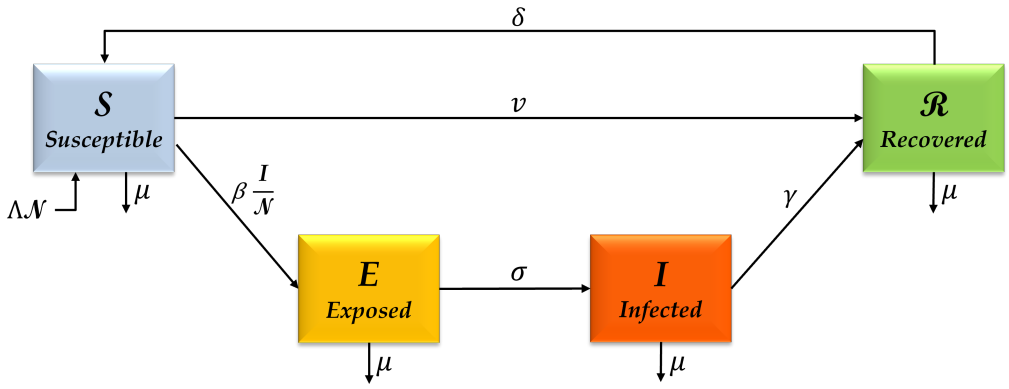

Figure 1.7: Flow chart for an SEIRS model with vital dynamic.

Numerical simulation:

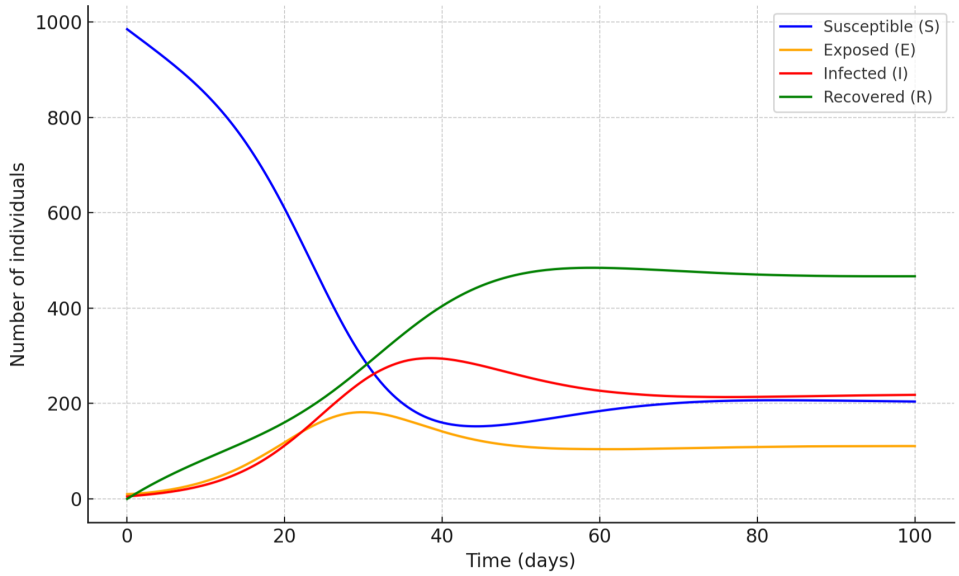

Figure 1.8: Numerical simulation of the SEIRS model with: $\beta = 0.5$, $\gamma = 0.1$ and the initial conditions $N = 1000$, $S(0) = 985$, $E(0) = 10$, $I(0) = 5$ and $R(0) = 0$.

1.7 The Fundamental Concepts in Fractional Calculus

In this section, we introduce key concepts in fractional calculus. The space under consideration is the Banach space of continuous functions $C([0, \ell], \mathbb{C})$, with the norm

$$\|\varphi\|_{\infty} = \sup_{t \in [0,\ell]} |\varphi(t)|. \tag{1.3}$$

Definition 1.8 ([26]). *The left-sided (arbitrary) fractional integral of order $\alpha > 0$ of a continuous function $\varphi : [0, \ell] \to \mathbb{R}$ is given by*

$$\mathcal{J}_{0^+}^{\alpha} \varphi(t) = \frac{1}{\Gamma(\alpha)} \int_0^t (t-\tau)^{\alpha-1} \varphi(\tau)\, d\tau,\ t \in [0, \ell]. \tag{1.4}$$

where $\Gamma(\alpha) = \int_0^{\infty} \tau^{\alpha-1} \exp(-\tau)\, d\tau$ is the Euler gamma function.

Definition 1.9 (Caputo's fractional derivative [26]). *The left-sided Caputo's fractional derivative of order $\alpha > 0$ of a function $\varphi : [0, \ell] \to \mathbb{R}$ is given by*

$${}^{C}\mathcal{D}_{0^+}^{\alpha} \varphi(t) = \begin{cases} \frac{d^m \varphi(t)}{dt^m}, \text{ for } \alpha = m \in \mathbb{N}_0, \\ \mathcal{J}_{0^+}^{m-\alpha} \frac{d^m \varphi(t)}{dt^m} = \int_0^t \frac{(t-\tau)^{m-\alpha-1}}{\Gamma(m-\alpha)} \frac{d^m \varphi(\tau)}{d\tau^m} d\tau, \text{ for } m-1 < \alpha < m \in \mathbb{N}. \end{cases} \tag{1.5}$$

Lemma 1.1 ([26]). *Assume that ${}^{C}\mathcal{D}_{0^+}^{\alpha} \varphi \in C([0, \ell], \mathbb{R})$, then we get for all $\alpha > 0$*

$$\mathcal{J}_{0^+}^{\alpha}\ {}^{C}\mathcal{D}_{0^+}^{\alpha} \varphi(t) = \varphi(t) - \sum_{k=0}^{n-1} \frac{\varphi^{(k)}(0)}{k!} t^k,\ n-1 < \alpha \leq n \in \mathbb{N}. \tag{1.6}$$

Lemma 1.2 (Gronwall [23]). *Let $\varphi(t)$ and $\omega(t)$ be nonnegative, continuous functions on $0 \leq t \leq \ell$, for which the inequality:*

$$\varphi(t) \leq \varphi(0) + \int_0^t \omega(\tau) \varphi(\tau)\, d\tau,\ t \in [0, \ell]. \tag{1.7}$$

where $\varphi(0)$ is a nonnegative constant. Then

$$\varphi(\tau) \leq \varphi(0) \exp\left(\int_0^t \omega(\tau)\, d\tau \right),\ t \in [0, \ell]. \tag{1.8}$$

Definition 1.10 (Banach's fixed point [52]). *Let P be a non-empty closed subset of a Banach space Ω, then any contraction mapping $\mathcal{T}$ of P into itself has a unique fixed point.*

Definition 1.11 (Schauder's fixed point [52]). *Let Ω be a Banach space, and P be a closed, convex and nonempty subset of Ω. Let $\mathcal{T} : P \to P$ be a continuous mapping such that $\mathcal{T}(P)$ is a relatively compact subset of Ω. Then $\mathcal{T}$ has at least one fixed point in P.*

CHAPTER 2

MALARIA TRANSMISSION DYNAMICS USING FRACTIONAL MODELS

This chapter examines malaria through fractional mathematical models that account for time delays and memory effects, providing greater accuracy in representing the disease dynamics.

2.1 Introduction

The transmission of diseases through mosquito bites highlights the important role of small pests in the spread of diseases. Malaria, which results from blood parasites of the genus Plasmodium and is transmitted through Anopheles mosquito bites, poses a major challenge to human health. This disease is notorious for its prevalence in tropical and subtropical regions, where the environment is conducive to mosquito breeding and transmission of blood parasites between humans. Global Health Organizations estimate that the number of malaria cases annually ranges from hundreds of thousands to millions, with developing countries being particularly affected.

Suitable environmental conditions such as stagnant water pools and high temperatures contribute to the spread of malaria, increase its severity, and exacerbate its complications. Those afflicted with malaria suffer from serious health effects, including organ failure such as kidney and liver failure, changes in blood composition, and central nervous system disorders. Individuals infected with malaria may experience symptoms such as high fever, severe headache, muscle pain, and confusion. In severe cases, death may occur if immediate and adequate treatment are not administered. Therefore, combating mosquitoes is of paramount importance for reducing the transmission of this disease and preserving public health.

This chapter contributes to the development of a fractional mathematical model aimed

at enhancing our understanding of the malaria transmission dynamics. The effectiveness of the model in accurately representing disease dynamics is ensured by analyzing the equilibrium points and studying the solution stability. Additionally, calculating the basic reproduction number provides crucial insights into the disease spread rate and influencing factors, which aids in better guiding health policies and preventive measures. Moreover, the model is used to validate the data and identify the factors contributing to disease transmission. Based on the results of the model, recommendations and strategies are offered to improve malaria control efforts and reduce their impact on public health.

In this chapter concerning the dynamics of the epidemic, we categorize the entire human population, represented as N, into three distinct classes: Susceptible (S_N), Infected (I_N), and Partially Immune (P_N) individuals.

Moreover, the mosquito population surrounding the human population, denoted as M, is partitioned into two distinct categories: Susceptible (S_M) and Infected (I_M) mosquitoes.

The parameters of the SIP(N)–SI(M) model are defined as follows:

- Λ indicates the rate of increase in the susceptible individuals.
- λ represents the rate of increase in the susceptible mosquitoes.
- $\mu < \Lambda$ is the rate of natural death for humans.
- $\upsilon < \lambda$ represents the rate of natural death of mosquitoes.
- β is the probability rate of disease transmission from I_M to S_N.
- γ is the probability rate of disease transmission from I_N to S_M.
- κ expresses the immunity acquisition rate for humans.
- δ represents the immunity loss rate for humans.

Motivated by the above-mentioned work, for $0 \leq t \leq \ell < \infty$, and $0 < \alpha \leq 1$, we have:

$$\begin{cases} {}^{C}\mathcal{D}^{\alpha}_{0+} S_N(t) &= \Lambda N(t) + \delta P_N(t) - \left(\dfrac{\beta I_M(t)}{M(t)} + \mu\right) S_N(t), \\ {}^{C}\mathcal{D}^{\alpha}_{0+} I_N(t) &= \dfrac{\beta I_M(t)}{M(t)} S_N(t) - (\kappa + \mu) I_N(t), \\ {}^{C}\mathcal{D}^{\alpha}_{0+} P_N(t) &= \kappa I_N(t) - (\delta + \mu) P_N(t), \\ {}^{C}\mathcal{D}^{\alpha}_{0+} S_M(t) &= \lambda M(t) - \left(\dfrac{\gamma I_N(t)}{N(t)} + \upsilon\right) S_M(t), \\ {}^{C}\mathcal{D}^{\alpha}_{0+} I_M(t) &= \dfrac{\gamma I_N(t)}{N(t)} S_M(t) - \upsilon I_M(t), \end{cases} \tag{2.1}$$

where the first three equations in system (2.1) represent human equations, while the last two equations express mosquito equations.

The changes in the transmission of malaria between humans and mosquitoes in SIP(N)–SI(M) model (2.1) can be interpreted as follows:

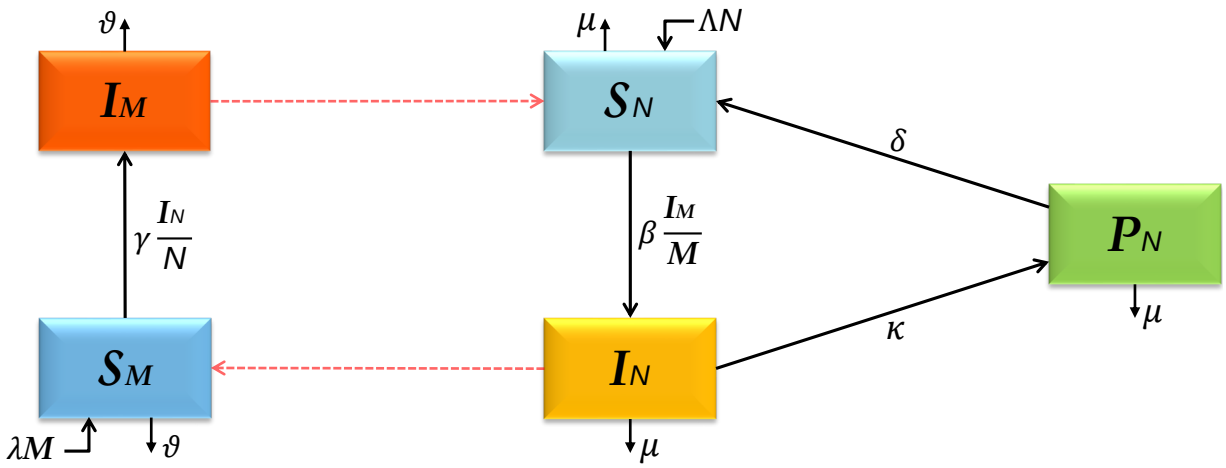

Figure 2.1: Flowchart of SIP(N)–SI(M).

In Figure 2.1, it is assumed that susceptible individuals S_N are recruited at a rate ΛN and die naturally at a rate μ. They become infected with malaria as a result of being bitten by infected mosquitoes and moving to infected class I_N at a transmission rate β.

For infected individuals, I_N is assumed to die naturally at a rate μ or acquire partial temporary immunity and move to the partially immune class P_N at a rate κ. Furthermore, partially immune individuals P_N may lose immunity and return to the susceptible class S_N at a rate δ or die naturally at a rate μ.

As for mosquitoes S_M, they are recruited into the susceptible category at a rate λM and die naturally at a rate υ. Susceptible mosquitoes S_M become infected with malaria at a rate γ after feeding on the blood of infected humans and move to the infected humans and move to the infected category I_M. Infected mosquitoes I_M also die naturally at a rate υ.

The chapter is structured to gain a thorough understanding of malaria transmission dynamics and the factors that influence them. We begin with exploring the feasibility region for the fractional SIP(N)–SI(M) mathematical model using the Caputo fractional derivative. This allows us define the boundaries in which we can effectively analyze the system's behavior and disease spread. This analysis helps in assessing the model's applicability and identifying the optimal conditions for its study.

Following this, attention is focused on studying the existence, uniqueness, and stability of solutions using Schauder's and Banach's fixed-point theorems, along with Ulam–Hyers' stability criteria. This analysis ensures that the model provides sustainable and applicable solutions, enhancing its credibility and ability to accurately represent real-world dynamics.

The basic reproduction number, $\mathfrak{Rb}$, is a critical indicator for assessing malaria transmission. Determining $\mathfrak{Rb}$ provides insights into disease spread rates and helps to identify points where control measures can be applied. In addition, we investigate the equilibrium points within the fractional SIP(N)–SI(M) model, analyze their stability to guide disease control strategies, and predict future trends. Mosquitoes play a crucial role in the transition between susceptible and infected states. Their recruitment, natural mortality, and infection dynamics are integral components of our model.

We validate the accuracy of our model using real data from the Algerian region. This allows us to identify the specific local factors contributing to the spread of malaria. The validation process enhances the precision of the model and assists in developing targeted disease-control strategies. Furthermore, we investigate the memory effect, which has enriched our understanding of the influence of temporal and historical dynamics on disease transmission.

2.2 Dynamic Analysis of the Feasible Region

2.2.1 Positivity and Boundedness of the Model

The SIP(N)–SI(M) model (2.1) is investigated within a biologically feasible region in $\mathbb{R}_+^5$, as defined in the subsequent lemma.

Lemma 2.1. *Assume that M_0 repersents the initial total mosquito population, let N_0 be the initial total human population at $t = 0$, where $0 \leq t \leq \ell < \infty$. Consequently, the solution to the considered model is confined to the feasible region, given by*

$$\Omega = \left\{ (S_N, I_N, P_N, S_M, I_M) \in \mathbb{R}_+^5 : 0 \leq N(t) \leq N_0 \exp\left(\frac{\Lambda \ell^\alpha}{\Gamma(\alpha+1)}\right),\ 0 \leq M(t) \leq M_0 \exp\left(\frac{\lambda \ell^\alpha}{\Gamma(\alpha+1)}\right) \right\}.$$

with

$$N(t) = S_N(t) + I_N(t) + P_N(t), \qquad M(t) = S_M(t) + I_M(t).$$

Proof. Let

$$N(t) = S_N(t) + I_N(t) + P_N(t),$$

then

$${}^C\mathcal{D}_{0^+}^\alpha N(t) = {}^C\mathcal{D}_{0^+}^\alpha S_N(t) + {}^C\mathcal{D}_{0^+}^\alpha I_N(t) + {}^C\mathcal{D}_{0^+}^\alpha P_N(t).$$

Now, summing all the human equations of (2.1), we get

$$\begin{aligned} {}^C\mathcal{D}_{0^+}^\alpha N(t) &= (\Lambda - \mu) N(t) \\ &\leq \Lambda N(t). \end{aligned}$$

After using lemma 1.1, we get

$$N(t) \leq N_0 + \Lambda \mathcal{J}_{0^+}^{\alpha} N(t).$$

Applying Gronwall lemma 1.2, we obtain

$$N(t) \leq N_0 \exp\left(\frac{\Lambda \ell^{\alpha}}{\Gamma(\alpha+1)}\right),$$

where N_0 is the total human population at $t = 0$.

In another way, let

$$M(t) = S_M(t) + I_M(t),$$

then

$${}^{C}\mathcal{D}_{0^+}^{\alpha} M(t) = {}^{C}\mathcal{D}_{0^+}^{\alpha} S_M(t) + {}^{C}\mathcal{D}_{0^+}^{\alpha} I_M(t).$$

Now, summing all the mosquito equations of (2.1), we obtain

$$\begin{aligned} {}^{C}\mathcal{D}_{0^+}^{\alpha} M(t) &= (\lambda - \upsilon) M(t) \\ &\leq \lambda M(t). \end{aligned}$$

Applying lemma 1.1, gives us

$$M(t) \leq M_0 + \lambda \mathcal{J}_{0^+}^{\alpha} M(t).$$

After using Gronwall lemma 1.2, we get

$$M(t) \leq M_0 \exp\left(\frac{\lambda \ell^{\alpha}}{\Gamma(\alpha+1)}\right),$$

where M_0 is the total mosquito population at $t = 0$. □

In subsequent sections of this chapter, we assume the existence of two positive constants:

$$\mathcal{N} \leq N_0 \exp\left(\tfrac{\Lambda \ell^{\alpha}}{\Gamma(\alpha+1)}\right), \qquad \mathcal{M} \leq M_0 \exp\left(\tfrac{\lambda \ell^{\alpha}}{\Gamma(\alpha+1)}\right),$$

where the total human population N and mosquito population M remained fixed throughout the chapter period and can be expressed as $N(t) = \mathcal{N}$ and $M(t) = \mathcal{M}$. This assumption was made to normalize the SIP(N)–SI(M) model (2.1). Therefore, we put:

$$\begin{aligned} \mathcal{S}(t) &= \tfrac{S_N(t)}{\mathcal{N}}, \qquad \mathcal{I}(t) = \tfrac{I_N(t)}{\mathcal{N}}, \qquad \mathcal{P}(t) = \tfrac{P_N(t)}{\mathcal{N}}, \\ \mathcal{V}(t) &= \tfrac{S_M(t)}{\mathcal{M}}, \qquad \mathcal{F}(t) = \tfrac{I_M(t)}{\mathcal{M}}, \end{aligned} \tag{2.2}$$

then we obtain

$$\begin{cases} {}^{C}\mathcal{D}_{0^+}^{\alpha}\mathcal{S}(t) &= \Lambda + \delta\mathcal{P}(t) - (\beta\mathcal{F}(t) + \mu)\mathcal{S}(t), \\ {}^{C}\mathcal{D}_{0^+}^{\alpha}\mathcal{I}(t) &= \beta\mathcal{F}(t)\mathcal{S}(t) - (\kappa + \mu)\mathcal{I}(t), \\ {}^{C}\mathcal{D}_{0^+}^{\alpha}\mathcal{P}(t) &= \kappa\mathcal{I}(t) - (\delta + \mu)\mathcal{P}(t), \\ {}^{C}\mathcal{D}_{0^+}^{\alpha}\mathcal{V}(t) &= \lambda - (\gamma\mathcal{I}(t) + \upsilon)\mathcal{V}(t), \\ {}^{C}\mathcal{D}_{0^+}^{\alpha}\mathcal{F}(t) &= \gamma\mathcal{I}(t)\mathcal{V}(t) - \upsilon\mathcal{F}(t), \end{cases} \tag{2.3}$$

along with the positive initial conditions

$$\mathcal{S}(0) = \varphi_1,\ \mathcal{I}(0) = \varphi_2,\ \mathcal{P}(0) = \varphi_3,\ \mathcal{V}(0) = \varphi_4,\ \mathcal{F}(0) = \varphi_5. \tag{2.4}$$

2.2.2 Existence Results of Solutions for the Normalized Model

In this section, we explore the existence and uniqueness of solutions to problem (2.6)–(2.7) through the field of fixed-point theory. Our investigation employs Banach's and Schauder's fixed-point theorems, as outlined in [53, 54, 23, 55, 56].

Let $\varphi = (\mathcal{S}, \mathcal{I}, \mathcal{P}, \mathcal{V}, \mathcal{F}) \in \Omega$, where $\Omega = [C([0, \ell], [0, 1])]^5$ is a Banach space with

$$\|\varphi\|_{\Omega} = \max\left\{\|\mathcal{S}\|_{\infty}, \|\mathcal{I}\|_{\infty}, \|\mathcal{P}\|_{\infty}, \|\mathcal{V}\|_{\infty}, \|\mathcal{F}\|_{\infty}\right\},$$

and let $\psi = (\psi_1, \psi_2, \psi_3, \psi_4, \psi_5)$, be such that

$$\begin{cases} \psi_1(t, \varphi(t)) &= \Lambda - (\beta\mathcal{F}(t) + \mu)\mathcal{S}(t) + \delta\mathcal{P}(t), \\ \psi_2(t, \varphi(t)) &= \beta\mathcal{F}(t)\mathcal{S}(t) - (\kappa + \mu)\mathcal{I}(t), \\ \psi_3(t, \varphi(t)) &= \kappa\mathcal{I}(t) - (\delta + \mu)\mathcal{P}(t), \\ \psi_4(t, \varphi(t)) &= \lambda - (\gamma\mathcal{I}(t) + \upsilon)\mathcal{V}(t), \\ \psi_5(t, \varphi(t)) &= \gamma\mathcal{I}(t)\mathcal{V}(t) - \upsilon\mathcal{F}(t). \end{cases} \tag{2.5}$$

It is clear that ψ is a continuous function.

By applying $\mathcal{J}_{0^+}^{\alpha}$ to both sides of the system

$${}^{C}\mathcal{D}_{0^+}^{\alpha}\varphi(t) = \psi(t, \varphi(t)), \tag{2.6}$$

taking into account the conditions

$$\varphi(0) = \varphi_0 = (\varphi_1, \varphi_2, \varphi_3, \varphi_4, \varphi_5), \tag{2.7}$$

and employing Lemma 1.1, we obtain the following system of fractional integral equations

$$\varphi(t) = \varphi_0 + \frac{1}{\Gamma(\alpha)}\int_0^t (t - \tau)^{\alpha - 1} f(\tau, \varphi(\tau))\, d\tau,$$

which is equivalent to the original problem (2.6)–(2.7).

Theorem 2.1. *Let* $\beta, \gamma, \delta, \kappa, \upsilon, \mu, \alpha, \ell \in \mathbb{R}_+$, *be such that* $\alpha \in (0, 1]$ *and*

$$\ell < \left(\frac{\Gamma(\alpha + 1)}{\max\{\beta + \mu, \kappa + \mu, \delta + \mu, \gamma + \upsilon\}} \right)^{\frac{1}{\alpha}}. \tag{2.8}$$

Then, there is at least one solution to problem (2.6)–(2.7) on $[0, \ell]$.

Proof. The proof begins with transformation of problem (2.6)–(2.7) into a fixed-point problem $\mathcal{T}\varphi(t) = \varphi(t)$, with

$$\mathcal{T}\varphi(t) = (\mathcal{T}_1\varphi(t), \mathcal{T}_2\varphi(t), \mathcal{T}_3\varphi(t), \mathcal{T}_4\varphi(t), \mathcal{T}_5\varphi(t))$$

and

$$\mathcal{T}\varphi(t) = \varphi_0 + \frac{1}{\Gamma(\alpha)} \int_0^t (t - \tau)^{\alpha - 1} \psi(\tau, \varphi(\tau))\, d\tau. \tag{2.9}$$

Observing that for $\varphi \in \Omega$, the operators $\mathcal{T}_i\varphi$ for $1 \leq i \leq 5$ are continuous, as demonstrated in Step 1. Consequently, $\mathcal{T}\varphi$ is an element of Ω, with

$$\|\mathcal{T}\varphi\|_\Omega = \max_{1 \leq i \leq 5} \|\mathcal{T}_i\varphi\|_\infty.$$

The equivalence between problems (2.6)–(2.7) and (2.9) implies that $\mathcal{T}$ includes fixed points for solving the aforementioned problem.

Step 1. $\mathcal{T}$ is a continuous operator.

Let $(\varphi_n)_{n \in \mathbb{N}_0} = (\mathcal{S}_n, \mathcal{I}_n, \mathcal{P}_n, \mathcal{V}_n, \mathcal{F}_n)$ be five nonnegative real sequences, such that $\lim_{n \to \infty} \varphi_n = \varphi$ in Ω. We obtain for all $t \in [0, \ell]$,

$$|\mathcal{T}_i\varphi_n(t) - \mathcal{T}_i\varphi(t)| \leq \frac{1}{\Gamma(\alpha)} \int_0^t (t - \tau)^{\alpha - 1} |\psi_i(\tau, \varphi_n(\tau)) - \psi_i(\tau, \varphi(\tau))|\, d\tau, \tag{2.10}$$

where ψ_i satisfies (2.5) for each $1 \leq i \leq 5$. We have

$$\begin{aligned}
|\psi_1(t, \varphi_n(t)) - \psi_1(t, \varphi(t))| &= |\delta(\mathcal{P}_n(t) - \mathcal{P}(t)) - [(\beta\mathcal{F}_n(t) + \mu)\mathcal{S}_n(t) \\
&\quad - (\beta\mathcal{F}(t) + \mu)\mathcal{S}(t)]| \\
&\leq \delta|\mathcal{P}_n(t) - \mathcal{P}(t)| + \mu|\mathcal{S}_n(t) - \mathcal{S}(t)| \\
&\quad + |\beta\mathcal{F}_n(t)\mathcal{S}_n(t) - \beta\mathcal{F}(t)\mathcal{S}(t)| \\
&\leq \delta|\mathcal{P}_n(t) - \mathcal{P}(t)| + (\beta + \mu)|\mathcal{S}_n(t) - \mathcal{S}(t)| \\
&\quad + \beta|\mathcal{F}_n(t) - \mathcal{F}(t)| \\
&\leq \max\{\delta, \beta + \mu\} \|\varphi_n - \varphi\|_\Omega.
\end{aligned} \tag{2.11}$$

Similarly, we obtain

$$\begin{aligned}
|\psi_2(t,\varphi_n(t)) - \psi_2(t,\varphi(t))| &\leq \max\{\beta, \kappa+\mu\}\|\varphi_n - \varphi\|_\Omega, \\
|\psi_3(t,\varphi_n(t)) - \psi_3(t,\varphi(t))| &\leq \max\{\kappa, \delta+\mu\}\|\varphi_n - \varphi\|_\Omega, \\
|\psi_4(t,\varphi_n(t)) - \psi_4(t,\varphi(t))| &\leq (\gamma+\upsilon)\|\varphi_n - \varphi\|_\Omega, \\
|\psi_5(t,\varphi_n(t)) - \psi_5(t,\varphi(t))| &\leq \max\{\gamma, \upsilon\}\|\varphi_n - \varphi\|_\Omega.
\end{aligned} \tag{2.12}$$

Since $\varphi_n \to \varphi$ in Ω as $n \to \infty$, we get $\psi_i(t,\varphi_n(t)) \to \psi_i(t,\varphi(t))$ for any $t \in [0,\ell]$, and each $i \in \overline{1,5}$.

Now, let $\mathcal{K} > 0$, be such that for each $t \in [0,\ell]$, we have

$$\begin{aligned}
\frac{(t-\tau)^{\alpha-1}}{\Gamma(\alpha)}|\psi_i(\tau,\varphi_n(\tau)) - \psi_i(\tau,\varphi(\tau))| &\leq \frac{(t-\tau)^{\alpha-1}}{\Gamma(\alpha)}(|\psi_i(\tau,\varphi_n(\tau))| + |\psi_i(\tau,\varphi(\tau))|) \\
&\leq \frac{2\mathcal{K}}{\Gamma(\alpha)}(t-\tau)^{\alpha-1}.
\end{aligned}$$

For each $i \in \overline{1,5}$, the function $\tau \to \frac{2\mathcal{K}}{\Gamma(\alpha)}(t-\tau)^{\alpha-1}$ is integrable on $[0,t]$, for each $t \in [0,\ell]$. Thus, the implication of Lebesgue's dominated convergence theorem gives us

$$|\mathcal{T}_i\varphi_n(t) - \mathcal{T}_i\varphi(t)| \to 0 \text{ as } n \to \infty,$$

and hence

$$\lim_{n\to\infty}\|\mathcal{T}\varphi_n - \mathcal{T}\varphi\|_\Omega = 0.$$

This signifies the continuity of $\mathcal{T}$.

Step 2. $\mathcal{T}$ is defined from a bounded, closed, and convex subset into itself.

Utilizing (2.8), we define

$$r \geq \frac{\varphi_i\Gamma(\alpha+1) + (\Lambda+\lambda)\ell^\alpha}{\Gamma(\alpha+1) - \max\{\beta+\mu, \kappa+\mu, \delta+\mu, \gamma+\upsilon\}\ell^\alpha},$$

where $\varphi^* = \max_{1\leq i\leq 5}\varphi_i$, and define the subset Ω_r as follows:

$$\Omega_r = \{\varphi \in \Omega : \|\varphi\|_\Omega \leq r\}.$$

It is clear that Ω_r is a subset of Ω, distinguished by its bounded, closed, and convex subset of Ω.

Consider the integral operator $\mathcal{T} : \Omega_r \to \Omega$ defined by (2.9). It follows that $\mathcal{T}(\Omega_r) \subset \Omega_r$.

Indeed, employing (2.11) and (2.12) provides us

$$\begin{aligned}
|\psi_1(t,\varphi(t))| &\leq \Lambda + \max\{\beta+\mu,\delta\}\|\varphi\|_\Omega,\\
|\psi_2(t,\varphi(t))| &\leq \max\{\beta,\kappa+\mu\}\|\varphi\|_\Omega,\\
|\psi_3(t,\varphi(t))| &\leq \max\{\kappa,\delta+\mu\}\|\varphi\|_\Omega,\\
|\psi_4(t,\varphi(t))| &\leq \lambda + (\gamma+\upsilon)\|\varphi\|_\Omega,\\
|\psi_5(t,\varphi(t))| &\leq \max\{\gamma,\upsilon\}\|\varphi\|_\Omega.
\end{aligned}$$

Then, in each case, for any $\varphi \in \Omega$

$$|\psi_i(t,\varphi(t))| \leq \eta r,\ \forall i \in \overline{1,5},$$

with

$$\eta = \frac{\Lambda+\lambda}{r} + \max\{\beta+\mu,\kappa+\mu,\delta+\mu,\gamma+\upsilon\}.$$

Thus

$$\begin{aligned}
|\mathcal{T}_i\varphi(t)| &\leq \varphi_i + \frac{1}{\Gamma(\alpha)}\int_0^t (t-\tau)^{\alpha-1}|\psi_i(\tau,\varphi(\tau))|\,d\tau\\
&\leq \varphi^* + \frac{\eta\ell^\alpha}{\Gamma(\alpha+1)}r\\
&\leq \varphi^* + \frac{(\Lambda+\lambda)\ell^\alpha}{\Gamma(\alpha+1)} + \frac{\max\{\beta+\mu,\kappa+\mu,\delta+\mu,\gamma+\upsilon\}\ell^\alpha}{\Gamma(\alpha+1)}r\\
&\leq r,\ \forall i \in \overline{1,5},
\end{aligned}$$

or $(\|\mathcal{T}_i\varphi\|_\infty)_{1\leq i\leq 5} \leq r$, then $\|\mathcal{T}\varphi\|_\Omega \leq r$. Consequently $\mathcal{T}(\Omega_r) \subset \Omega_r$.

Step 3. $\mathcal{T}(\Omega_r)$ is equicontinuous subset of Ω.

Let $t_1, t_2 \in [0,\ell]$, $t_1 < t_2$ and $\varphi \in \Omega_r$. Then, for every $i \in \overline{1,5}$, we get

$$\begin{aligned}
|\mathcal{T}_i\varphi(t_2) - \mathcal{T}_i\varphi(t_1)| &= \Big|\frac{1}{\Gamma(\alpha)}\int_0^{t_2}(t_2-\tau)^{\alpha-1}\psi_i(\tau,\varphi(\tau))\,d\tau\\
&\quad - \frac{1}{\Gamma(\alpha)}\int_0^{t_1}(t_1-\tau)^{\alpha-1}\psi_i(\tau,\varphi(\tau))\,d\tau\Big|\\
&\leq \frac{1}{\Gamma(\alpha)}\int_0^{t_1}\left|\left((t_2-\tau)^{\alpha-1}-(t_1-\tau)^{\alpha-1}\right)\psi_i(\tau,\varphi(\tau))\right|d\tau\\
&\quad + \frac{1}{\Gamma(\alpha)}\int_{t_1}^{t_2}(t_2-\tau)^{\alpha-1}|\psi_i(\tau,\varphi(\tau))|\,d\tau\\
&\leq \frac{\eta r}{\Gamma(\alpha)}\left(\int_0^{t_1}\left|(t_2-\tau)^{\alpha-1}-(t_1-\tau)^{\alpha-1}\right|d\tau\right.\\
&\quad \left.+\int_{t_1}^{t_2}(t_2-\tau)^{\alpha-1}\,d\tau\right).
\end{aligned} \tag{2.13}$$

We have

$$(t_2-\tau)^{\alpha-1}-(t_1-\tau)^{\alpha-1}=-\frac{1}{\alpha}\frac{d}{d\tau}\left((t_2-\tau)^{\alpha}-(t_1-\tau)^{\alpha}\right),$$

then

$$\int_0^{t_1}\left|(t_2-\tau)^{\alpha-1}-(t_1-\tau)^{\alpha-1}\right|d\tau\leq\frac{1}{\alpha}\left[(t_2-t_1)^{\alpha}+(t_2^{\alpha}-t_1^{\alpha})\right],$$

we also have

$$\begin{aligned}\int_{t_1}^{t_2}(t_2-\tau)^{\alpha-1}\,d\tau&=-\frac{1}{\alpha}\left[(t_2-\tau)^{\alpha}\right]_{t_1}^{t_2}\\&\leq\frac{1}{\alpha}(t_2-t_1)^{\alpha}.\end{aligned}$$

Then, (2.13) gives

$$|\mathcal{T}_i\varphi(t_2)-\mathcal{T}_i\varphi(t_1)|\leq\frac{\eta r}{\Gamma(\alpha+1)}\left[2(t_2-t_1)^{\alpha}+(t_2^{\alpha}-t_1^{\alpha})\right].$$

The right-hand side of the inequality above approaches zero as $t_1\to t_2$ for every $i\in\overline{1,5}$.

Based on Steps 1–3, assisted by the Ascoli-Arzelà theorem, we infer the continuity of $\mathcal{T}:\Omega_r\to\Omega_r$, its compactness, and its satisfaction with Schauder's fixed-point theorem assumptions. Therefore, $\mathcal{T}$ possesses a fixed point that solves problem (2.6)–(2.7) on $[0,\ell]$. □

Theorem 2.2. *We give $\alpha\in(0,1]$, $\ell>0$, and*

$$\eta=\max\{\beta+\mu,\kappa+\mu,\delta+\mu,\gamma+\upsilon\},$$

for some $\beta,\delta,\kappa,\gamma,\upsilon,\mu\in\mathbb{R}_+$. If

$$\frac{\eta\ell^{\alpha}}{\Gamma(\alpha+1)}<1,\tag{2.14}$$

thus, there is a unique solution to the problem (2.6)–(2.7) on $[0,\ell]$.

Proof. Similar to the steps taken to prove Theorem 2.1, problem (2.6)–(2.7) has already been transformed into fixed-point problem (2.9).

Let $\varphi,\omega\in\Omega$, then

$$|\mathcal{T}_i\varphi(t)-\mathcal{T}_i\omega(t)|\leq\frac{1}{\Gamma(\alpha)}\int_0^t(t-\tau)^{\alpha-1}\left|\psi_i(\tau,\varphi(\tau))-\psi_i(\tau,\omega(\tau))\right|d\tau,\ \forall i\in\overline{1,5}.\tag{2.15}$$

For all $t \in [0, \ell]$, we have

$$\begin{aligned}
|\psi_1(t, \varphi(t)) - \psi_1(t, \omega(t))| &\leq \max\{\beta + \mu, \delta\} \|\varphi - \omega\|_\Omega, \\
|\psi_2(t, \varphi(t)) - \psi_2(t, \omega(t))| &\leq \max\{\beta, \kappa + \mu\} \|\varphi - \omega\|_\Omega, \\
|\psi_3(t, \varphi(t)) - \psi_3(t, \omega(t))| &\leq \max\{\kappa, \delta + \mu\} \|\varphi - \omega\|_\Omega, \\
|\psi_4(t, \varphi(t)) - \psi_4(t, \omega(t))| &\leq (\gamma + \upsilon) \|\varphi - \omega\|_\Omega, \\
|\psi_5(t, \varphi(t)) - \psi_5(t, \omega(t))| &\leq \max\{\gamma, \upsilon\} \|\varphi - \omega\|_\Omega.
\end{aligned}$$

Then

$$|\psi_i(t, \varphi(t)) - \psi_i(t, \omega(t))| \leq \eta \|\varphi - \omega\|_\Omega, \ \forall i \in \overline{1, 5}. \tag{2.16}$$

From (2.15), we find

$$\|\mathcal{T}_i\varphi - \mathcal{T}_i\omega\|_\infty \leq \frac{\eta \ell^\alpha}{\Gamma(\alpha + 1)} \|\varphi - \omega\|_\Omega, \ \forall i \in \overline{1, 5}.$$

and

$$\|\mathcal{T}\varphi - \mathcal{T}\omega\|_\Omega \leq \frac{\eta \ell^\alpha}{\Gamma(\alpha + 1)} \|\varphi - \omega\|_\Omega.$$

Referring to (2.14), $\mathcal{T}$ is considered as a contraction operator. By employing Banach's Contraction Principle, it can be deduced that $\mathcal{T}$ possesses a unique fixed point, which corresponds to the unique solution of the problem (2.6)–(2.7) on $[0, \ell]$. □

2.2.3 Ulam-Hyers Stability for the Normalized Model

Definition 2.1. *The system of Caputo-type fractional differential equations (2.6) is Ulam-Hyers stable if there exists a real number $c > 0$ such that for each $\varepsilon = \max\{\varepsilon_1, \ldots, \varepsilon_5\}$ with $\varepsilon_i > 0$, $i \in \overline{1, 5}$, and for each solution $\omega \in \Omega$ of the inequality*

$$\left|{}^C\mathcal{D}^\alpha_{0^+}\omega_i(t) - \psi_i(t, \omega(t))\right| \leq \varepsilon_i, \quad t \in [0, \ell], \ i \in \overline{1, 5}, \tag{2.17}$$

there exists $\varphi \in \Omega$ a solution of (2.6) with

$$\|\omega - \varphi\|_\Omega \leq c\varepsilon.$$

Definition 2.2. *The system of Caputo-type fractional differential equations (2.6) is generalized Ulam-Hyers stable if there exists $\xi \in C(\mathbb{R}_+, \mathbb{R}_+)$, $\xi(0) = 0$, such that for each solution $\omega \in \Omega$ of inequality (2.17), there exists a solution $\varphi \in \Omega$ of (2.6) with*

$$\|\omega - \varphi\|_\Omega \leq \xi(\varepsilon).$$

Remark 2.1 ([57]). *If $\omega \in \Omega$ is a solution of inequality (2.17), then there exist $(\varepsilon_i)_{i\in\overline{1,5}} > 0$ and $\phi \in \Omega$, such that*

1. ${}^{C}\mathcal{D}^{\alpha}_{0^+}\omega_i(t) = \psi_i(t,\omega(t)) + \phi_i(t), t \in [0,\ell], i \in \overline{1,5}$,
2. $|\phi_i(t)| \leq \varepsilon_i$, *for all* $t \in [0,\ell]$, *and each* $i \in \overline{1,5}$.

The subsequent lemma aids in establishing the stability of system (2.6).

Lemma 2.2. *If $\omega \in \Omega$ is the solution of inequality (2.17), then there exist $(\varepsilon_i)_{i\in\overline{1,5}} > 0$ such that ω will be the solution of the inequality*

$$\left|\omega_i(t) - \omega_i(0) - \frac{1}{\Gamma(\alpha)}\int_0^t (t-\tau)^{\alpha-1}\psi_i(\tau,\omega(\tau))\,d\tau\right| \leq \frac{\ell^{\alpha}\varepsilon_i}{\Gamma(\alpha+1)},$$

for each $i \in \overline{1,5}$.

Proof. If ω is a solution of (2.17), we have from Remark 2.1

$$\begin{cases} {}^{C}\mathcal{D}^{\alpha}_{0^+}\omega_i(t) = \psi_i(t,\omega(t)) + \phi_i(t), & t \in [0,\ell], i \in \overline{1,5}, \\ |\phi_i(t)| \leq \varepsilon_i, & (\varepsilon_i)_{i\in\overline{1,5}} > 0, \end{cases}$$

hence

$$\omega_i(t) = \omega_i(0) + \frac{1}{\Gamma(\alpha)}\int_0^t (t-\tau)^{\alpha-1}\left[\psi_i(\tau,\omega(\tau)) + \phi_i(\tau)\right]d\tau.$$

Also,

$$\begin{aligned} & \left|\omega_i(t) - \omega_i(0) - \frac{1}{\Gamma(\alpha)}\int_0^t (t-\tau)^{\alpha-1}\psi_i(\tau,\omega(\tau))\,d\tau\right| \\ = & \left|\omega_i(0) + \frac{1}{\Gamma(\alpha)}\int_0^t (t-\tau)^{\alpha-1}\left[\psi_i(\tau,\omega(\tau)) + \phi_i(\tau)\right]d\tau\right. \\ & \left. - \omega_i(0) - \frac{1}{\Gamma(\alpha)}\int_0^t (t-\tau)^{\alpha-1}\psi_i(\tau,\omega(\tau))\,d\tau\right| \\ \leq & \frac{1}{\Gamma(\alpha)}\int_0^t (t-\tau)^{\alpha-1}|\phi_i(\tau)|\,d\tau \\ \leq & \frac{\ell^{\alpha}\varepsilon_i}{\Gamma(\alpha+1)}, \quad \forall i \in \overline{1,5}. \end{aligned}$$

That establishes the lemma. □

Theorem 2.3. *Assuming that (2.14) holds, system (2.6) is Ulam-Hyers stable. Furthermore, it can also be asserted that (2.6) is a generalized Ulam-Hyers stable system.*

Proof. Let $(\varepsilon_i)_{i\in\overline{1,5}} > 0$, we define $\omega \in \Omega$ as a solution of the inequality

$$\left|{}^{C}\mathcal{D}^{\alpha}_{0+}\omega_i(t) - \psi_i(t,\omega(t))\right| \leq \varepsilon_i, \quad t \in [0,\ell], \ i \in \overline{1,5},$$

and $\varphi \in \Omega$ is the unique solution of system (2.6) with the conditions

$$\varphi_i(0) = \omega_i(0), \quad \forall i \in \overline{1,5}.$$

Then

$$\varphi_i(t) = \omega_i(0) + \frac{1}{\Gamma(\alpha)}\int_0^t (t-\tau)^{\alpha-1}\psi_i(\tau,\varphi(\tau))\,d\tau,$$

and

$$\begin{aligned}
|\omega_i(t) - \varphi_i(t)| &= \left|\omega_i(t) - \omega_i(0) - \frac{1}{\Gamma(\alpha)}\int_0^t (t-\tau)^{\alpha-1}\psi_i(\tau,\varphi(\tau))\,d\tau\right| \\
&\leq \left|\omega_i(t) - \omega_i(0) - \frac{1}{\Gamma(\alpha)}\int_0^t (t-\tau)^{\alpha-1}\psi_i(\tau,\omega(\tau))\,d\tau\right| \\
&\quad + \frac{1}{\Gamma(\alpha)}\int_0^t (t-\tau)^{\alpha-1}|\psi_i(\tau,\omega(\tau)) - \psi_i(\tau,\varphi(\tau))|\,d\tau.
\end{aligned}$$

Using (2.16), and Lemma 2.2, we get

$$|\omega_i(t) - \varphi_i(t)| \leq \frac{\ell^{\alpha}}{\Gamma(\alpha+1)}\left(\varepsilon_i + \eta\|\varphi-\omega\|_{\Omega}\right), \quad \forall t \in [0,\ell], \ \forall i \in \overline{1,5}.$$

Taking the maximum from both sides, we obtain

$$\|\varphi-\omega\|_{\Omega} \leq \frac{\ell^{\alpha}}{\Gamma(\alpha+1)}\left(\varepsilon + \eta\|\varphi-\omega\|_{\Omega}\right).$$

Thus

$$\|\varphi-\omega\|_{\Omega} \leq c\varepsilon,$$

where $c = \frac{\ell^{\alpha}}{\Gamma(\alpha+1)-\eta\ell^{\alpha}}$. This implies that system (2.6) is stable in the Ulam-Hyers sense and is consequently generalized Ulam-Hyers stable if we set $\xi(t) = ct$. □

2.3 Analysis for the Fractional SIP(N)–SI(M) Model

2.3.1 Basic Reproduction Number and Equilibrium Points

Theorem 2.4. *The basic reproduction number of system (2.3) is determined by*

$$\mathfrak{Rb} = \sqrt{\frac{\beta\gamma\lambda\Lambda}{\upsilon^2\mu(\kappa+\mu)}}. \tag{2.18}$$

Proof. Because the SIP(N)–SI(M) model is composed of infection components $\mathcal{I}$, $\mathcal{P}$, and $\mathcal{F}$, we obtain:

$$y_i - z_i = \begin{pmatrix} \beta\mathcal{F}(t)\,\mathcal{S}(t) - (\kappa+\mu)\,\mathcal{I}(t) \\ \kappa\mathcal{I}(t) - (\delta+\mu)\,\mathcal{P}(t) \\ \gamma\mathcal{I}(t)\,\mathcal{V}(t) - \upsilon\mathcal{F}(t) \end{pmatrix}.$$

Accordingly,

$$y_i = \begin{pmatrix} \beta\mathcal{F}(t)\,\mathcal{S}(t) \\ 0 \\ \gamma\mathcal{I}(t)\,\mathcal{V}(t) \end{pmatrix}, z_i = \begin{pmatrix} (\kappa+\mu)\,\mathcal{I}(t) \\ (\delta+\mu)\,\mathcal{P}(t) - \kappa\mathcal{I}(t) \\ \upsilon\mathcal{F}(t) \end{pmatrix}.$$

Here, y_i denotes the rate of new infections appearing in compartment i, and z_i denotes the rate of transitions between compartment i and other infected compartments for each $i \in \{1,2,3\}$.

The new infection matrix $\mathcal{Y}$ and transition matrix $\mathcal{Z}$ are assessed at the disease-free equilibrium point $\mathfrak{D}\mathfrak{f}\mathfrak{p}$ (Theorem 2.5), as follows:

$$\mathcal{Y} = \begin{pmatrix} 0 & 0 & \beta\bar{\mathcal{S}} \\ 0 & 0 & 0 \\ \gamma\bar{\mathcal{V}} & 0 & 0 \end{pmatrix}, \quad \mathcal{Z} = \begin{pmatrix} \kappa+\mu & 0 & 0 \\ -\kappa & \delta+\mu & 0 \\ 0 & 0 & \upsilon \end{pmatrix}.$$

Following the next-generation matrix principle, the basic reproduction number is defined as the spectral radius of matrix $\mathcal{Y}\mathcal{Z}^{-1}$ and is given by (2.18). □

The initial step in comprehending a differential equation is to identify equilibrium points. In epidemiology, we are concerned with two types of equilibrium point:

- Disease-free equilibrium is defined as the point at which no disease (or death from disease) is introduced into the population and is depicted in the model as $\mathcal{I} = \mathcal{P} = \mathcal{F} = 0$.
- Other equilibrium points, where $\mathcal{I} \neq 0$ and $\mathcal{F} \neq 0$, are indicated as endemic equilibrium points (or outbreak equilibrium points).

We define the positive real values

$$m_1 = \kappa + \mu, \qquad m_2 = \delta + \mu,$$

to facilitate the calculations and establish the following theorem.

Theorem 2.5. *The system (2.3) has two types of equilibrium points*

1. *Disease-free equilibrium*

$$\mathfrak{Dfp} = \left(\bar{\mathcal{S}}, \bar{\mathcal{I}}, \bar{\mathcal{P}}, \bar{\mathcal{V}}, \bar{\mathcal{F}}\right) = \left(\frac{\Lambda}{\mu}, 0, 0, \frac{\lambda}{\upsilon}, 0\right).$$

2. *Endemic equilibrium point* $E_2 = (\mathcal{S}^*, \mathcal{I}^*, \mathcal{P}^*, \mathcal{V}^*, \mathcal{F}^*)$*, which is*

$$\mathfrak{Eqp} = \left(\bar{\mathcal{S}}\left(1 - \frac{\mu\left(\delta + m_1\right)}{\Lambda m_2}\mathcal{I}^*\right), \mathcal{I}^*, \frac{\kappa}{m_2}\mathcal{I}^*, \frac{\lambda}{\gamma\mathcal{I}^* + \upsilon}, \frac{\gamma\lambda\mathcal{I}^*}{\upsilon\left(\gamma\mathcal{I}^* + \upsilon\right)}\right),$$

where

$$\mathcal{I}^* = \frac{m_1 m_2 \upsilon^2}{\gamma\left[m_1 m_2 \upsilon + \beta\lambda\left(\delta + m_1\right)\right]}\left(\mathfrak{Rb}^2 - 1\right).$$

The existence of the endemic equilibrium point depends on $\mathfrak{Rb} > 1$.

Proof. To determine the equilibrium points for system (2.3), we set ${}^{C}\mathcal{D}^{\alpha}_{0^+}\varphi\left(t\right) = \vec{0}$, with $\varphi = (\mathcal{S}, \mathcal{I}, \mathcal{P}, \mathcal{V}, \mathcal{F})$. Therefore

$$\begin{cases} 0 &= \Lambda + \delta\mathcal{P}\left(t\right) - \left(\beta\mathcal{F}\left(t\right) + \mu\right)\mathcal{S}\left(t\right), & (eq1) \\ 0 &= \beta\mathcal{F}\left(t\right)\mathcal{S}\left(t\right) - \left(\kappa + \mu\right)\mathcal{I}\left(t\right), & (eq2) \\ 0 &= \kappa\mathcal{I}\left(t\right) - \left(\delta + \mu\right)\mathcal{P}\left(t\right), & (eq3) \\ 0 &= \lambda - \left(\gamma\mathcal{I}\left(t\right) + \upsilon\right)\mathcal{V}\left(t\right), & (eq4) \\ 0 &= \gamma\mathcal{I}\left(t\right)\mathcal{V}\left(t\right) - \upsilon\mathcal{F}\left(t\right). & (eq5) \end{cases}$$

From equations $(eq3)$ and $(eq4)$, we have

$$\mathcal{P}\left(t\right) = \frac{\kappa}{m_2}\mathcal{I}\left(t\right) \quad \text{and} \quad \mathcal{V}\left(t\right) = \frac{\lambda}{\gamma\mathcal{I}\left(t\right) + \upsilon}.$$

Substituting the expression of $\mathcal{V}\left(t\right)$ in equation $(eq5)$, we get

$$\mathcal{F}\left(t\right) = \frac{\gamma\lambda\mathcal{I}\left(t\right)}{\upsilon\left(\gamma\mathcal{I}\left(t\right) + \upsilon\right)}.$$

If we add $(eq1)$ to $(eq2)$ we obtain

$$\mathcal{S}\left(t\right) = \bar{\mathcal{S}}\left(1 - \frac{\mu\left(\delta + m_1\right)}{\Lambda m_2}\mathcal{I}\left(t\right)\right).$$

1. If $\mathcal{I} = 0$, we can easily obtain the first disease-free equilibrium point $\mathfrak{Dfp}$.

2. When $\mathcal{I} \neq 0$, equation $(eq2)$ gives us

$$\mathcal{I}^* = \frac{m_1 m_2 \upsilon^2}{\gamma\left[m_1 m_2 \upsilon + \beta\lambda\left(\delta + m_1\right)\right]}\left(\mathfrak{Rb}^2 - 1\right).$$

Consequently, we obtain the required endemic equilibrium point $\mathfrak{Eqp}$, which exists for $\mathfrak{Rb} > 1$.

Hence, the theorem is proved. □

2.3.2 Stability Study of Disease-Free Equilibrium Point

Local Stability Analysis of $\mathfrak{Dfp}$

Theorem 2.6. *The disease-free equilibrium point of system (2.3) is locally asymptotically stable when* $\mathfrak{Rb} < 1$.

Proof. The Jacobian matrix for system (2.3) is written as follows

$$J = \begin{pmatrix} \frac{\partial \psi_1}{\partial \mathcal{S}} & \frac{\partial \psi_1}{\partial \mathcal{I}} & \frac{\partial \psi_1}{\partial \mathcal{P}} & \frac{\partial \psi_1}{\partial \mathcal{V}} & \frac{\partial \psi_1}{\partial \mathcal{F}} \\ \frac{\partial \psi_2}{\partial \mathcal{S}} & \frac{\partial \psi_2}{\partial \mathcal{I}} & \frac{\partial \psi_2}{\partial \mathcal{P}} & \frac{\partial \psi_2}{\partial \mathcal{V}} & \frac{\partial \psi_2}{\partial \mathcal{F}} \\ \frac{\partial \psi_3}{\partial \mathcal{S}} & \frac{\partial \psi_3}{\partial \mathcal{I}} & \frac{\partial \psi_3}{\partial \mathcal{P}} & \frac{\partial \psi_3}{\partial \mathcal{V}} & \frac{\partial \psi_3}{\partial \mathcal{F}} \\ \frac{\partial \psi_4}{\partial \mathcal{S}} & \frac{\partial \psi_4}{\partial \mathcal{I}} & \frac{\partial \psi_4}{\partial \mathcal{P}} & \frac{\partial \psi_4}{\partial \mathcal{V}} & \frac{\partial \psi_4}{\partial \mathcal{F}} \\ \frac{\partial \psi_5}{\partial \mathcal{S}} & \frac{\partial \psi_5}{\partial \mathcal{I}} & \frac{\partial \psi_5}{\partial \mathcal{P}} & \frac{\partial \psi_5}{\partial \mathcal{V}} & \frac{\partial \psi_5}{\partial \mathcal{F}} \end{pmatrix}$$

where $\psi_{1\leq i\leq 5}\left(t, \varphi\left(t\right)\right)$ represents the right-hand side of (2.3). Then

$$J = \begin{pmatrix} -\left(\beta\mathcal{F}+\mu\right) & 0 & \delta & 0 & -\beta\mathcal{S} \\ \beta\mathcal{F} & -m_1 & 0 & 0 & \beta\mathcal{S} \\ 0 & \kappa & -m_2 & 0 & 0 \\ 0 & -\gamma\mathcal{V} & 0 & -\left(\gamma\mathcal{I}+\upsilon\right) & 0 \\ 0 & \gamma\mathcal{V} & 0 & \gamma\mathcal{I} & -\upsilon \end{pmatrix}.$$

The eigenvalues of $J\left(\mathfrak{Dfp}\right)$ are given as the roots of the following characteristic polynomial

$$P_1\left(X\right) = -\left(\mu+X\right)\left(m_2+X\right)\left(\upsilon+X\right)\left[X^2+\left(m_1+\upsilon\right)X+m_1\upsilon\left(1-\mathfrak{Rb}^2\right)\right].$$

The roots of $P_1\left(X\right)$ are negative reals or complexes of negative real parts, which makes $\mathfrak{Dfp}$ locally asymptotically stable. □

Global Stability Analysis of $\mathfrak{Dfp}$

Theorem 2.7. *The disease-free equilibrium point* $\mathfrak{Dfp}$ *of system (2.3) is globally asymptotically stable if* $\mathfrak{Rb} < 1$.

Proof. To prove the theorem, we examine the following Lyapunov function

$$W\left(\mathcal{S},\mathcal{I},\mathcal{P},\mathcal{V},\mathcal{F}\right) = c_1\mathcal{I}+c_2\mathcal{P}+c_3\mathcal{F}.$$

We consider c_i to be positive constants for $i \in 1, 2, 3$, to be determined later. The fractional derivative of W along with the solution of system (2.3) is calculated as follows:

$$\begin{aligned}
{}^{C}\mathcal{D}^{\alpha}_{0+}W &= c_1\,{}^{C}\mathcal{D}^{\alpha}_{0+}\mathcal{I} + c_2\,{}^{C}\mathcal{D}^{\alpha}_{0+}\mathcal{P} + c_3\,{}^{C}\mathcal{D}^{\alpha}_{0+}\mathcal{F} \\
&= c_1\left[\beta\mathcal{F}\mathcal{S} - (\kappa+\mu)\,\mathcal{I}\right] + c_2\left[\kappa\mathcal{I} - (\delta+\mu)\,\mathcal{P}\right] + c_3\left[\gamma\mathcal{I}\mathcal{V} - \upsilon\mathcal{F}\right] \\
&\leq c_1\left[\frac{\beta\Lambda}{\mu}\mathcal{F} - (\kappa+\mu)\,\mathcal{I}\right] + c_2\left[\kappa\mathcal{I} - (\delta+\mu)\,\mathcal{P}\right] + c_3\left[\frac{\gamma\lambda}{\upsilon}\mathcal{I} - \upsilon\mathcal{F}\right] \\
&= \left[-c_1\,(\kappa+\mu) + c_2\kappa + c_3\frac{\gamma\lambda}{\upsilon}\right]\mathcal{I} - c_2\,(\delta+\mu)\,\mathcal{P} + \left[c_1\frac{\beta\Lambda}{\mu} - c_3\upsilon\right]\mathcal{F}.
\end{aligned}$$

By choosing $c_1 = \upsilon$, $c_2 = 0$, and $c_3 = \frac{\beta\Lambda}{\mu}$, we obtain

$${}^{C}\mathcal{D}^{\alpha}_{0+}W \leq \upsilon\,(\kappa+\mu)\left(\mathfrak{Rb}^2 - 1\right)\mathcal{I}.$$

Thus, if $\mathfrak{Rb} < 1$, we get ${}^{C}\mathcal{D}^{\alpha}_{0+}W \leq 0$, then $\frac{dW}{dt} < 0$. According to LaSalle's invariance principle [58], this implies that $\mathfrak{Dfp}$ is globally asymptotically stable. □

2.3.3 Stability Study of Endemic Equilibrium Point

Local Stability Analysis of $\mathfrak{Eqp}$

Let g_0, g_1, and g_2, be such that

$$\begin{aligned}
g_0 &= (\gamma\mathcal{I}^* + \upsilon)\left(\frac{\kappa\delta + (m_1+\delta)\,(\beta\mathcal{F}^* + \mu)}{m_2}\right), \\
g_1 &= m_1\,(\gamma\mathcal{I}^* + \upsilon) + \frac{\beta\mathcal{F}^*\left[\delta\mu + m_1\,(\gamma\mathcal{I}^* + \upsilon + \mu) + m_2\,(\gamma\mathcal{I}^* + \upsilon)\right] + \mu m_2\,(m_1 + \gamma\mathcal{I}^* + \upsilon)}{\mu + m_2}, \\
g_2 &= (\beta\mathcal{F}^* + \mu)\,m_2 + (m_1 + \gamma\mathcal{I}^* + \upsilon)\,(\beta\mathcal{F}^* + \mu + m_2) + m_1\,(\gamma\mathcal{I}^* + \upsilon).
\end{aligned}$$

Theorem 2.8. *If we put*

$$\beta\gamma\mathcal{V}^*\mathcal{S}^* < \min\left\{g_0, g_1, g_2\right\},$$

the endemic equilibrium point $\mathfrak{Eqp}$ *of system (2.3) is locally asymptotically stable when* $\mathfrak{Rb} > 1$.

Proof. As shown in the previous section, the Jacobian matrix $J\left(\mathfrak{Eqp}\right)$ for (2.3) is

$$J_{\mathfrak{Eqp}} = \begin{pmatrix}
-\left(\beta\mathcal{F}^* + \mu\right) & 0 & \delta & 0 & -\beta\mathcal{S}^* \\
\beta\mathcal{F}^* & -m_1 & 0 & 0 & \beta\mathcal{S}^* \\
0 & \kappa & -m_2 & 0 & 0 \\
0 & -\gamma\mathcal{V}^* & 0 & -\left(\gamma\mathcal{I}^* + \upsilon\right) & 0 \\
0 & \gamma\mathcal{V}^* & 0 & \gamma\mathcal{I}^* & -\upsilon
\end{pmatrix}.$$

The characteristic polynomial is given by

$$P_2(X) = -(\upsilon + X)\left(X^4 + a_3X^3 + a_2X^2 + a_1X + a_0\right),$$

where

$$\begin{aligned} a_0 &= \mu m_2 (g_0 - \beta\gamma\mathcal{V}^*\mathcal{S}^*), \\ a_1 &= (m_2 + \mu)(g_1 - \beta\gamma\mathcal{V}^*\mathcal{S}^*), \\ a_2 &= g_2 - \beta\gamma\mathcal{V}^*\mathcal{S}^*, \\ a_3 &= \beta\mathcal{F}^* + \gamma\mathcal{I}^* + m_1 + m_2 + \mu + \upsilon. \end{aligned}$$

According to Descartes' rule, the roots of $P_2(X)$ are negative reals or complexes of negative real parts. Therefore, the required result is obtained. □

Global Stability Analysis of $\mathfrak{Eqp}$

From system (2.3), we obtain

$$\begin{cases} \Lambda = -\delta\mathcal{P}^* + (\beta\mathcal{F}^* + \mu)\mathcal{S}^*, \\ (\kappa + \mu)\mathcal{S}^* = \beta\mathcal{S}^*\mathcal{F}^*, \\ (\delta + \mu)\mathcal{P}^* = \kappa\mathcal{I}^*, \\ \lambda = (\gamma\mathcal{I}^* + \upsilon)\mathcal{V}^*, \\ \upsilon\mathcal{F}^* = \gamma\mathcal{I}^*\mathcal{V}^*. \end{cases}$$

Theorem 2.9. *Suppose that*

$$\frac{\mathcal{P}^*}{\mathcal{P}} \leq 1 \leq \min\left\{\left(\frac{\mathcal{S}^*}{\mathcal{S}} - 1\right)^2 + \frac{\mathcal{F}\mathcal{I}^*}{\mathcal{F}^*\mathcal{I}}, \left(\frac{\mathcal{V}^*}{\mathcal{V}} - 1\right)^2 + \frac{\mathcal{F}\mathcal{I}^*}{\mathcal{F}^*\mathcal{I}}\right\}.$$

Therefore, the endemic equilibrium point $\mathfrak{Eqp}$ of the system (2.3) is globally asymptotically stable when $\mathfrak{Rb} > 1$.

Proof. We analyze the following nonlinear Lyapunov function of the Goh-Volterra form:

$$\begin{aligned} W(\mathcal{S},\mathcal{I},\mathcal{P},\mathcal{V},\mathcal{F}) = &\left[\mathcal{S}(t) - \mathcal{S}^* - \mathcal{S}^*\log\frac{\mathcal{S}(t)}{\mathcal{S}^*}\right] + \left[\mathcal{I}(t) - \mathcal{I}^* - \mathcal{I}^*\log\frac{\mathcal{I}(t)}{\mathcal{I}^*}\right] \\ &+ \frac{\delta}{\delta+\mu}\left[\mathcal{P}(t) - \mathcal{P}^* - \mathcal{P}^*\log\frac{\mathcal{P}(t)}{\mathcal{P}^*}\right] \\ &+ \frac{\beta\mathcal{S}^*}{\upsilon}\left[\mathcal{V}(t) - \mathcal{V}^* - \mathcal{V}^*\log\frac{\mathcal{V}(t)}{\mathcal{V}^*}\right] \\ &+ \frac{\beta\mathcal{S}^*}{\upsilon}\left[\mathcal{F}(t) - \mathcal{F}^* - \mathcal{F}^*\log\frac{\mathcal{F}(t)}{\mathcal{F}^*}\right]. \end{aligned}$$

By leveraging the fidings on Volterra-type Lyapunov functions for fractional-order epidemic systems outlined in [59], and subsequently employing the Caputo derivative on both sides, the following inequality can be established:

$$
\begin{aligned}
{}^{C}\mathcal{D}_{0+}^{\alpha} W \leq & \left(1-\frac{\mathcal{S}^{*}}{\mathcal{S}}\right) {}^{C}\mathcal{D}_{0+}^{\alpha} \mathcal{S}(t)+\left(1-\frac{\mathcal{I}^{*}}{\mathcal{I}}\right) {}^{C}\mathcal{D}_{0+}^{\alpha} \mathcal{I}(t)+\frac{\delta}{\delta+\mu}\left(1-\frac{\mathcal{P}^{*}}{\mathcal{P}}\right) {}^{C}\mathcal{D}_{0+}^{\alpha} \mathcal{P}(t) \\
& +\frac{\beta \mathcal{S}^{*}}{\upsilon}\left(1-\frac{\mathcal{V}^{*}}{\mathcal{V}}\right) {}^{C}\mathcal{D}_{0+}^{\alpha} \mathcal{V}(t)+\frac{\beta \mathcal{S}^{*}}{\upsilon}\left(1-\frac{\mathcal{F}^{*}}{\mathcal{F}}\right) {}^{C}\mathcal{D}_{0+}^{\alpha} \mathcal{F}(t) .
\end{aligned}
$$

A simple calculation provides the following result

$$
\begin{aligned}
\left(1-\frac{\mathcal{S}^{*}}{\mathcal{S}}\right) {}^{C}\mathcal{D}_{0+}^{\alpha} \mathcal{S} &= \left(1-\frac{\mathcal{S}^{*}}{\mathcal{S}}\right)\left[\Lambda+\delta \mathcal{P}-(\beta \mathcal{F}+\mu) \mathcal{S}\right] \\
&= \left(1-\frac{\mathcal{S}^{*}}{\mathcal{S}}\right)\left[-\delta \mathcal{P}^{*}+\left(\beta \mathcal{F}^{*}+\mu\right) \mathcal{S}^{*}+\delta \mathcal{P}-(\beta \mathcal{F}+\mu) \mathcal{S}\right] \\
&= \mu \mathcal{S}^{*}\left(2-\frac{\mathcal{S}^{*}}{\mathcal{S}}-\frac{\mathcal{S}}{\mathcal{S}^{*}}\right)+\beta \mathcal{F}^{*} \mathcal{S}^{*}\left(1-\frac{\mathcal{S}^{*}}{\mathcal{S}}\right)-\beta \mathcal{F} \mathcal{S}+\delta \mathcal{P}-\delta \mathcal{P}^{*} \\
&\quad +\beta \mathcal{F} \mathcal{S}^{*}-\delta \mathcal{P} \frac{\mathcal{S}^{*}}{\mathcal{S}}+\delta \mathcal{P}^{*} \frac{\mathcal{S}^{*}}{\mathcal{S}} .
\end{aligned}
$$

In same way, we find

$$
\begin{aligned}
\left(1-\frac{\mathcal{I}^{*}}{\mathcal{I}}\right) {}^{C}\mathcal{D}_{0+}^{\alpha} \mathcal{I} &= \left(1-\frac{\mathcal{I}^{*}}{\mathcal{I}}\right)\left[\beta \mathcal{F} \mathcal{S}-(\kappa+\mu) \mathcal{I}\right] \\
&= \beta \mathcal{F} \mathcal{S}-(\kappa+\mu) \mathcal{I}-\beta \mathcal{F} \mathcal{S} \frac{\mathcal{I}^{*}}{\mathcal{I}}+(\kappa+\mu) \mathcal{I}^{*} .
\end{aligned}
$$

Next

$$
\begin{aligned}
\frac{\delta}{\delta+\mu}\left(1-\frac{\mathcal{P}^{*}}{\mathcal{P}}\right) {}^{C}\mathcal{D}_{0+}^{\alpha} \mathcal{P} &= \frac{\delta}{\delta+\mu}\left(1-\frac{\mathcal{P}^{*}}{\mathcal{P}}\right)\left[\kappa \mathcal{I}-(\delta+\mu) \mathcal{P}\right] \\
&= \delta \mathcal{P}^{*}-\delta \mathcal{P}+\frac{\delta \kappa}{\delta+\mu} \mathcal{I}-\frac{\delta \kappa}{\delta+\mu} \mathcal{I} \frac{\mathcal{P}^{*}}{\mathcal{P}} .
\end{aligned}
$$

Also

$$
\begin{aligned}
\frac{\beta \mathcal{S}^{*}}{\upsilon}\left(1-\frac{\mathcal{V}^{*}}{\mathcal{V}}\right) {}^{C}\mathcal{D}_{0+}^{\alpha} \mathcal{V} &= \frac{\beta \mathcal{S}^{*}}{\upsilon}\left(1-\frac{\mathcal{V}^{*}}{\mathcal{V}}\right)\left[\lambda-(\gamma \mathcal{I}+\upsilon) \mathcal{V}\right] \\
&= \frac{\beta \mathcal{S}^{*}}{\upsilon}\left(1-\frac{\mathcal{V}^{*}}{\mathcal{V}}\right)\left[\left(\gamma \mathcal{I}^{*}+\upsilon\right) \mathcal{V}^{*}-(\gamma \mathcal{I}+\upsilon) \mathcal{V}\right] \\
&= \beta \mathcal{S}^{*} \mathcal{V}^{*}\left(2-\frac{\mathcal{V}^{*}}{\mathcal{V}}-\frac{\mathcal{V}}{\mathcal{V}^{*}}\right)+\frac{\beta \mathcal{S}^{*}}{\upsilon} \gamma \mathcal{I}^{*} \mathcal{V}^{*}-\frac{\beta \mathcal{S}^{*}}{\upsilon} \gamma \mathcal{I} \mathcal{V} \\
&\quad +\frac{\beta \mathcal{S}^{*}}{\upsilon} \gamma \mathcal{I} \mathcal{V}^{*}-\frac{\beta \mathcal{S}^{*}}{\upsilon} \gamma \mathcal{I}^{*} \mathcal{V}^{*} \frac{\mathcal{V}^{*}}{\mathcal{V}} .
\end{aligned}
$$

and

$$
\begin{aligned}
\frac{\beta \mathcal{S}^{*}}{\upsilon}\left(1-\frac{\mathcal{F}^{*}}{\mathcal{F}}\right) {}^{C}\mathcal{D}_{0+}^{\alpha} \mathcal{F} &= \frac{\beta \mathcal{S}^{*}}{\upsilon}\left(1-\frac{\mathcal{F}^{*}}{\mathcal{F}}\right)\left[\gamma \mathcal{I} \mathcal{V}-\upsilon \mathcal{F}\right] \\
&= \frac{\beta \mathcal{S}^{*}}{\upsilon} \gamma \mathcal{I} \mathcal{V}-\beta \mathcal{S}^{*} \mathcal{F}-\frac{\beta \mathcal{S}^{*}}{\upsilon} \gamma \mathcal{I} \mathcal{V} \frac{\mathcal{F}^{*}}{\mathcal{F}}+\beta \mathcal{S}^{*} \mathcal{F}^{*} .
\end{aligned}
$$

Then

$$
\begin{aligned}
{}^{C}\mathcal{D}^{\alpha}_{0+}W \;\leq\; & \mu\mathcal{S}^{*}\left(2-\frac{\mathcal{S}^{*}}{\mathcal{S}}-\frac{\mathcal{S}}{\mathcal{S}^{*}}\right)+\beta\mathcal{F}^{*}\mathcal{S}^{*}\left(4-\frac{\mathcal{S}^{*}}{\mathcal{S}}-\frac{\mathcal{V}^{*}}{\mathcal{V}}-\frac{\mathcal{I}\mathcal{V}\mathcal{F}^{*}}{\mathcal{I}^{*}\mathcal{V}^{*}\mathcal{F}}-\frac{\mathcal{F}\mathcal{S}\mathcal{I}^{*}}{\mathcal{F}^{*}\mathcal{S}^{*}\mathcal{I}}\right)\\
& +\beta\mathcal{S}^{*}\mathcal{V}^{*}\left(2-\frac{\mathcal{V}^{*}}{\mathcal{V}}-\frac{\mathcal{V}}{\mathcal{V}^{*}}\right)+\delta\mathcal{P}^{*}\left(\frac{\mathcal{S}^{*}}{\mathcal{S}}-\frac{\mathcal{S}^{*}\mathcal{P}}{\mathcal{S}\mathcal{P}^{*}}-\frac{\mathcal{P}^{*}\mathcal{I}}{\mathcal{P}\mathcal{I}^{*}}+\frac{\mathcal{I}}{\mathcal{I}^{*}}\right).
\end{aligned}
$$

with

$$
\begin{cases}
2-\frac{\mathcal{S}^{*}}{\mathcal{S}}-\frac{\mathcal{S}}{\mathcal{S}^{*}}\leq 0, & \text{and} \quad 2-\frac{\mathcal{V}^{*}}{\mathcal{V}}-\frac{\mathcal{V}}{\mathcal{V}^{*}}\leq 0,\\
\frac{\mathcal{S}^{*}}{\mathcal{S}}-\frac{\mathcal{S}^{*}\mathcal{P}}{\mathcal{S}\mathcal{P}^{*}}-\frac{\mathcal{P}^{*}\mathcal{I}}{\mathcal{P}\mathcal{I}^{*}}+\frac{\mathcal{I}}{\mathcal{I}^{*}}\leq 0, & \text{for} \quad \frac{\mathcal{P}^{*}}{\mathcal{P}}\leq 1,\\
4-\frac{\mathcal{S}^{*}}{\mathcal{S}}-\frac{\mathcal{V}^{*}}{\mathcal{V}}-\frac{\mathcal{I}\mathcal{V}\mathcal{F}^{*}}{\mathcal{I}^{*}\mathcal{V}^{*}\mathcal{F}}-\frac{\mathcal{F}\mathcal{S}\mathcal{I}^{*}}{\mathcal{F}^{*}\mathcal{S}^{*}\mathcal{I}}\leq 0, & \text{for} \quad \min\left\{\left(\frac{\mathcal{S}^{*}}{\mathcal{S}}-1\right)^{2}+\frac{\mathcal{F}\mathcal{I}^{*}}{\mathcal{F}^{*}\mathcal{I}},\left(\frac{\mathcal{V}^{*}}{\mathcal{V}}-1\right)^{2}+\frac{\mathcal{F}\mathcal{I}^{*}}{\mathcal{F}^{*}\mathcal{I}}\right\}\geq 1.
\end{cases}
$$

Because all parameters are nonnegative, we obtain ${}^{C}\mathcal{D}^{\alpha}_{0+}W \leq 0$, which follows that $\frac{dW}{dt}\leq 0$ when $\mathfrak{Rb}>1$. According to LaSalle's invariance principle [58], $(\mathcal{S},\mathcal{I},\mathcal{P},\mathcal{V},\mathcal{F})\to(\mathcal{S}^{*},\mathcal{I}^{*},\mathcal{P}^{*},\mathcal{V}^{*},\mathcal{F}^{*})$ as $t\to\infty$. □

2.4 Data Fitting Analysis through Numerical Simulation

In this section, we validate our analytical findings by determining specific parameter values and using the Adams-type predictor-corrector method [60, 61] to perform a numerical simulation of the proposed nonlinear system (2.1) to obtain an approximate solution for the model.

The *nlinfit* function in MATLAB is a powerful tool for nonlinear regressions. It is used to model predictive relationships between variables when the data or the relationship between variables is complex and does not fit simple linear models. It also provides a convenient interface for data-fitting problems.

Using this tool, we identified the parameter values closest to those in Table 2.2, resulting in a minimum error for the fractional-order model. These estimated parameters were then incorporated into the fractional-order SIP(N)–SI(M) model (2.1). To ensure consistent physical dimensions, we modified the units of all model parameters to align with the dimension $(time)^{-\alpha}$, which corresponds to the fractional derivatives with dimension (order α).

2.4.1 Numerical Scheme for the Fractional SIP(N)–SI(M) Model

In this subsection, we outline the generalized predictor-corrector scheme associated with the Adams–Bashforth–Moulton algorithm [62], which can be used to solve fractional

epidemic systems. The chosen method is stable, converges faster, and has superior accuracy compared to other methods [61, 62, 63], making it an optimal choice for our SIP(N)–SI(M) model (2.1).

Consider the following Cauchy problem of Caputo fractional derivative of order $\alpha > 0$

$$\begin{aligned} {}^{C}\mathcal{D}_{0^+}^{\alpha}\varphi(t) &= \psi(t,\varphi(t)), \qquad 0 \le t \le \ell, \quad \alpha \in (m-1,m] \\ \varphi^{(k)}(0) &= \varphi_0^{(k)}, \qquad k = 0,1,\ldots,m-1, \quad m \in \mathbb{N}. \end{aligned}$$

where ψ is a nonlinear function. The Cauchy problem is equivalent to the Volterra integral equation:

$$\varphi(t) = \sum_{k=0}^{m-1} \frac{t^k}{k!}\varphi_0^{(k)} + \frac{1}{\Gamma(\alpha)}\int_0^t (t-\tau)^{\alpha-1}\psi(\tau,\varphi(\tau))\,d\tau.$$

Consider a uniform grid $\{t_n = nh, \text{ with } n = 0,1,\ldots,L\}$ for some integer L and $h = \frac{\ell}{L}$. Let $\varphi_h(t_n)$ denote the approximation of $\varphi(t_n)$. Assume that we have already calculated approximations $\varphi_h(t_j)$, for $j = 1,2,\ldots,n$, and we want to obtain $\varphi_h(t_{n+1})$ using equation (2.4.1).

$$\begin{aligned} \varphi_h(t_{n+1}) &= \sum_{k=0}^{m-1} \frac{t_{n+1}^k}{k!}\varphi_0^{(k)} + \frac{h^\alpha}{\Gamma(\alpha+2)}\psi(t_{n+1},\varphi_h^{pr}(t_{n+1})) \\ &\quad + \frac{h^\alpha}{\Gamma(\alpha+2)}\sum_{j=0}^{n} a_{j,n+1}\psi(t_j\varphi_h(t_j)), \end{aligned}$$

where

$$\alpha_{j,n+1} = \begin{cases} n^{\alpha+1} - (n-\alpha)(n+1)^\alpha, & \text{if } j = 0, \\ (n-j+2)^{\alpha+1} + (n-j)^{\alpha+1} - 2(n-j+1)^{\alpha+1}, & \text{if } 1 \le j \le n, \\ 1, & \text{if } j = n+1. \end{cases} \tag{2.19}$$

The preliminary approximation $\varphi_h^{pr}(t_{n+1})$ is called predictor and is given by

$$\varphi_h^{pr}(t_{n+1}) = \sum_{k=0}^{m-1} \frac{t_{n+1}^k}{k!}\varphi_0^{(k)} + \frac{1}{\Gamma(\alpha)}\sum_{j=0}^{n} b_{j,n+1}\psi(t_j,\varphi_h(t_j)),$$

with

$$b_{j,n+1} = \frac{h^\alpha}{\alpha}\left[(n+1-j)^\alpha - (n-j)^\alpha\right]. \tag{2.20}$$

Error in this method is

$$\max_{n=0,1,\ldots,L} |\varphi(t_n) - \varphi_h(t_n)| = O\left(h^\Theta\right),$$

where $\Theta = \min(2, 1+\alpha)$. Consequently, by taking $\varphi_h(t_n) = (S_{N_n}, I_{N_n}, P_{N_n}, S_{M_n}, I_{M_n})$ and

$$\psi(t_n,\varphi_h(t_n)) = (\psi_1(t_n,\varphi_h(t_n)), \psi_2(t_n,\varphi_h(t_n)), \psi_3(t_n,\varphi_h(t_n)), \psi_4(t_n,\varphi_h(t_n)), \psi_5(t_n,\varphi_h(t_n))),$$

where $(\psi_i)_{1\leq i\leq 5}$ satisfy (2.5). We explore the numerical scheme corresponding to the SIP(N)–SI(M) model (2.1):

$$\begin{aligned}
S_{N_{n+1}} &= S_{N_0}+\tfrac{h^\alpha}{\Gamma(\alpha+2)}\left(\Lambda N-\left(\tfrac{\beta I^{pr}_{M_{n+1}}}{M}+\mu\right)S^{pr}_{N_{n+1}}+\delta R^{pr}_{N_{n+1}}\right)\\
&+ \tfrac{h^\alpha}{\Gamma(\alpha+2)}\sum_{j=0}^{n}a_{j,n+1}\left(\Lambda N-\left(\tfrac{\beta I_{M_j}}{M}+\mu\right)S_{N_j}+\delta R_{N_j}\right),\\
I_{N_{n+1}} &= I_{N_0}+\tfrac{h^\alpha}{\Gamma(\alpha+2)}\left(\tfrac{\beta I^{pr}_{M_{n+1}}}{M}S^{pr}_{N_{n+1}}-(\kappa+\mu)\,I^{pr}_{N_{n+1}}\right)\\
&+ \tfrac{h^\alpha}{\Gamma(\alpha+2)}\sum_{j=0}^{n}a_{j,n+1}\left(\tfrac{\beta I_{M_j}}{M}S_{N_j}-(\kappa+\mu)\,I_{N_j}\right),\\
P_{N_{n+1}} &= P_{N_0}+\tfrac{h^\alpha}{\Gamma(\alpha+2)}\left(\kappa I^{pr}_{N_{n+1}}-(\delta+\mu)\,R^{pr}_{N_{n+1}}\right)\\
&+ \tfrac{h^\alpha}{\Gamma(\alpha+2)}\sum_{j=0}^{n}a_{j,n+1}\left(\kappa I_{N_j}-(\delta+\mu)\,R_{N_j}\right),\\
S_{M_{n+1}} &= S_{M_0}+\tfrac{h^\alpha}{\Gamma(\alpha+2)}\left(\lambda M-\left(\tfrac{\gamma I^{pr}_{N_{n+1}}}{N}+\upsilon\right)S^{pr}_{M_{n+1}}\right)\\
&+ \tfrac{h^\alpha}{\Gamma(\alpha+2)}\sum_{j=0}^{n}a_{j,n+1}\left(\lambda M-\left(\tfrac{\gamma I_{N_j}}{N}+\upsilon\right)S_{M_j}\right),\\
I_{M_{n+1}} &= I_{M_0}+\tfrac{h^\alpha}{\Gamma(\alpha+2)}\left(\tfrac{\gamma I^{pr}_{N_{n+1}}}{N}S^{pr}_{M_{n+1}}-\upsilon I^{pr}_{M_{n+1}}\right)\\
&+ \tfrac{h^\alpha}{\Gamma(\alpha+2)}\sum_{j=0}^{n}a_{j,n+1}\left(\tfrac{\gamma I_{N_j}}{N}S_{M_j}-\upsilon I_{M_j}\right),
\end{aligned}$$

where $a_{j,n+1}$ are given by (2.19). Similarly, the predicted values are

$$\begin{aligned}
S^{pr}_{N_{n+1}} &= S_{N_0}+\tfrac{1}{\Gamma(\alpha)}\sum_{j=0}^{n}b_{j,n+1}\left(\Lambda N-\left(\tfrac{\beta I_{M_j}}{M}+\mu\right)S_{N_j}+\delta R_{N_j}\right),\\
I^{pr}_{N_{n+1}} &= I_{N_0}+\tfrac{1}{\Gamma(\alpha)}\sum_{j=0}^{n}b_{j,n+1}\left(\tfrac{\beta I_{M_j}}{M}S_{N_j}-(\kappa+\mu)\,I_{N_j}\right),\\
P^{pr}_{N_{n+1}} &= P_{N_0}+\tfrac{1}{\Gamma(\alpha)}\sum_{j=0}^{n}b_{j,n+1}\left(\kappa I_{N_j}-(\delta+\mu)\,P_{N_j}\right),\\
S^{pr}_{M_{n+1}} &= S_{M_0}+\tfrac{1}{\Gamma(\alpha)}\sum_{j=0}^{n}b_{j,n+1}\left(\lambda M-\left(\tfrac{I_{N_j}}{N}+\upsilon\right)S_{M_j}\right),\\
I^{pr}_{M_{n+1}} &= I_{M_0}+\tfrac{1}{\Gamma(\alpha)}\sum_{j=0}^{n}b_{j,n+1}\left(\tfrac{I_{N_j}}{N}S_{M_j}-\upsilon I_{M_j}\right),
\end{aligned}$$

where $b_{j,n+1}$ are given by (2.20).

2.4.2 Fitted Data Analysis of Malaria in Algeria

This section presents a numerical study to contribute to a comprehensive understanding and effective management of malaria in Algeria using data from reliable health sources. Statistical and graphical methods were employed to examine the key epidemiological indicators and provide insights into the malaria situation in the country.

The total population of Algeria was $N = 30\,774\,621$ in 2000 [70]. Initial reported malaria cases $I_N(0) = 541$ from the World Health Organization [71].

In our analtsis, we assume that the total population N remains constant; however, a significant increase in population was observed from 2000 to 2021. Therefore, we cannot directly compare the infection rate in 2000, where there were 541 cases out of a population of $30\,774\,621$, to the infection rate in 2021, where there were $1\,164$ cases out of a population of $44\,177\,969$. To ensure accuracy, we will adjust the infection rate for each year based on the initial total population in 2000 (Table 2.1), enabling a precise comparison of infection rates over time. Based on these considerations, we will calculate the average recruitment and natural death rates for the entire period from 2000 to 2021 [72].

Interpretation	**Ref.**	2000	2001	$\cdots$	2020	2021	**Average**
Population of Algeria	[70]	30 774 621	31 200 985	$\cdots$	43 451 666	44 177 969	-
Initial malaria cases	[71]	541	435	$\cdots$	2 726	1 164	-
Adjusted malaria cases	-	541	429	$\cdots$	1 931	811	-
Recruitment rate Λ	[72]	0.0196	0.0193	$\cdots$	0.0224	0.0215	0.022818
Natural death rate μ	[72]	0.005	0.0049	$\cdots$	0.0054	0.0045	0.0046818

Table 2.1: Adjusted parameters and initial data of infected population in Algeria from 2000 to 2021.

Lemma 2.1 ensures that the population does not exceed a specified limit. This constraint is integral to maintaining the validity of our model, as it reflects real-world limitations on population growth and size. Indeed, we have

$$N_0 = N_{2000} = 30\,774\,621 \quad \text{and} \quad N(t) \leq N_{2021} = 44\,177\,969.$$

Subsequently, it must hold that:

$$\begin{aligned} N_{2021} &\leq N_{2000} \exp\left(\frac{\Lambda \ell^{\alpha}}{\Gamma(\alpha+1)}\right) \\ &\leq \min\left\{N_{2000} \times \exp\left(\frac{0.022818 \ell^{\alpha}}{\Gamma(\alpha+1)}\right)\right\}. \end{aligned}$$

Our numerical simulation shows that the greatest value that ℓ can take is 36 when we select $0.79 \leq \alpha \leq 1$. This decision makes the existence and uniqueness of the solution for the SIP(N)–SI(M) model on $[0, \ell]$ more evident. As a result, N should not be greater than 4.67×10^7, in accordance with the limitations of Lemma 2.1.

Figure 2.2 shows the simulation of the model predictions for real-world malaria cases. The predicted parameter values, biological descriptions, and pertinent references are displayed in the table below.

Parameter	Interpretation	Baseline Value	Reference
Λ	Recruitment rate of human	0.022818	Estimated [72]
$S_N(0)$	Initial number of S_N	$30\,773\,545$	Calculated
$I_N(0)$	Initial number of I_N	541	[71]
$P_N(0)$	Initial number of P_N	535	Assumed
$S_M(0)$	Initial number of S_M	$288\,232$	Assumed
$I_M(0)$	Initial number of I_M	$19\,310$	Assumed
β	Rate of transmission from I_M to S_N	0.294482673	Fitted
δ	Immunity loss rate of humans	$0,0314446765$	Fitted
κ	Immunity acquisition rate of humans	$0,512191861$	Fitted
λ	Recruitment rate of mosquito	0.104576629	Fitted
γ	Rate of transmission from I_N to S_M	0.126616512	Fitted
υ	Natural death rate of mosquitoes	0.456197917	Fitted
μ	Natural death rate of humans	0.0046818	Estimated [72]

Table 2.2: Parameters and initial data of the SIP(N)–SI(M) model.

The basic reproduction number in this case is:

$$\mathfrak{Rb} \simeq 0.4203 < 1.$$

Moreover, following Theorem 2.2, if we choose $0.79 \leq \alpha \leq 1$, then SIP(N)–SI(M) model admits a unique solution on $[0, \ell]$, with

$$\ell < 1.8083 \text{ (unit)}.$$

As malaria statistics are collected annually or over several months, we chose a unit of 20 years. In this context, the value of ℓ should not exceed 36 years.

Figure 2.2 presents a chronological table spanning 21 years (beginning in 2000) of confirmed malaria cases. This illustrates fluctuations in the number of infections, reflecting variations in the symptoms and disease severity. Additionally, the data revealed a notable increase in cases coinciding with the emergence of COVID-19.

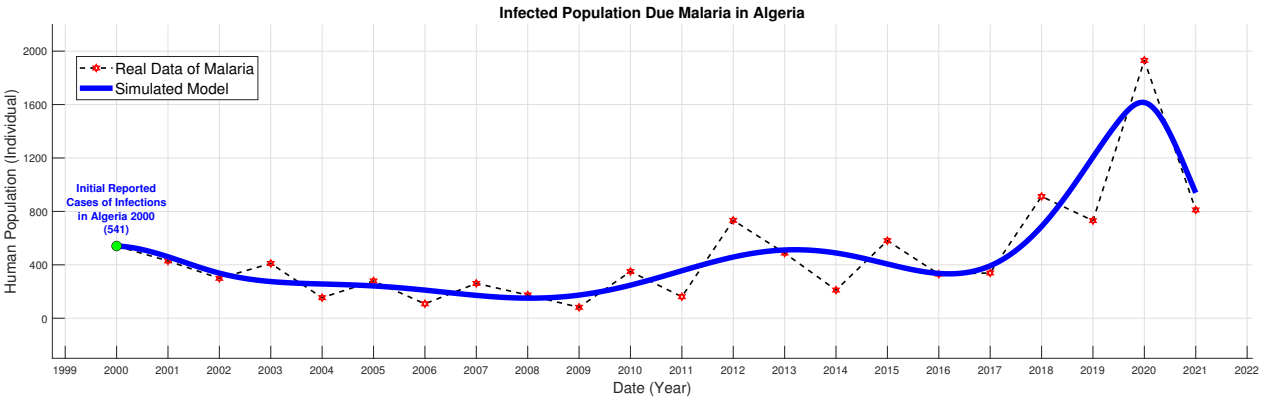

Figure 2.2: The reported cases of malaria in Algeria (shown with red markers) compared to the predicted cumulative infected cases provided by the proposed model (represented by blue line) for $\alpha = 0.79$.

In the context of Caputo's model, various values of α are examined to represent different scenarios or conditions. Figures 2.3 and 2.4 illustrate the simulation findings with the numerical results employed to analyze the dynamics of two human classes and two categories of mosquitoes.

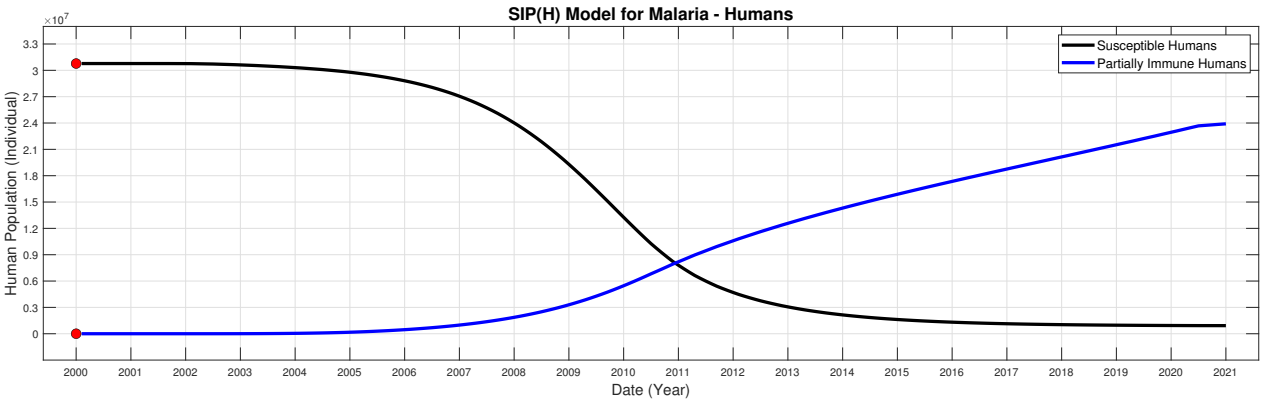

Figure 2.3: Numerical simulation results for the model for the human population.

It is essential to note that the SIP(N) model assumes a well-mixed population, homoge-

neous mixing, and constant parameters over time. However, it may not fully capture all aspects of disease transmission such as birth, death, or variations in immunity. Furthermore, the suitability of the SIP(N) model varies depending on the specific disease being modeled and the context of the outbreak.

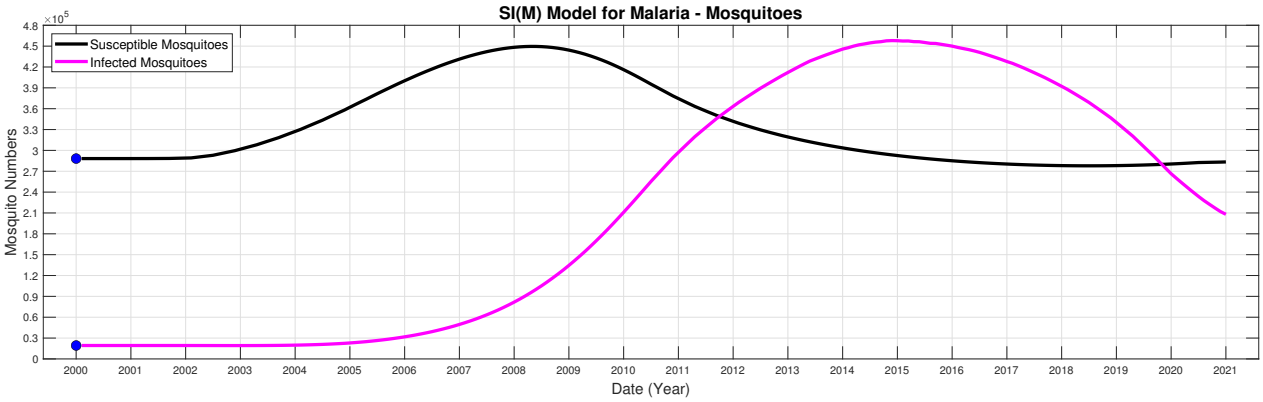

Figure 2.4: Numerical simulation results for the model for the mosquito population.

Next, we demonstrate the behavior of the fractional system (2.1) using four specific values of $\alpha \in (0, 1]$. The simulation results of the model are presented in Figure 2.5, showing the dynamics of both human and mosquito populations over time for various values of α.

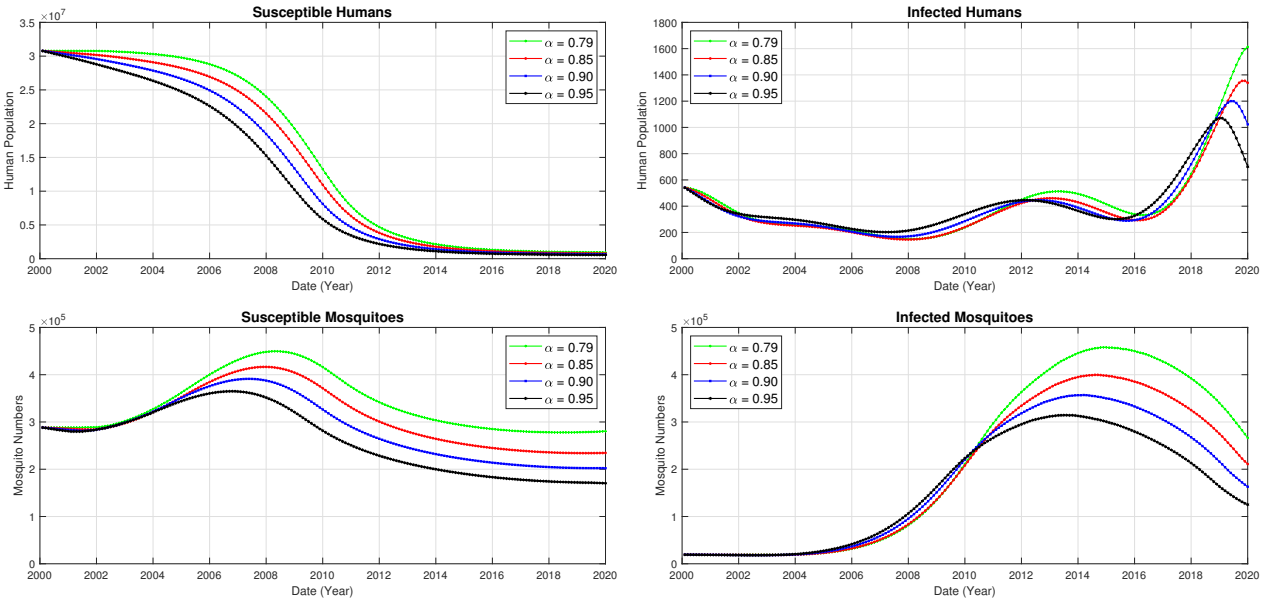

Figure 2.5: The dynamics of Caputo's fractional model for various values of α and using the estimation parameters in Table 2.2.

The first graph shows the susceptible human populations from 2000 to 2020. As the

parameter α increases, the decline in the susceptible population accelerates, signifying a more rapid spread of the disease. This observation suggests that higher memory effects (corresponding to larger α values) lead to a swifter depletion of the susceptible human population, thereby intensifying disease transmission dynamics.

Moving to the second graph, we examine the infected human population during the same period. For lower α values, the infection peak experiences a delay, whereas higher α values cause the peak to manifest earlier and with greater intensity. This temporal shift in the infection peak for smaller α values provides a critical window for implementing intervention strategies that can mitigate the impact of the disease.

The third graph depicts the susceptible mosquito populations over time. Analogous to the human population, an increase in α results in a more rapid reduction in the number of susceptible mosquitoes. This behavior reflects the heightened transmission dynamics associated with larger α values.

These simulation results and accompanying graphs emphasize the pivotal role of the fractional-order parameter α in malaria transmission dynamics between humans and mosquitoes. Higher α values lead to rapid and intense disease spread, which affects human susceptibility and infection peaks. Conversely, smaller α values allow for delayed infection peaks, thereby creating an opportunity for early intervention. These insights underscore the significance of fractional models for understanding disease spread and optimizing public health strategies.

After the initial analysis, adjustments were made to the crucial parameter β, which represents the disease transmission rate among the infected individuals. Gradual and diverse modifications are applied to return to the initial baseline value, and the resulting impact on the populations of infected individuals is illustrated in Figure 2.6 for the fractional cases, specifically with $\alpha = 0.85$ and $\alpha = 0.95$.

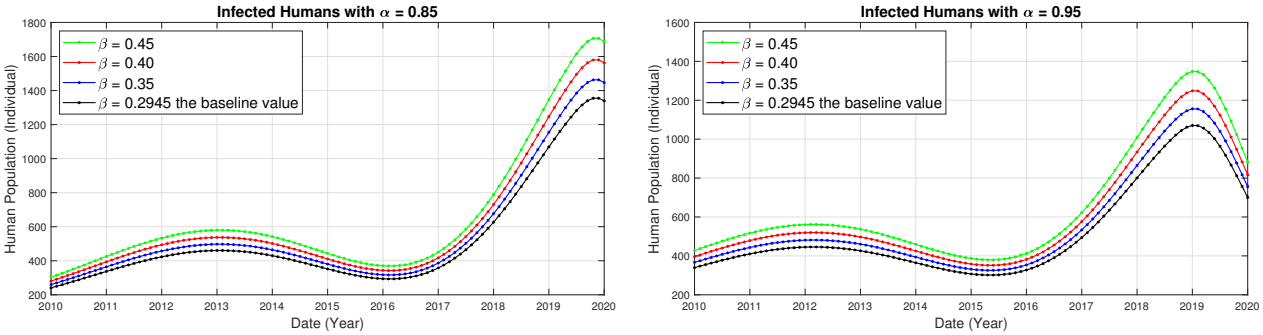

Figure 2.6: Impact of β on the infected population for different values of α with $\alpha = 0.85$, $\alpha = 0.95$ and using the estimation parameters in Table 2.2.

The graphical results reveal a pronounced reduction in the peaks of the infection curves within each population category as the contact rate β decreases. Notably, smaller values of the fractional parameter α correspond to a slower and more sustained disease spread, effectively capturing the memory effect inherent in the model. This biological interpretation underscores that increasing α accelerates disease transmission, whereas lower values delay the appearance of infection peaks, a behavior contingent upon the impact of preceding events.

Furthermore, our graphical analysis emphasizes the critical role of preventive measures. Neglecting interventions such as reducing human-mosquito contact, leads to a substantial increase in infections, facilitating a longer and swifter disease spread. Therefore, targeted efforts to minimize the contact between humans and mosquitoes should be central to intervention strategies. Implementing insecticides and medications to reduce mosquito populations significantly contributes to the maintenance of human population stability and curbing disease transmission.

2.4.3 Significance and Closing Remarks on Numerical Simulation

In Algeria, concerted efforts by authorities aim to raise public awareness about the critical importance of implementing safety measures to prevent malaria transmission. These preventive measures include targeted pesticide spraying in high-risk areas, distribution of treated mosquito bed nets for nocturnal protection, and provision of medications for treatment and prevention. Implementing these preventive strategies is pivotal for managing the spread of malaria as they effectively reduce the risk of infection and subsequent transmission.

In our mathematical model, these preventive measures directly impact the parameter β, which represents the rate of infection transmission from mosquitoes to humans. Our simulations explore how variations in this parameter influence disease progression and spread. Figures 2.5 and 2.6 illustrate how different values of the fractional-order parameter α affect the duration of the critical disease state, particularly the number of infected individuals. Specifically, $\alpha \in (0, 1)$ quantifies memory during epidemics. As α approaches zero, the system exhibits perfect memory, whereas approaching one signifies no memory. Notably, an increase in β leads to a rapid surge in the number of infected individuals, emphasizing that neglecting safety measures significantly accelerates disease spread.

A comparison of our results with those of recent studies employing traditional models reveals that the fractional-order model better captures the intricate dynamics of disease transmission, particularly in the context of malaria. Recent research utilizing fractional-order models has demonstrated their efficacy in providing more accurate epidemic predictions, especially when accounting for natural delays in transmission processes. Our model aligns with these findings, but introduces a novel dimension by explicitly considering the impact of memory on disease spread, an aspect overlooked in traditional models.

CHAPTER 3

DENGUE FEVER DYNAMICS USING ADVANCED MATHEMATICAL APPROACHES

This chapter presents a traditional mathematical model for studying the dynamics of dengue fever, focusing on environmental factors and their impact on the rate of disease transmission.

3.1 Introduction

Dengue fever is one of the most widespread viral diseases transmitted by mosquitoes globally, threatening the lives of millions in over 100 countries, particularly in the tropical and subtropical regions. The virus that causes dengue fever is primarily transmitted through the bite of Aedes aegypti or Aedes albopictus mosquitoes, which thrive in humid urban environments. The main symptoms of this disease include a high fever, headache, and muscle and joint pain. In severe cases, the disease can lead to dengue hemorrhagic fever or shock syndrome, which can be fatal if not properly treated [82].

Dengue fever presents an escalating global health challenge, with the World Health Organization (WHO) estimating approximately 390 million infections annually, 96 million of which are symptomatic [82]. The rapid spread of this disease can be attributed to multiple factors, including rapid urbanization, increased population density in cities, and climate change, which expands the habitat of virus-carrying mosquitoes. Therefore, finding innovative solutions to curb the spread of this disease through preventive measures or effective health strategies is of utmost importance [65].

In the epidemic dynamics discussed in this chapter, we divide the total human population (denoted as N) into four distinct classes:

- S_N: Susceptible individuals.
- I_N: Infected individuals.
- H_N: Hospitalized individuals.
- R_N: Recovered individuals.

Additionally, the mosquito population surrounding the human population (denoted as M) is divided into:

- S_M: Susceptible mosquitoes.
- E_M: Exposed mosquitoes.
- I_M: Infected mosquitoes.

The parameters of the SIHR(N)–SEI(M) model are defined as follows:

- Λ: Rate of increase in susceptible individuals.
- λ: Rate of increase in susceptible mosquitoes.
- $\mu < \Lambda$: Natural death rate for humans.
- $\upsilon < \lambda$: Natural death rate of mosquitoes.
- θ: Rate of death due to disease infection in I_N. Dengue-induced mortality in I_N.
- β: Probability rate of disease transmission from I_M to S_N.
- γ: Probability rate of disease transmission from I_N to S_M.
- κ: Immunity loss rate for humans.
- p: Transfer rate of humans from I_N to T_N.
- q and τ: Recovery rates from infectious populations I_N and T_N, respectively.
- δ: Infection rate of mosquitoes.

Motivated by the above-mentioned works, we propose the following system of ordinary differential equations for $0 \leq t \leq \ell < \infty$:

$$\begin{cases} \dfrac{dS_N(t)}{dt} &= \Lambda N(t) + \kappa R_N(t) - \left(\dfrac{\beta I_M(t)}{M(t)} + \mu\right) S_N(t) \\ \dfrac{dI_N(t)}{dt} &= \dfrac{\beta I_M(t)}{M(t)} S_N(t) - (p+q+\theta+\mu) I_N(t) \\ \dfrac{dH_N(t)}{dt} &= pI_N(t) - (\tau+\mu) H_N(t) \\ \dfrac{dR_N(t)}{dt} &= qI_N(t) + \tau H_N(t) - (\kappa+\mu) R_N(t) \\ \dfrac{dS_M(t)}{dt} &= \lambda M(t) - \left(\dfrac{\gamma I_N(t)}{N(t)} + \upsilon\right) S_M(t) \\ \dfrac{dE_M(t)}{dt} &= \dfrac{\gamma I_N(t)}{N} S_M(t) - (\delta+\upsilon) E_M(t) \\ \dfrac{dI_M(t)}{dt} &= \delta E_M(t) - \upsilon I_M(t). \end{cases} \tag{3.1}$$

In system (3.1), the first four equations represent the human population dynamics, whereas the last three equations describe the mosquito population dynamics.

To better understand the transmission dynamics of infectious diseases between humans and mosquitoes in the SIHR(N)–SEI(M) model (3.1), we refer to the following chart:

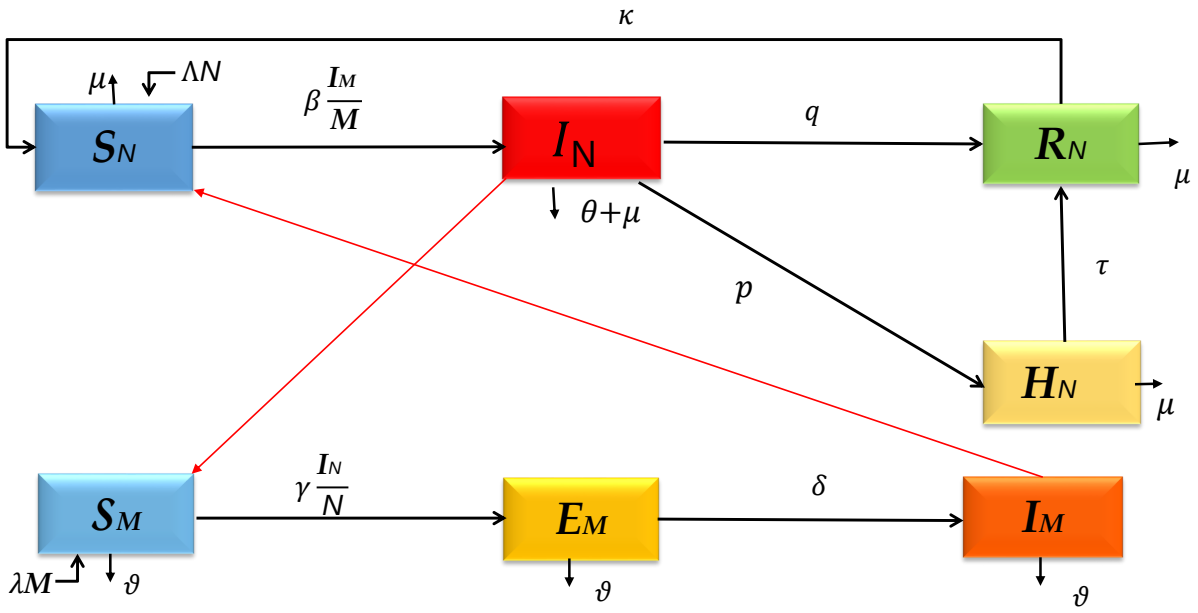

Figure 3.1: Flowchart of SIHR(N)–SEI(M).

This chapter aims to provide a comprehensive understanding of the dynamics of dengue fever transmission and its influencing factors. We begin by analyzing the behavior of the SIHR(H)–SEI(M) mathematical model to apply it after that in studying recent health data from a range of countries. This analysis allows us to identify the effective application domains of the model and assess the behavior of the disease spread across diverse environments.

We then chapter the existence and uniqueness of the solutions using Banach's fixed-point theory, ensuring that the solutions provided by the model are sustainable and applicable in various contexts. The basic reproduction number, $\mathfrak{Rb}$, is a vital indicator for assessing dengue fever transmission, helping us understand disease spread rates, and identifying points where effective control measures can be implemented.

Additionally, we explore the equilibrium points within the model and analyze their stability to guide disease control strategies and predict future trends. We validate the accuracy of our model using real data from multiple countries and identify specific local factors that contribute to the spread of dengue fever. This validation process enhances the

precision of the model and aids the development of targeted and effective strategies for disease control.

3.2 Dynamic Analysis of the Feasible Region

3.2.1 Positivity and Boundedness of the Model

The SIHR(N)–SEI(M) model (3.1) is investigated within a biologically feasible region in $\mathbb{R}^7_+$, as defined in the subsequent lemma.

Lemma 3.1. *Assume that M_0 represents the initial total mosquito population, and let N_0 be the initial total human population at $t = 0$, where $0 \leq t \leq \ell < \infty$. Consequently, the solution to the considered model is confined to the feasible region, given by*

$$\Omega = \left\{(S_N, I_N, H_N, R_N, S_M, E_M, I_M) \in \mathbb{R}^7_+ : 0 \leq N(t) \leq N_0 \exp\left((\Lambda - \mu)\ell\right),\ 0 \leq M(t) \leq M_0 \exp(\lambda\ell)\right\}$$

with

$$N(t) = S_N(t) + I_N(t) + H_N(t) + R_N(t), \qquad M(t) = S_M(t) + E_M(t) + I_M(t).$$

Proof. Let

$$N(t) = S_N(t) + I_N(t) + H_N(t) + R_N(t),$$

then

$$\frac{dN(t)}{dt} = \frac{dS_N(t)}{dt} + \frac{dI_N(t)}{dt} + \frac{dH_N(t)}{dt} + \frac{dR_N(t)}{dt}.$$

Now, summing all the human equations of (3.1), we get

$$\begin{aligned} \frac{dN(t)}{dt} &= (\Lambda - \mu) N(t) - \theta I_N(t) \\ &\leq (\Lambda - \mu) N(t). \end{aligned}$$

Consequently,

$$N(t) \leq N_0 + \int_0^t (\Lambda - \mu) N(\tau)\, d\tau.$$

Applying Gronwall lemma [23], we obtain

$$N(t) \leq N_0 \exp\left((\Lambda - \mu)\ell\right),$$

where N_0 is the total human population at $t = 0$.
In another way, let

$$M(t) = S_M(t) + E_M(t) + I_M(t),$$

then

$$\frac{dM(t)}{dt} = \frac{dS_M(t)}{dt} + \frac{dE_M(t)}{dt} + \frac{dI_M(t)}{dt}.$$

Now, summing all the mosquitoes equations of (3.1), we obtain

$$\begin{aligned} \frac{dM(t)}{dt} &= (\lambda - \upsilon) M(t) \\ &\leq \lambda M(t). \end{aligned}$$

Or

$$M(t) \leq M_0 + \int_0^t \lambda M(\tau)\, d\tau.$$

Therefore,

$$M(t) \leq M_0 \exp(\lambda \ell),$$

where M_0 is the total mosquito population at $t = 0$. □

In subsequent sections of this chapter, we assume the existence of two positive constants:

$$\mathcal{N} \leq N_0 \exp((\Lambda - \mu)\ell), \qquad \mathcal{M} \leq M_0 \exp(\lambda \ell),$$

where the total human population N and mosquito population M remained fixed throughout the chapter period and can be expressed as $N(t) = \mathcal{N}$ and $M(t) = \mathcal{M}$. This assumption was made to normalize the SIHR(N)–SEI(M) model (3.1). Therefore, we put:

$$\begin{aligned} &\mathcal{S}(t) = \tfrac{S_N(t)}{\mathcal{N}}, \quad \mathcal{I}(t) = \tfrac{I_N(t)}{\mathcal{N}}, \quad \mathcal{H}(t) = \tfrac{H_N(t)}{\mathcal{N}}, \quad \mathcal{R}(t) = \tfrac{R_N(t)}{\mathcal{N}}, \\ &\mathcal{V}(t) = \tfrac{S_M(t)}{\mathcal{M}}, \quad \mathcal{E}(t) = \tfrac{E_M(t)}{\mathcal{M}}, \quad \mathcal{F}(t) = \tfrac{I_M(t)}{\mathcal{M}}, \end{aligned} \tag{3.2}$$

then we obtain

$$\begin{cases} \frac{d\mathcal{S}(t)}{dt} &= \Lambda + \kappa \mathcal{R}(t) - (\beta \mathcal{F}(t) + \mu)\mathcal{S}(t) \\ \frac{d\mathcal{I}(t)}{dt} &= \beta \mathcal{F}(t) S(t) - (p + q + \theta + \mu)\mathcal{I}(t) \\ \frac{d\mathcal{H}(t)}{dt} &= p\mathcal{I}(t) - (\tau + \mu)\mathcal{H}(t) \\ \frac{d\mathcal{R}(t)}{dt} &= q\mathcal{I}(t) + \tau \mathcal{H}(t) - (\kappa + \mu)\mathcal{R}(t) \\ \frac{d\mathcal{V}(t)}{dt} &= \lambda - (\gamma \mathcal{I}(t) + \upsilon)\mathcal{V}(t) \\ \frac{d\mathcal{E}(t)}{dt} &= \gamma \mathcal{I}(t)\mathcal{V}(t) - (\delta + \upsilon)\mathcal{E}(t) \\ \frac{d\mathcal{F}(t)}{dt} &= \delta \mathcal{E}(t) - \upsilon \mathcal{F}(t). \end{cases} \tag{3.3}$$

along with the positive initial conditions

$$\mathcal{S}(0) = \varphi_1,\ \mathcal{I}(0) = \varphi_2,\ \mathcal{H}(0) = \varphi_3,\ \mathcal{R}(0) = \varphi_4,\ \mathcal{V}(0) = \varphi_5,\ \mathcal{E}(0) = \varphi_6,\ \mathcal{F}(0) = \varphi_7. \tag{3.4}$$

3.2.2 Existence Results of Solutions for the Normalized Model

In this section, we explore the existence and uniqueness of solutions to problem (3.6)–(3.7) using Banach's fixed-point theorem.

Let $\varphi = (\mathcal{S}, \mathcal{I}, \mathcal{H}, \mathcal{R}, \mathcal{V}, \mathcal{E}, \mathcal{F}) \in \Omega$, where $\Omega = [C([0, \ell], [0, 1])]^7$ is a Banach space with

$$\|\varphi\|_{\Omega} = \max\left\{\|\mathcal{S}\|_{\infty}, \|\mathcal{I}\|_{\infty}, \|\mathcal{H}\|_{\infty}, \|\mathcal{R}\|_{\infty}, \|\mathcal{V}\|_{\infty}, \|\mathcal{E}\|_{\infty}, \|\mathcal{F}\|_{\infty}\right\}$$

and let $\psi = (\psi_1, \psi_2, \psi_3, \psi_4, \psi_5, \psi_6, \psi_7)$, be such that

$$\begin{cases} \psi_1(t, \varphi(t)) &= \Lambda - (\beta\mathcal{F}(t) + \mu)\mathcal{S}(t) + \kappa\mathcal{R}(t), \\ \psi_2(t, \varphi(t)) &= \beta\mathcal{F}(t)\mathcal{S}(t) - (p + q + \theta + \mu)\mathcal{I}(t), \\ \psi_3(t, \varphi(t)) &= p\mathcal{I}(t) - (\tau + \mu)\mathcal{H}(t), \\ \psi_4(t, \varphi(t)) &= q\mathcal{I}(t) + \tau\mathcal{H}(t) - (\kappa + \mu)\mathcal{R}(t), \\ \psi_5(t, \varphi(t)) &= \lambda - (\gamma\mathcal{I}(t) + \upsilon)\mathcal{V}(t), \\ \psi_6(t, \varphi(t)) &= \gamma\mathcal{I}(t)\mathcal{V}(t) - (\delta + \upsilon)\mathcal{E}(t), \\ \psi_7(t, \varphi(t)) &= \delta\mathcal{E}(t) - \upsilon\mathcal{F}(t). \end{cases} \tag{3.5}$$

It is evident that ψ is a continuous function.

Applying an integral to both sides of the system yields

$$\frac{d\varphi(t)}{dt} = \psi(t, \varphi(t)), \tag{3.6}$$

taking into account the conditions

$$\varphi(0) = \varphi_0 = (\varphi_1, \varphi_2, \varphi_3, \varphi_4, \varphi_5, \varphi_6, \varphi_7), \tag{3.7}$$

we obtain the following system of integral equations

$$\varphi(t) = \varphi_0 + \int_0^t \psi(\tau, \varphi(\tau))\, d\tau,$$

which is equivalent to the original problem (3.6)–(3.7).

Theorem 3.1. *Let $\beta, \gamma, \delta, \kappa, p, q, \tau, \theta, \upsilon, \mu, \ell \in \mathbb{R}_+$, be such that*

$$\eta = \max\{\beta + \mu, p + q + \theta + \mu, \tau + \mu, \kappa + \mu, \gamma + \upsilon, \delta + \upsilon\}.$$

If

$$\eta\ell < 1, \tag{3.8}$$

thus, there is a unique solution to problem (3.6)–(3.7) on $[0, \ell]$.

Proof. The proof begins with transformation of problem (3.6)–(3.7) into a fixed-point problem $\mathcal{T}\varphi(t) = \varphi(t)$, with

$$\mathcal{T}\varphi(t) = (\mathcal{T}_1\varphi(t), \mathcal{T}_2\varphi(t), \mathcal{T}_3\varphi(t), \mathcal{T}_4\varphi(t), \mathcal{T}_5\varphi(t), \mathcal{T}_6\varphi(t), \mathcal{T}_7\varphi(t))$$

and

$$\mathcal{T}\varphi(t) = \varphi_0 + \int_0^t \psi(\tau, \varphi(\tau))\, d\tau. \tag{3.9}$$

Observing that for $\varphi \in \Omega$, the operators $\mathcal{T}_i\varphi$ for $1 \leq i \leq 7$ are continuous.

Consequently, $\mathcal{T}\varphi$ is an element of Ω, with

$$\|\mathcal{T}\varphi\|_\Omega = \max_{1\leq i\leq 7} \|\mathcal{T}_i\varphi\|_\infty .$$

The equivalence between problems (3.6)–(3.7) and (3.9) implies that $\mathcal{T}$ includes fixed points for solving the aforementioned problem.

Let $\varphi, \omega \in \Omega$, then

$$|\mathcal{T}_i\varphi(t) - \mathcal{T}_i\omega(t)| \leq \int_0^t |\psi_i(\tau, \varphi(\tau)) - \psi_i(\tau, \omega(\tau))|\, d\tau, \ \forall i \in \overline{1,7}. \tag{3.10}$$

For all $t \in [0, \ell]$, we have

$$\begin{aligned}
|\psi_1(t, \varphi(t)) - \psi_1(t, \omega(t))| &= |\kappa(\mathcal{R}_\varphi(t) - \mathcal{R}_\omega(t)) - [(\beta\mathcal{F}_\varphi(t) + \mu)\mathcal{S}_\varphi(t) \\
&\quad - (\beta\mathcal{F}_\omega(t) + \mu)\mathcal{S}_\omega(t)]| \\
&\leq \kappa|\mathcal{R}_\varphi(t) - \mathcal{R}_\omega(t)| + \mu|\mathcal{S}_\varphi(t) - \mathcal{S}_\omega(t)| \\
&\quad + |\beta\mathcal{F}_\varphi(t)\mathcal{S}_\varphi(t) - \beta\mathcal{F}_\omega(t)\mathcal{S}_\omega(t)| \\
&\leq \kappa|\mathcal{R}_\varphi(t) - \mathcal{R}_\omega(t)| + (\beta + \mu)|\mathcal{S}_\varphi(t) - \mathcal{S}_\omega(t)| \\
&\quad + \beta|\mathcal{F}_\varphi(t) - \mathcal{F}_\omega(t)| \\
&\leq \max\{\kappa, \beta + \mu\}\|\varphi - \omega\|_\Omega .
\end{aligned} \tag{3.11}$$

Similarly, we obtain

$$\begin{aligned}
|\psi_2(t, \varphi(t)) - \psi_2(t, \omega(t))| &\leq \max\{\beta, p + q + \theta + \mu\}\|\varphi - \omega\|_\Omega , \\
|\psi_3(t, \varphi(t)) - \psi_3(t, \omega(t))| &\leq \max\{p, \tau + \mu\}\|\varphi - \omega\|_\Omega , \\
|\psi_4(t, \varphi(t)) - \psi_4(t, \omega(t))| &\leq \max\{p, q, \kappa + \mu\}\|\varphi - \omega\|_\Omega , \\
|\psi_5(t, \varphi(t)) - \psi_5(t, \omega(t))| &\leq (\gamma + \upsilon)\|\varphi - \omega\|_\Omega , \\
|\psi_6(t, \varphi(t)) - \psi_6(t, \omega(t))| &\leq \max\{\gamma, \delta + \upsilon\}\|\varphi - \omega\|_\Omega , \\
|\psi_7(t, \varphi(t)) - \psi_7(t, \omega(t))| &\leq \max\{\delta, \upsilon\}\|\varphi - \omega\|_\Omega .
\end{aligned}$$

Then,

$$|\psi_i(t,\varphi(t)) - \psi_i(t,\omega(t))| \leq \eta \|\varphi - \omega\|_\Omega, \ \forall i \in \overline{1,7}. \tag{3.12}$$

From (3.10), we find

$$\|\mathcal{T}_i\varphi - \mathcal{T}_i\omega\|_\infty \leq \eta\ell \|\varphi - \omega\|_\Omega, \ \forall i \in \overline{1,7}$$

and

$$\|\mathcal{T}\varphi - \mathcal{T}\omega\|_\Omega \leq \eta\ell \|\varphi - \omega\|_\Omega.$$

Referring to (3.8), $\mathcal{T}$ is considered a contraction operator. By employing Banach's Contraction Principle, it can be deduced that $\mathcal{T}$ possesses a unique fixed point, which corresponds to the unique solution of the problem (3.6)–(3.7) on $[0,\ell]$. □

3.2.3 Ulam-Hyers Stability for the Normalized Model

Definition 3.1. *The system of differential equations (3.6) is Ulam-Hyers stable if there exists a real number $c > 0$ such that for each $\varepsilon = \max\{\varepsilon_1,\ldots,\varepsilon_7\}$ with $\varepsilon_i > 0,\ i \in \overline{1,7}$, and for each solution $\omega \in \Omega$ of the inequality*

$$\left|\frac{d}{dt}\omega_i(t) - \psi_i(t,\omega(t))\right| \leq \varepsilon_i, \quad t \in [0,\ell],\ i \in \overline{1,7}, \tag{3.13}$$

there exists $\varphi \in \Omega$ a solution of (3.6) with

$$\|\omega - \varphi\|_\Omega \leq c\varepsilon.$$

Definition 3.2. *The system of differential equations (3.6) is generalized Ulam-Hyers stable if there exists $\xi \in C(\mathbb{R}_+,\mathbb{R}_+),\ \xi(0) = 0$, such that for each solution $\omega \in \Omega$ of inequality (3.13), there exists a solution $\varphi \in \Omega$ of (3.6) with*

$$\|\omega - \varphi\|_\Omega \leq \xi(\varepsilon).$$

Remark 3.1 ([24, 21])**.** *If $\omega \in \Omega$ is a solution of inequality (3.13), then there exist $(\varepsilon_i)_{i\in\overline{1,7}} > 0$ and $\phi \in \Omega$, such that*

1. $\frac{d}{dt}\omega_i(t) = \psi_i(t,\omega(t)) + \phi_i(t),\ t \in [0,\ell],\ i \in \overline{1,7}$,
2. $|\phi_i(t)| \leq \varepsilon_i$, *for all* $t \in [0,\ell]$, *and each* $i \in \overline{1,7}$.

The subsequent lemma aids in establishing the stability of system (3.6).

Lemma 3.2. *If $\omega \in \Omega$ is the solution of inequality (3.13), then there exist $(\varepsilon_i)_{i\in\overline{1,7}} > 0$ such that ω will be the solution of the inequality*

$$\left|\omega_i(t) - \omega_i(0) - \int_0^t \psi_i(\tau, \omega(\tau))\, d\tau\right| \leq \ell\varepsilon_i,$$

for each $i \in \overline{1,7}$.

Proof. If ω is a solution of (3.13), we have from Remark 3.1

$$\begin{cases} \frac{d}{dt}\omega_i(t) = \psi_i(t, \omega(t)) + \phi_i(t), & t \in [0,\ell],\ i \in \overline{1,7}, \\ |\phi_i(t)| \leq \varepsilon_i, & (\varepsilon_i)_{i\in\overline{1,7}} > 0, \end{cases}$$

hence

$$\omega_i(t) = \omega_i(0) + \int_0^t [\psi_i(\tau, \omega(\tau)) + \phi_i(\tau)]\, d\tau.$$

Also,

$$\begin{aligned} \left|\omega_i(t) - \omega_i(0) - \int_0^t \psi_i(\tau, \omega(\tau))\, d\tau\right| &= \left|\omega_i(0) + \int_0^t [\psi_i(\tau, \omega(\tau)) + \phi_i(\tau)]\, d\tau \right. \\ &\quad \left. - \omega_i(0) - \int_0^t \psi_i(\tau, \omega(\tau))\, d\tau\right| \\ &\leq \int_0^t |\phi_i(\tau)|\, d\tau \leq \ell\varepsilon_i, \quad \forall i \in \overline{1,7}. \end{aligned}$$

That establishes the lemma. □

Theorem 3.2. *Assuming that (3.8) holds, system (3.6) is Ulam-Hyers stable. Furthermore, it can also be asserted that (3.6) is a generalized Ulam-Hyers stable system.*

Proof. Let $(\varepsilon_i)_{i\in\overline{1,7}} > 0$, we define $\omega \in \Omega$ as a solution of the inequality

$$\left|\frac{d}{dt}\omega_i(t) - \psi_i(t, \omega(t))\right| \leq \varepsilon_i, \quad t \in [0,\ell],\ i \in \overline{1,7},$$

and $\varphi \in \Omega$ is the unique solution of system (3.6) with the conditions

$$\varphi_i(0) = \omega_i(0), \quad \forall i \in \overline{1,7}.$$

Then

$$\varphi_i(t) = \omega_i(0) + \int_0^t \psi_i(\tau, \varphi(\tau))\, d\tau,$$

and

$$\begin{aligned}|\omega_i(t)-\varphi_i(t)| &= \left|\omega_i(t)-\omega_i(0)-\int_0^t \psi_i(\tau,\varphi(\tau))\,d\tau\right| \\ &\leq \left|\omega_i(t)-\omega_i(0)-\int_0^t \psi_i(\tau,\omega(\tau))\,d\tau\right| \\ &\quad+\int_0^t |\psi_i(\tau,\omega(\tau))-\psi_i(\tau,\varphi(\tau))|\,d\tau.\end{aligned}$$

Using (3.12), and Lemma 3.2, we get

$$|\omega_i(t)-\varphi_i(t)| \leq \ell\left(\varepsilon_i+\eta\|\varphi-\omega\|_\Omega\right), \quad \forall t\in[0,\ell],\ \forall i\in\overline{1,7}.$$

Taking the maximum from both sides, we obtain

$$\|\varphi-\omega\|_\Omega \leq \ell\left(\varepsilon+\eta\|\varphi-\omega\|_\Omega\right).$$

Thus

$$\|\varphi-\omega\|_\Omega \leq c\varepsilon,$$

where $c=\frac{\ell}{1-\eta\ell}$. This implies that system (3.6) is stable in the Ulam-Hyers sense and is consequently generalized Ulam-Hyers stable if we set $\xi(t)=ct$. □

3.3 Analysis for the SIHR(N)–SEI(M) Model

3.3.1 Basic Reproduction Number and Equilibrium Points

Theorem 3.3. *The basic reproduction number of system (3.3) is determined by*

$$\mathfrak{Rb}=\sqrt{\frac{\beta\gamma\delta\lambda\Lambda}{\mu\upsilon^2(\delta+\upsilon)(p+q+\theta+\mu)}}. \tag{3.14}$$

Proof. Because the SIHR(N)–SEI(M) model is composed of infection components $\mathcal{I}$, $\mathcal{H}$, $\mathcal{E}$, and $\mathcal{F}$, we obtain:

$$y_i-z_i=\begin{pmatrix}\beta\mathcal{F}\mathcal{S}-(p+q+\theta+\mu)\mathcal{I}\\ p\mathcal{I}-(\tau+\mu)\mathcal{H}\\ \gamma\mathcal{I}\mathcal{V}(t)-(\delta+\upsilon)\mathcal{E}\\ \delta\mathcal{E}-\upsilon\mathcal{F}\end{pmatrix}.$$

Accordingly,

$$y_i = \begin{pmatrix} \beta\mathcal{F}\mathcal{S} \\ 0 \\ \gamma\mathcal{I}\mathcal{V} \\ 0 \end{pmatrix}, \; z_i = \begin{pmatrix} (p+q+\theta+\mu)\,\mathcal{I} \\ -p\mathcal{I} + (\tau+\mu)\,\mathcal{H} \\ (\delta+\upsilon)\,\mathcal{E} \\ -\delta\mathcal{E} + \upsilon\mathcal{F} \end{pmatrix}.$$

Here, y_i denotes the rate of new infections appearing in compartment i, and z_i denotes the rate of transitions between compartment i and other infected compartments for each $i \in \{1, 2, 3, 4\}$.

The new infection matrix $\mathcal{Y}$ and transition matrix $\mathcal{Z}$ are assessed at the disease-free equilibrium point $\mathfrak{Dfp}$ (Theorem 3.4), as follows:

$$\mathcal{Y} = \begin{pmatrix} 0 & 0 & 0 & \beta\bar{\mathcal{S}} \\ 0 & 0 & 0 & 0 \\ \gamma\bar{\mathcal{V}} & 0 & 0 & 0 \\ 0 & 0 & 0 & 0 \end{pmatrix}, \; \mathcal{Z} = \begin{pmatrix} p+q+\theta+\mu & 0 & 0 & 0 \\ -p & \tau+\mu & 0 & 0 \\ 0 & 0 & \delta+\upsilon & 0 \\ 0 & 0 & -\delta & \upsilon \end{pmatrix}.$$

Following the next-generation matrix principle, the basic reproduction number is defined as the spectral radius of matrix $\mathcal{Y}\mathcal{Z}^{-1}$ and is given by (3.14). □

The initial step in comprehending a differential equation is to identify equilibrium points. In epidemiology, we are concerned with two types of equilibrium point:

- Disease-free equilibrium is defined as the point at which no disease (or death from disease) is introduced into the population and is depicted in the model as $\mathcal{I} = \mathcal{H} = \mathcal{E} = \mathcal{F} = 0$.
- Other equilibrium points, where $\mathcal{I} \neq 0$, $\mathcal{H} \neq 0$, and $\mathcal{F} \neq 0$, are indicated as endemic equilibrium points (or outbreak equilibrium points).

We define the positive real values

$$\begin{aligned} \lambda_1 &= p+q+\theta+\mu, & \lambda_2 &= \tau+\mu, \\ \lambda_3 &= \kappa+\mu, & \lambda_4 &= \delta+\upsilon, \end{aligned}$$

to facilitate the calculations and establish the following theorem.

Theorem 3.4. *System (3.3) has two types of equilibrium points*

1. *Disease-free equilibrium*

$$\mathfrak{Dfp} = (\bar{\mathcal{S}}, \bar{\mathcal{I}}, \bar{\mathcal{T}}, \bar{\mathcal{R}}, \bar{\mathcal{V}}, \bar{\mathcal{E}}, \bar{\mathcal{F}}) = \left(\frac{\Lambda}{\mu}, 0, 0, 0, \frac{\lambda}{\upsilon}, 0, 0\right).$$

2. *Endemic equilibrium point* $E_2 = (\mathcal{S}^*, \mathcal{I}^*, \mathcal{H}^*, \mathcal{R}^*, \mathcal{V}^*, \mathcal{E}^*, \mathcal{F}^*)$ *which is*

$$\mathfrak{Eqp} = \left(\mathcal{S}^*, \mathcal{I}^*, \frac{p}{\lambda_2}\mathcal{I}^*, \frac{q\lambda_2 + \tau p}{\lambda_2\lambda_3}\mathcal{I}^*, \frac{\lambda}{\gamma\mathcal{I}^* + \upsilon}, \frac{\lambda\gamma\mathcal{I}^*}{\lambda_4\left(\gamma\mathcal{I}^* + \upsilon\right)}, \frac{\gamma\delta\lambda\mathcal{I}^*}{\upsilon\lambda_4\left(\gamma\mathcal{I}^* + \upsilon\right)}\right),$$

where

$$\mathcal{S}^* = \bar{\mathcal{S}} - \frac{\mu\left(\lambda_1\lambda_2 + \kappa\left(p + \theta + \mu\right)\right) + \kappa\tau\left(\theta + \mu\right)}{\mu\lambda_2\lambda_3}\mathcal{I}^*,$$

also

$$\mathcal{I}^* = \frac{\mu\upsilon^2\lambda_1\lambda_2\lambda_3\lambda_4}{\gamma\upsilon\lambda_1\lambda_2\lambda_3\lambda_4 + \kappa\tau\left(\theta + \mu\right) + \mu\left(\lambda_1\lambda_2 + \kappa\left(p + \theta + \mu\right)\right)}\left(\mathfrak{Rb}^2 - 1\right),$$

The existence of the endemic equilibrium point depends on $\mathfrak{Rb} > 1$.

Proof. To determine the equilibrium points for system (3.3), we set $\frac{d\varphi\left(t\right)}{dt} = \vec{0}$, with $\varphi = (\mathcal{S}, \mathcal{I}, \mathcal{H}, \mathcal{R}, \mathcal{V}, \mathcal{E}, \mathcal{F})$. Therefore

$$\begin{cases} 0 = \Lambda + \kappa\mathcal{R}\left(t\right) - \left(\beta\mathcal{F}\left(t\right) + \mu\right)\mathcal{S}\left(t\right), & (eq1) \\ 0 = \beta\mathcal{F}\left(t\right)\mathcal{S}\left(t\right) - \lambda_1\mathcal{I}\left(t\right), & (eq2) \\ 0 = p\mathcal{I}\left(t\right) - \lambda_2\mathcal{H}\left(t\right), & (eq3) \\ 0 = q\mathcal{I}\left(t\right) + \tau\mathcal{V}\left(t\right) - \lambda_3\mathcal{R}\left(t\right), & (eq4) \\ 0 = \lambda - \left(\gamma\mathcal{I}\left(t\right) + \upsilon\right)\mathcal{V}\left(t\right), & (eq5) \\ 0 = \gamma\mathcal{I}\left(t\right)\mathcal{V}\left(t\right) - \lambda_4\mathcal{E}\left(t\right), & (eq6) \\ 0 = \delta\mathcal{E}\left(t\right) - \upsilon\mathcal{F}\left(t\right), & (eq7) \end{cases}$$

From equations $(eq3)$ and $(eq5)$, we have

$$\mathcal{H}\left(t\right) = \frac{p}{\lambda_2}\mathcal{I}\left(t\right) \quad \text{and} \quad \mathcal{V}\left(t\right) = \frac{\lambda}{\gamma\mathcal{I}\left(t\right) + \upsilon}.$$

then we replace it in $(eq4)$, $(eq6)$, and $(eq7)$, to get

$$\mathcal{R}\left(t\right) = \frac{q\lambda_2 + \tau p}{\lambda_2\lambda_3}\mathcal{I}\left(t\right), \qquad \mathcal{E}\left(t\right) = \frac{\lambda\gamma\mathcal{I}\left(t\right)}{\lambda_4\left(\gamma\mathcal{I}\left(t\right) + \upsilon\right)}, \qquad \mathcal{F}\left(t\right) = \frac{\gamma\delta\lambda\mathcal{I}\left(t\right)}{\upsilon\lambda_4\left(\gamma\mathcal{I}\left(t\right) + \upsilon\right)}.$$

If we add $(eq1)$ to $(eq2)$ we obtain

$$\mathcal{S}\left(t\right) = \bar{\mathcal{S}} - \frac{\mu\left(\lambda_1\lambda_2 + \kappa\left(p + \theta + \mu\right)\right) + \kappa\tau\left(\theta + \mu\right)}{\mu\lambda_2\lambda_3}\mathcal{I}\left(t\right),$$

1. If $\mathcal{I} = 0$, we can easily obtain the first disease-free equilibrium point $\mathfrak{Dfp}$.

2. When $\mathcal{I} \neq 0$, equation $(eq2)$ gives us

$$\mathcal{I}^* = \frac{\mu\upsilon^2\lambda_1\lambda_2\lambda_3\lambda_4}{\gamma\upsilon\lambda_1\lambda_2\lambda_3\lambda_4 + \kappa\tau\left(\theta + \mu\right) + \mu\left(\lambda_1\lambda_2 + \kappa\left(p + \theta + \mu\right)\right)}\left(\mathfrak{Rb}^2 - 1\right).$$

Consequently, we obtain the required endemic equilibrium point $\mathfrak{Eqp}$, which exists when $\mathfrak{Rb} > 1$.

Hence, the theorem is proven. □

3.3.2 Stability Study of Disease-Free Equilibrium Point

Local Stability Analysis of $\mathfrak{Dfp}$

Theorem 3.5. *The disease-free equilibrium point of system (3.3) is locally asymptotically stable when* $\mathfrak{Rb} < 1$.

Proof. The Jacobian matrix for system (3.3) can be written as

$$J = \begin{pmatrix} \frac{\partial \psi_1}{\partial \mathcal{S}} & \frac{\partial \psi_1}{\partial \mathcal{I}} & \frac{\partial \psi_1}{\partial \mathcal{H}} & \frac{\partial \psi_1}{\partial \mathcal{R}} & \frac{\partial \psi_1}{\partial \mathcal{V}} & \frac{\partial \psi_1}{\partial \mathcal{E}} & \frac{\partial \psi_1}{\partial \mathcal{F}} \\ \frac{\partial \psi_2}{\partial \mathcal{S}} & \frac{\partial \psi_2}{\partial \mathcal{I}} & \frac{\partial \psi_2}{\partial \mathcal{H}} & \frac{\partial \psi_2}{\partial \mathcal{R}} & \frac{\partial \psi_2}{\partial \mathcal{V}} & \frac{\partial \psi_2}{\partial \mathcal{E}} & \frac{\partial \psi_2}{\partial \mathcal{F}} \\ \frac{\partial \psi_3}{\partial \mathcal{S}} & \frac{\partial \psi_3}{\partial \mathcal{I}} & \frac{\partial \psi_3}{\partial \mathcal{H}} & \frac{\partial \psi_3}{\partial \mathcal{R}} & \frac{\partial \psi_3}{\partial \mathcal{V}} & \frac{\partial \psi_3}{\partial \mathcal{E}} & \frac{\partial \psi_3}{\partial \mathcal{F}} \\ \frac{\partial \psi_4}{\partial \mathcal{S}} & \frac{\partial \psi_4}{\partial \mathcal{I}} & \frac{\partial \psi_4}{\partial \mathcal{H}} & \frac{\partial \psi_4}{\partial \mathcal{R}} & \frac{\partial \psi_4}{\partial \mathcal{V}} & \frac{\partial \psi_4}{\partial \mathcal{E}} & \frac{\partial \psi_4}{\partial \mathcal{F}} \\ \frac{\partial \psi_5}{\partial \mathcal{S}} & \frac{\partial \psi_5}{\partial \mathcal{I}} & \frac{\partial \psi_5}{\partial \mathcal{H}} & \frac{\partial \psi_5}{\partial \mathcal{R}} & \frac{\partial \psi_5}{\partial \mathcal{V}} & \frac{\partial \psi_5}{\partial \mathcal{E}} & \frac{\partial \psi_5}{\partial \mathcal{F}} \\ \frac{\partial \psi_6}{\partial \mathcal{S}} & \frac{\partial \psi_6}{\partial \mathcal{I}} & \frac{\partial \psi_6}{\partial \mathcal{H}} & \frac{\partial \psi_6}{\partial \mathcal{R}} & \frac{\partial \psi_6}{\partial \mathcal{V}} & \frac{\partial \psi_6}{\partial \mathcal{E}} & \frac{\partial \psi_6}{\partial \mathcal{F}} \\ \frac{\partial \psi_7}{\partial \mathcal{S}} & \frac{\partial \psi_7}{\partial \mathcal{I}} & \frac{\partial \psi_7}{\partial \mathcal{H}} & \frac{\partial \psi_7}{\partial \mathcal{R}} & \frac{\partial \psi_7}{\partial \mathcal{V}} & \frac{\partial \psi_7}{\partial \mathcal{E}} & \frac{\partial \psi_7}{\partial \mathcal{F}} \end{pmatrix}$$

where $\psi_{1\leq i\leq 7}\left(t,\varphi\left(t\right)\right)$ represents the right-hand side of (3.3). Then

$$J = \begin{pmatrix} -\left(\beta\mathcal{F}+\mu\right) & 0 & 0 & \kappa & 0 & 0 & -\beta\mathcal{S} \\ \beta\mathcal{F} & -\lambda_1 & 0 & 0 & 0 & 0 & \beta\mathcal{S} \\ 0 & p & -\lambda_2 & 0 & 0 & 0 & 0 \\ 0 & q & \tau & -\lambda_3 & 0 & 0 & 0 \\ 0 & -\gamma\mathcal{V} & 0 & 0 & -\left(\gamma\mathcal{I}+\upsilon\right) & 0 & 0 \\ 0 & \gamma\mathcal{V} & 0 & 0 & \gamma\mathcal{I} & -\lambda_4 & 0 \\ 0 & 0 & 0 & 0 & 0 & \delta & -\upsilon \end{pmatrix}.$$

The eigenvalues of $J\left(\mathfrak{Dfp}\right)$ are given as the roots of the characteristic polynomial

$$\begin{aligned} P_1\left(X\right) = &-\left(\mu+X\right)\left(\upsilon+X\right)\left(\lambda_2+X\right)\left(\lambda_3+X\right)\left[X^3+\left(\lambda_1+\lambda_4+\upsilon\right)X^2\right. \\ &\left.+\left(\lambda_1\lambda_4+\upsilon\lambda_1+\upsilon\lambda_4\right)X+\upsilon\lambda_1\lambda_4\left(1-\mathfrak{Rb}^2\right)\right]. \end{aligned}$$

According to Descartes' rule, the roots of $P_1\left(X\right)$ are negative reals or complexes of negative real parts, which makes $\mathfrak{Dfp}$ locally asymptotically stable. □

Global Stability Analysis of $\mathfrak{Dfp}$

Theorem 3.6. *The disease-free equilibrium point* $\mathfrak{Dfp}$ *of system (3.3) is globally asymptotically stable if* $\mathfrak{Rb} < 1$.

Proof. To prove the theorem, we examine the following Lyapunov function

$$W(\mathcal{S},\mathcal{I},\mathcal{H},\mathcal{R},\mathcal{V},\mathcal{E},\mathcal{F}) = c_1\mathcal{I} + c_2\mathcal{H} + c_3\mathcal{E} + c_4\mathcal{F}.$$

We consider c_i to be positive constants for $i \in \{1,2,3,4\}$, which will be determined later. The derivative of W along with the solution of system (3.3) is calculated as follows:

$$\begin{aligned}
\frac{dW}{dt} &= c_1\frac{d\mathcal{I}}{dt} + c_2\frac{d\mathcal{H}}{dt} + c_3\frac{d\mathcal{E}}{dt} + c_4\frac{d\mathcal{F}}{dt} \\
&= c_1\left[\beta\mathcal{F}\mathcal{S} - \lambda_1\mathcal{I}\right] + c_2\left[p\mathcal{I} - \lambda_2\mathcal{H}\right] + c_3\left[\gamma\mathcal{I}\mathcal{V} - \lambda_4\mathcal{E}\right] \\
&+ c_4\left[\delta\mathcal{E} - \upsilon\mathcal{F}\right] \\
&\leq c_1\left[\frac{\beta\Lambda}{\mu}\mathcal{F} - \lambda_1\mathcal{I}\right] + c_2\left[p\mathcal{I} - \lambda_2\mathcal{H}\right] + c_3\left[\frac{\gamma\lambda}{\upsilon}\mathcal{I} - \lambda_4\mathcal{E}\right] \\
&+ c_4\left[\delta\mathcal{E} - \upsilon\mathcal{F}\right] \\
&= \left[-c_1\lambda_1 + c_2p + c_3\frac{\gamma\lambda}{\upsilon}\right]\mathcal{I} - c_2\lambda_2\mathcal{H} \\
&+ \left[-c_3\lambda_4 + c_4\delta\right]\mathcal{E} + \left[c_1\frac{\beta\Lambda}{\mu} - c_4\upsilon\right]\mathcal{F}.
\end{aligned}$$

By choosing $c_1 = \upsilon\lambda_4$, $c_2 = 0$, $c_3 = \frac{\beta\delta\Lambda}{\mu}$, and $c_4 = \frac{\beta\Lambda\lambda_4}{\mu}$, we obtain

$$\frac{dW}{dt} \leq \upsilon\lambda_1\lambda_4\left(\mathfrak{Rb}^2 - 1\right)\mathcal{E}.$$

Thus, if $\mathfrak{Rb} < 1$, then $\frac{dW}{dt} < 0$. According to LaSalle's invariance principle [58], this implies that $\mathfrak{Dfp}$ is globally asymptotically stable. □

3.3.3 Stability Study of Endemic Equilibrium Point

Local Stability Analysis of $\mathfrak{Eqp}$

Let g_0, g_1, g_2, and g_3 be such that

$$\begin{aligned}
g_0 &= \frac{\lambda_4\left(\gamma\mathcal{I}^* + \upsilon\right)\left(\mu\lambda_1\lambda_2\lambda_3 + \beta\mathcal{F}^*\lambda_9\right)}{\mu\lambda_2\lambda_3}, \\
g_1 &= \frac{\left(\gamma\mathcal{I}^* + \upsilon\right)\left(\mu\lambda_7 + \beta\mathcal{F}^*\left[\lambda_{10} + \mu p\left(\lambda_2 + \kappa\right) + \lambda_2\left(\mu q + \lambda_3\left(\theta + \mu\right)\right)\right]\right)}{\mu\lambda_2 + \mu\lambda_3 + \lambda_2\lambda_3} \\
&\quad + \frac{\lambda_1\lambda_2\lambda_3\lambda_4\left(\gamma\mathcal{I}^* + \upsilon + \mu\right) + \beta\mathcal{F}^*\lambda_4\lambda_9}{\mu\lambda_2 + \mu\lambda_3 + \lambda_2\lambda_3}, \\
g_2 &= \frac{\lambda_1\lambda_2\lambda_3\lambda_4 + \lambda_7\left(\gamma\mathcal{I}^* + \upsilon + \mu\right) + \left(\gamma\mathcal{I}^* + \upsilon\right)\left(\mu\lambda_6 + \beta\mathcal{F}^*\lambda_8\right) + \beta\mathcal{F}^*\left(\lambda_9 + \lambda_{10}\right)}{\mu + \lambda_2 + \lambda_3}, \\
g_3 &= \lambda_7 + \beta\mathcal{F}^*\lambda_8 + \lambda_5\left(\beta\mathcal{F}^* + \mu\right)\left(\gamma\mathcal{I}^* + \upsilon\right) + \lambda_6\left(\gamma\mathcal{I}^* + \upsilon + \mu\right),
\end{aligned}$$

where

$$\begin{aligned}
\lambda_5 &= \lambda_1+\lambda_2+\lambda_3+\lambda_4,\\
\lambda_6 &= \lambda_1\lambda_2+\lambda_1\lambda_3+\lambda_1\lambda_4+\lambda_2\lambda_3+\lambda_2\lambda_4+\lambda_3\lambda_4,\\
\lambda_7 &= \lambda_1\lambda_2\lambda_3+\lambda_1\lambda_2\lambda_4+\lambda_1\lambda_3\lambda_4+\lambda_2\lambda_3\lambda_4,\\
\lambda_8 &= \lambda_1\lambda_2+\lambda_1\lambda_4+\lambda_2\lambda_3+\lambda_2\lambda_4+\lambda_3\lambda_4+\lambda_3\left(p+\theta+\mu\right)+\mu q,\\
\lambda_9 &= \mu p\left(\lambda_3+\tau\right)+\lambda_2\left(\mu q+\lambda_3\left(\theta+\mu\right)\right),\\
\lambda_{10} &= \lambda_4\left(\lambda_1\lambda_2+\lambda_2\lambda_3+\lambda_3\left(p+\theta+\mu\right)+\mu q\right).
\end{aligned}$$

Theorem 3.7. *If we put*

$$\beta\gamma\delta\mathcal{V}^*\mathcal{S}^* < \min\left\{g_0, g_1, g_2, g_3\right\},$$

then the endemic equilibrium point $\mathfrak{Eqp}$ *of system (3.3) is locally asymptotically stable if* $\mathfrak{Rb} > 1$.

Proof. As shown in the previous section, the Jacobian matrix $J\left(\mathfrak{Eqp}\right)$ for (3.3) is

$$J_{E_2} = \begin{pmatrix}
-\left(\beta\mathcal{F}^*+\mu\right) & 0 & 0 & \kappa & 0 & 0 & -\beta\mathcal{S}^*\\
\beta\mathcal{F}^* & -\lambda_1 & 0 & 0 & 0 & 0 & \beta\mathcal{S}^*\\
0 & p & -\lambda_2 & 0 & 0 & 0 & 0\\
0 & q & \tau & -\lambda_3 & 0 & 0 & 0\\
0 & -\gamma\mathcal{V}^* & 0 & 0 & -\left(\gamma\mathcal{I}^*+\upsilon\right) & 0 & 0\\
0 & \gamma\mathcal{V}^* & 0 & 0 & \gamma\mathcal{I}^* & -\lambda_4 & 0\\
0 & 0 & 0 & 0 & 0 & \delta & -\upsilon
\end{pmatrix}.$$

The characteristic polynomial is given by

$$P_2\left(X\right) = -\left(\upsilon+X\right)\left(X^6+a_5X^5+a_4X^4+a_3X^3+a_2X^2+a_1X+a_0\right),$$

where

$$\begin{aligned}
a_0 &= \mu\lambda_2\lambda_3\left(g_0-\beta\gamma\delta\mathcal{V}^*\mathcal{S}^*\right),\\
a_1 &= \left(\mu\lambda_2+\mu\lambda_3+\lambda_2\lambda_3\right)\left(g_1-\beta\gamma\delta\mathcal{V}^*\mathcal{S}^*\right),\\
a_2 &= \left(\mu+\lambda_2+\lambda_3\right)\left(g_2-\beta\gamma\delta\mathcal{V}^*\mathcal{S}^*\right),\\
a_3 &= g_3-\beta\gamma\delta\mathcal{V}^*\mathcal{S}^*,\\
a_4 &= \lambda_6+\lambda_5\left(\beta\mathcal{F}^*+\gamma\mathcal{I}^*+\upsilon+\mu\right)+\left(\beta\mathcal{F}^*+\mu\right)\left(\gamma\mathcal{I}^*+\upsilon\right),\\
a_5 &= \lambda_5+\gamma\mathcal{I}^*+\beta\mathcal{F}^*+\upsilon+\mu.
\end{aligned}$$

According to Descartes' rule, the roots of $P_2\left(X\right)$ are negative reals or complexes of negative real parts. Therefore, the required result is obtained. □

Global Stability Analysis of $\mathfrak{Eqp}$

From system (3.3), we obtain

$$\begin{cases} \Lambda = (\beta\mathcal{F}^* + \mu)\,\mathcal{S}^* - \kappa\mathcal{R}^*, \\ \lambda_1 I^* = \beta F^* \mathcal{S}^*, \\ p\mathcal{I}^* = \lambda_2 \mathcal{H}^*, \\ \lambda_3 \mathcal{R}^* = q\mathcal{I}^* + \tau\mathcal{H}^*, \\ \lambda = (\gamma\mathcal{I}^* + \upsilon)\,\mathcal{V}^*, \\ \lambda_4 \mathcal{E}^* = \gamma\mathcal{I}^*\mathcal{V}^*, \\ \upsilon\mathcal{F}^* = \delta\mathcal{E}^*. \end{cases}$$

Now, let us define

$$\begin{cases} \mathcal{Z}_1 = \frac{\lambda_1\mathcal{S}^*}{\mathcal{S}^*\mathcal{I}}\,(\mathcal{I}^* - \mathcal{I}) + \beta\,(\mathcal{F} - \mathcal{F}^*) + \frac{\kappa}{\mathcal{S}}\,(\mathcal{R}^* - \mathcal{R}), \\ \mathcal{Z}_2 = \frac{\beta\mathcal{S}}{\mathcal{I}}\,(\mathcal{F}^* - \mathcal{F}) + \gamma\,(\mathcal{V} - \mathcal{V}^*) + \frac{\gamma\mathcal{V}}{\mathcal{E}}\,(\mathcal{E}^* - \mathcal{E}) + \frac{q}{\mathcal{R}}\,(\mathcal{R}^* - \mathcal{R}), \\ \mathcal{Z}_3 = \frac{p}{\mathcal{I}}\,(\mathcal{I}^* - \mathcal{I}) + \frac{\tau}{\mathcal{R}}\,(\mathcal{R}^* - \mathcal{R}), \\ \mathcal{Z}_4 = \frac{\delta}{\mathcal{F}}\,(\mathcal{F}^* - \mathcal{F}) + \frac{\lambda_4\mathcal{E}^*}{\mathcal{V}^*\mathcal{E}}\,(\mathcal{V} - \mathcal{V}^*). \end{cases}$$

To prove the theorem concerning global stability, we propose the following hypothesis.

Hyp. There exist four nonnegative constants $\mathcal{X}_1$, $\mathcal{X}_2$, $\mathcal{X}_3$, and $\mathcal{X}_4$ such that

$$\begin{cases} \mathcal{Z}_1 = \left(\mathcal{X}_1 - \frac{\lambda_1\mathcal{I}^*}{\mathcal{S}^*} - \mu\right)\frac{\mathcal{S}-\mathcal{S}^*}{\mathcal{S}}, \\ \mathcal{Z}_2 = (\mathcal{X}_2 - \lambda_1)\,\frac{\mathcal{I}-\mathcal{I}^*}{\mathcal{I}}, \\ \mathcal{Z}_3 = (\mathcal{X}_3 - \lambda_2)\,\frac{\mathcal{H}-\mathcal{H}^*}{\mathcal{H}}, \\ \mathcal{Z}_4 = (\mathcal{X}_4 - \lambda_4)\,\frac{\mathcal{E}-\mathcal{E}^*}{\mathcal{E}}. \end{cases}$$

Theorem 3.8. *Assume that hypothesis (**Hyp**) holds. Then, the endemic equilibrium point $\mathfrak{Eqp}$ of system (3.3) is globally asymptotically stable if $\mathfrak{Rb} > 1$.*

Proof. We analyze the following nonlinear Lyapunov function of the Goh-Volterra form

$$\begin{aligned} W(\mathcal{S},\mathcal{I},\mathcal{H},\mathcal{R},\mathcal{V},\mathcal{E},\mathcal{F}) &= \left[\mathcal{S}(t) - \mathcal{S}^* - \mathcal{S}^*\log\tfrac{\mathcal{S}(t)}{\mathcal{S}^*}\right] + \left[\mathcal{I}(t) - \mathcal{I}^* - \mathcal{I}^*\log\tfrac{\mathcal{I}(t)}{\mathcal{I}^*}\right] \\ &+ \left[\mathcal{H}(t) - \mathcal{H}^* - \mathcal{H}^*\log\tfrac{\mathcal{H}(t)}{\mathcal{H}^*}\right] + \left[\mathcal{R}(t) - \mathcal{R}^* - \mathcal{R}^*\log\tfrac{\mathcal{R}(t)}{\mathcal{R}^*}\right] \\ &+ \left[\mathcal{V}(t) - \mathcal{V}^* - \mathcal{V}^*\log\tfrac{\mathcal{V}(t)}{\mathcal{V}^*}\right] + \left[\mathcal{E}(t) - \mathcal{E}^* - \mathcal{E}^*\log\tfrac{\mathcal{E}(t)}{\mathcal{E}^*}\right] \\ &+ \left[\mathcal{F}(t) - \mathcal{F}^* - \mathcal{F}^*\log\tfrac{\mathcal{F}(t)}{\mathcal{F}^*}\right]. \end{aligned}$$

By calculating the derivative of W with respect to time along the solutions of system (3.3), we obtain

$$\begin{aligned} \frac{dW}{dt} &= \left(1 - \frac{\mathcal{S}^*}{\mathcal{S}}\right)\frac{d\mathcal{S}}{dt} + \left(1 - \frac{\mathcal{I}^*}{\mathcal{I}}\right)\frac{d\mathcal{I}}{dt} + \left(1 - \frac{\mathcal{H}^*}{\mathcal{H}}\right)\frac{d\mathcal{H}}{dt} + \left(1 - \frac{\mathcal{R}^*}{\mathcal{R}}\right)\frac{d\mathcal{R}}{dt} \\ &+ \left(1 - \frac{\mathcal{V}^*}{\mathcal{V}}\right)\frac{d\mathcal{V}}{dt} + \left(1 - \frac{\mathcal{E}^*}{\mathcal{E}}\right)\frac{d\mathcal{E}}{dt} + \left(1 - \frac{\mathcal{F}^*}{\mathcal{F}}\right)\frac{d\mathcal{F}}{dt}. \end{aligned}$$

A simple calculation provides the following result

$$\begin{aligned}\left(1-\frac{\mathcal{S}^*}{\mathcal{S}}\right)\frac{d\mathcal{S}}{dt} &= \left(1-\frac{\mathcal{S}^*}{\mathcal{S}}\right)\left[\Lambda+\kappa\mathcal{R}-(\beta\mathcal{F}+\mu)\,\mathcal{S}\right]\\ &= \left(1-\frac{\mathcal{S}^*}{\mathcal{S}}\right)\left[-\kappa\mathcal{R}^*+(\beta\mathcal{F}^*+\mu)\,\mathcal{S}^*+\kappa\mathcal{R}-(\beta\mathcal{F}+\mu)\,\mathcal{S}\right]\\ &= \frac{\mathcal{S}-\mathcal{S}^*}{\mathcal{S}}\left[-\mu\,(\mathcal{S}-\mathcal{S}^*)-\kappa\,(\mathcal{R}^*-\mathcal{R})-\beta\mathcal{F}\mathcal{S}+\beta\mathcal{F}^*\mathcal{S}^*\right].\end{aligned}$$

As

$$\beta\mathcal{F}^*\mathcal{S}^*-\beta\mathcal{F}\mathcal{S}=\beta\mathcal{F}^*\mathcal{S}^*-\beta\mathcal{F}^*\mathcal{S}+\beta\mathcal{F}^*\mathcal{S}-\beta\mathcal{F}\mathcal{S}-\beta\mathcal{S}\,(\mathcal{F}-\mathcal{F}^*)-\frac{\lambda_1\mathcal{E}^*}{\mathcal{S}^*}\,(\mathcal{S}-\mathcal{S}^*)\,, \quad (3.15)$$

then

$$\left(1-\frac{\mathcal{S}^*}{\mathcal{S}}\right)\frac{d\mathcal{S}}{dt}=-\left(\frac{\lambda_1\mathcal{E}^*}{\mathcal{S}^*}+\mu\right)\frac{(\mathcal{S}-\mathcal{S}^*)}{\mathcal{S}}-(\mathcal{S}-\mathcal{S}^*)\left[\beta\,(\mathcal{F}-\mathcal{F}^*)+\frac{\kappa}{\mathcal{S}}\,(\mathcal{R}^*-\mathcal{R})\right].$$

In same way, we find

$$\begin{aligned}\left(1-\frac{\mathcal{I}^*}{\mathcal{I}}\right)\frac{d\mathcal{I}}{dt} &= \left(1-\frac{\mathcal{I}^*}{\mathcal{I}}\right)\left[\beta\mathcal{F}\mathcal{S}-\lambda_1\mathcal{I}\right]=\frac{\mathcal{I}-\mathcal{I}^*}{\mathcal{I}}\left[\beta\mathcal{F}\mathcal{S}-\lambda_1\,(\mathcal{I}-\mathcal{I}^*)-\lambda_1\mathcal{I}^*\right]\\ &= -\lambda_1\frac{(\mathcal{I}-\mathcal{I}^*)^2}{\mathcal{I}}-\frac{\mathcal{I}^*-\mathcal{I}}{\mathcal{I}}\left[\beta\mathcal{F}\mathcal{S}-\beta\mathcal{F}^*\mathcal{S}^*\right].\end{aligned}$$

Using (3.15) gives us

$$\left(1-\frac{\mathcal{I}^*}{\mathcal{I}}\right)\frac{d\mathcal{I}}{dt} = -\lambda_1\frac{(\mathcal{I}-\mathcal{I}^*)^2}{\mathcal{I}}-\frac{\lambda_1\mathcal{I}^*}{\mathcal{S}^*\mathcal{I}}\,(\mathcal{I}^*-\mathcal{I})\,(\mathcal{S}-\mathcal{S}^*)-\frac{\beta\mathcal{S}}{\mathcal{I}}\,(\mathcal{I}^*-\mathcal{I})\,(\mathcal{F}-\mathcal{F}^*).$$

Next

$$\begin{aligned}\left(1-\frac{\mathcal{H}^*}{\mathcal{H}}\right)\frac{d\mathcal{H}}{dt} &= \left(\frac{\mathcal{H}-\mathcal{H}^*}{\mathcal{H}}\right)\left[p\mathcal{I}-\lambda_2\mathcal{H}\right]=\left(\frac{\mathcal{H}-\mathcal{H}^*}{\mathcal{H}}\right)\left[p\mathcal{I}-\lambda_2\,(\mathcal{H}-\mathcal{H}^*)-\lambda_2\mathcal{H}^*\right]\\ &= -\lambda_2\frac{(\mathcal{H}-\mathcal{H}^*)^2}{\mathcal{H}}-\frac{p}{\mathcal{H}}\,(\mathcal{H}-\mathcal{H}^*)\,(\mathcal{I}^*-\mathcal{I}).\end{aligned}$$

Also

$$\begin{aligned}\left(1-\frac{\mathcal{R}^*}{\mathcal{R}}\right)\frac{d\mathcal{R}}{dt} &= \left(1-\frac{\mathcal{R}^*}{\mathcal{R}}\right)\left[q\mathcal{I}+\tau\mathcal{H}-\lambda_3\mathcal{R}\right]\\ &= \left(\frac{\mathcal{R}-\mathcal{R}^*}{\mathcal{R}}\right)\left[p\mathcal{I}+\tau\mathcal{H}-\lambda_3\,(\mathcal{R}-\mathcal{R}^*)-\lambda_3\mathcal{R}^*\right]\\ &= -\lambda_3\frac{(\mathcal{R}-\mathcal{R}^*)^2}{\mathcal{R}}-(\mathcal{R}^*-\mathcal{R})\left[\frac{q}{\mathcal{R}}\,(\mathcal{R}-\mathcal{R}^*)+\frac{\tau}{\mathcal{R}}\,(\mathcal{H}-\mathcal{H}^*)\right]\end{aligned}$$

and

$$\begin{aligned}\left(1-\frac{\mathcal{V}^*}{\mathcal{V}}\right)\frac{d\mathcal{V}}{dt} &= \left(1-\frac{\mathcal{V}^*}{\mathcal{V}}\right)\left[\lambda-(\gamma\mathcal{I}+\upsilon)\,\mathcal{V}\right]=\left(1-\frac{\mathcal{V}^*}{\mathcal{V}}\right)\left[(\gamma\mathcal{I}^*+\upsilon)\,\mathcal{V}^*-(\gamma\mathcal{I}+\upsilon)\,\mathcal{V}\right]\\ &= -\upsilon\frac{(\mathcal{V}-\mathcal{V}^*)^2}{\mathcal{V}}+\frac{\mathcal{V}-\mathcal{V}^*}{\mathcal{V}}\left[\gamma\mathcal{I}^*\mathcal{V}^*-\gamma\mathcal{I}\mathcal{V}\right].\end{aligned}$$

As

$$\gamma\mathcal{I}^*\mathcal{V}^* - \gamma\mathcal{I}\mathcal{V} = \gamma\mathcal{I}^*\mathcal{V}^* + \gamma\mathcal{I}^*\mathcal{V} - \gamma\mathcal{I}^*\mathcal{V} - \gamma\mathcal{I}\mathcal{V} = -\gamma\mathcal{V}\left(\mathcal{I}-\mathcal{I}^*\right) - \frac{\lambda_4\mathcal{E}^*}{\mathcal{V}^*}\left(\mathcal{V}-\mathcal{V}^*\right), \quad (3.16)$$

then

$$\left(1-\frac{\mathcal{V}^*}{\mathcal{V}}\right)\frac{d\mathcal{V}}{dt} = -\left(\frac{\lambda_4\mathcal{E}^*}{\mathcal{V}^*}+\upsilon\right)\frac{\left(\mathcal{V}-\mathcal{V}^*\right)^2}{\mathcal{V}} - \gamma\left(\mathcal{V}-\mathcal{V}^*\right)\left(\mathcal{I}-\mathcal{I}^*\right).$$

Next

$$\begin{aligned}\left(1-\frac{\mathcal{E}^*}{\mathcal{E}}\right)\frac{d\mathcal{E}}{dt} &= \left(1-\frac{\mathcal{E}^*}{\mathcal{E}}\right)\left[\gamma\mathcal{I}\mathcal{V}-\lambda_4\mathcal{E}\right] = \frac{\mathcal{E}-\mathcal{E}^*}{\mathcal{E}}\left[\gamma\mathcal{I}\mathcal{V}-\upsilon\left(\mathcal{E}-\mathcal{E}^*\right)-\lambda_4\mathcal{E}^*\right]\\ &= -\lambda_4\frac{\left(\mathcal{E}-\mathcal{E}^*\right)^2}{\mathcal{E}} - \frac{\mathcal{E}^*-\mathcal{E}}{\mathcal{E}}\left[\gamma\mathcal{I}^*\mathcal{V}^*-\gamma\mathcal{I}\mathcal{V}\right].\end{aligned}$$

Using (3.16) gives us

$$\left(1-\frac{\mathcal{E}^*}{\mathcal{E}}\right)\frac{d\mathcal{E}}{dt} = -\lambda_4\frac{\left(\mathcal{E}-\mathcal{E}^*\right)^2}{\mathcal{E}} - \frac{\lambda_4\mathcal{E}^*}{\mathcal{V}^*\mathcal{E}}\left(\mathcal{E}^*-\mathcal{E}\right)\left(\mathcal{V}-\mathcal{V}^*\right) - \frac{\gamma\mathcal{V}}{\mathcal{E}}\left(\mathcal{E}^*-\mathcal{E}\right)\left(\mathcal{I}-\mathcal{I}^*\right).$$

Also

$$\begin{aligned}\left(1-\frac{\mathcal{F}^*}{\mathcal{F}}\right)\frac{d\mathcal{F}}{dt} &= \left(\frac{\mathcal{F}-\mathcal{F}^*}{\mathcal{F}}\right)\left[\delta\mathcal{E}-\upsilon\mathcal{F}\right] = \left(\frac{\mathcal{F}-\mathcal{F}^*}{\mathcal{F}}\right)\left[\delta\mathcal{E}-\upsilon\left(\mathcal{F}-\mathcal{F}^*\right)-\upsilon\mathcal{F}^*\right]\\ &= -\upsilon\frac{\left(\mathcal{F}-\mathcal{F}^*\right)^2}{\mathcal{F}} - \frac{\delta}{\mathcal{F}}\left(\mathcal{E}-\mathcal{E}^*\right)\left(\mathcal{F}^*-\mathcal{F}\right).\end{aligned}$$

Then

$$\begin{aligned}\frac{dW}{dt} \leq &-\left(\frac{\lambda_1\mathcal{I}^*}{\mathcal{S}^*}+\mu\right)\frac{\left(\mathcal{S}-\mathcal{S}^*\right)^2}{\mathcal{S}} - \lambda_1\frac{\left(\mathcal{I}-\mathcal{I}^*\right)^2}{\mathcal{I}} - \lambda_2\frac{\left(\mathcal{H}-\mathcal{H}^*\right)^2}{\mathcal{H}} - \lambda_3\frac{\left(\mathcal{R}-\mathcal{R}^*\right)^2}{\mathcal{R}}\\ &-\left(\frac{\lambda_4\mathcal{E}^*}{\mathcal{V}^*}+\upsilon\right)\frac{\left(\mathcal{V}-\mathcal{V}^*\right)^2}{\mathcal{V}} - \lambda_4\frac{\left(\mathcal{E}-\mathcal{E}^*\right)^2}{\mathcal{E}} - \upsilon\frac{\left(\mathcal{F}-\mathcal{F}^*\right)^2}{\mathcal{F}}\\ &-\mathcal{Z}_1\left(\mathcal{S}-\mathcal{S}^*\right) - \mathcal{Z}_2\left(\mathcal{I}-\mathcal{I}^*\right) - \mathcal{Z}_3\left(\mathcal{H}-\mathcal{H}^*\right) - \mathcal{Z}_4\left(\mathcal{E}-\mathcal{E}^*\right).\end{aligned}$$

By employing (**Hyp**), we get

$$\begin{aligned}\frac{dW}{dt} \leq &-\mathcal{X}_1\frac{\left(\mathcal{S}-\mathcal{S}^*\right)^2}{\mathcal{S}} - \mathcal{X}_2\frac{\left(\mathcal{I}-\mathcal{I}^*\right)^2}{\mathcal{I}} - \mathcal{X}_3\frac{\left(\mathcal{H}-\mathcal{H}^*\right)^2}{\mathcal{H}} - \lambda_3\frac{\left(\mathcal{R}-\mathcal{R}^*\right)^2}{\mathcal{R}}\\ &-\left(\frac{\lambda_4\mathcal{E}^*}{\mathcal{V}^*}+\upsilon\right)\frac{\left(\mathcal{V}-\mathcal{V}^*\right)^2}{\mathcal{V}} - \mathcal{X}_4\frac{\left(\mathcal{E}-\mathcal{E}^*\right)^2}{\mathcal{E}} - \upsilon\frac{\left(\mathcal{F}-\mathcal{F}^*\right)^2}{\mathcal{F}}.\end{aligned}$$

Because all parameters are nonnegative, we obtain $\frac{dW}{dt} \leq 0$ when $\mathfrak{Rb} > 1$. According to LaSalle's invariance principle [58], $(\mathcal{S},\mathcal{I},\mathcal{H},\mathcal{R},\mathcal{V},\mathcal{E},\mathcal{F}) \to (\mathcal{S}^*,\mathcal{I}^*,\mathcal{H}^*,\mathcal{R}^*,\mathcal{V}^*,\mathcal{E}^*,\mathcal{F}^*)$ as $t \to \infty$. □

3.4 Data Fitting Analysis through Numerical Simulation

In this section, we validate our analytical results by specifying particular parameter values and applying a numerical solution method to the model. The parameters, as detailed in Table 3.5, are based on consistent scaling to ensure that they align with the correct physical dimensions. For clarity, all model parameters are adjusted to conform to the time dimension, ensuring consistency with the model requirements.

3.4.1 Evaluating Dengue Control in Low $\mathfrak{Rb}$ Countries

Fitted Data Analysis of Dengue in Singapore

This section presents a numerical study that contributes to a comprehensive understanding and effective management of dengue in Singapore, using data from reliable health sources. Statistical and graphical methods were employed to examine the key epidemiological indicators and provide insights into the dengue situation in the country.

Singapore has a tropical, humid climate year-round, making it prone to continuous mosquito breeding and dengue transmission. Although Singapore has a highly developed healthcare infrastructure and strong monitoring system, persistent climatic conditions pose an ongoing challenge in controlling mosquito populations. Continuous efforts in environmental management and raising health awareness among the population are crucial to minimize the spread of the disease.

The total population of Singapore was $N = 3\,022\,209$ in 1990 [74], with initial reported dengue cases of $I_N(0) = 218\,939$ [73].

In our analysis, we assume that the total population N remains constant; however, a significant increase in population was observed from 1990 to 2021. Therefore, we cannot directly compare the infection rate in 1990, where there were $218\,939$ cases out of a population of $3\,022\,209$, to the infection rate in 2021, where there were $485\,139$ cases out of a population of $5\,941\,060$. To ensure accuracy, we will adjust the infection rate for each year based on the initial total population in 1990 (Table 3.1), enabling a precise comparison of infection rates over time. Based on these considerations, we will calculate the average recruitment and natural death rates for the entire period from 1990 to 2021 [75].

Interpretation	Ref.	1990	1991	$\cdots$	2020	2021	Average
Population of Singapore	[74]	3 022 209	3 120 620	$\cdots$	5 909 869	5 941 060	-
Initial dengue cases	[73]	218 939	228 484	$\cdots$	469 646	485 139	-
Adjusted dengue cases	-	218 939	221 279	$\cdots$	240 169	246 790	-
Recruitment rate Λ	[75]	0.0182	0.0171	$\cdots$	0.0085	0.0086	0.0117375
Natural death rate μ	[75]	0.0047	0.0046	$\cdots$	0.0052	0.0058	0.00465

Table 3.1: Adjusted parameters and initial data of infected population in Singapore from 1990 to 2021.

Lemma 3.1 ensures that the population does not exceed a specified limit, maintaining our model's validity and reflecting real-world population constraints. Indeed, we have

$$N_0 = N_{1990} = 3\,022\,209 \quad \text{and} \quad N(t) \leq N_{2021} = 25\,941\,060.$$

Subsequently, it must hold that:

$$\begin{aligned} N_{2021} &\leq N_{1990} \exp\left((\Lambda - \mu)\,\ell\right) \\ &\leq \min\left\{N_{1990} \times \exp\left((0.0117375 - 0.00465)\,\ell\right)\right\}. \end{aligned}$$

Our numerical simulation shows that the highest value that ℓ can take is 77. This decision makes the existence and uniqueness of the solution for the SIHR(N)–SEI(M) model on $[0, \ell]$ more evident. As a result, N should not be greater than 5.2318×10^6, in accordance with the limitations of Lemma 3.1.

The basic reproduction number in this case is:

$$\mathfrak{Rb} \simeq 0.374530069 < 1.$$

Moreover, following Theorem 3.1, then SIHR(N)–SEI(M) model admits a unique solution on $[0, \ell]$, with

$$\ell < 1.5485 \text{ (unit)}.$$

Because dengue statistics are collected annually or over several months, we chose a unit of 50 years. In this context, the value of ℓ should not exceed 77 years.

Figure 3.2 shows the development of confirmed dengue cases in Singapore over 31 years starting in 1990. The curve demonstrates noticeable fluctuations in recorded infections, with different phases indicating variations in the disease spread rates. The graph highlights periods of increase and decrease, reflecting changes in environmental and health conditions, and improvements in prevention and treatment strategies. The data suggest a gradual improvement in disease control in recent years despite ongoing fluctuations.

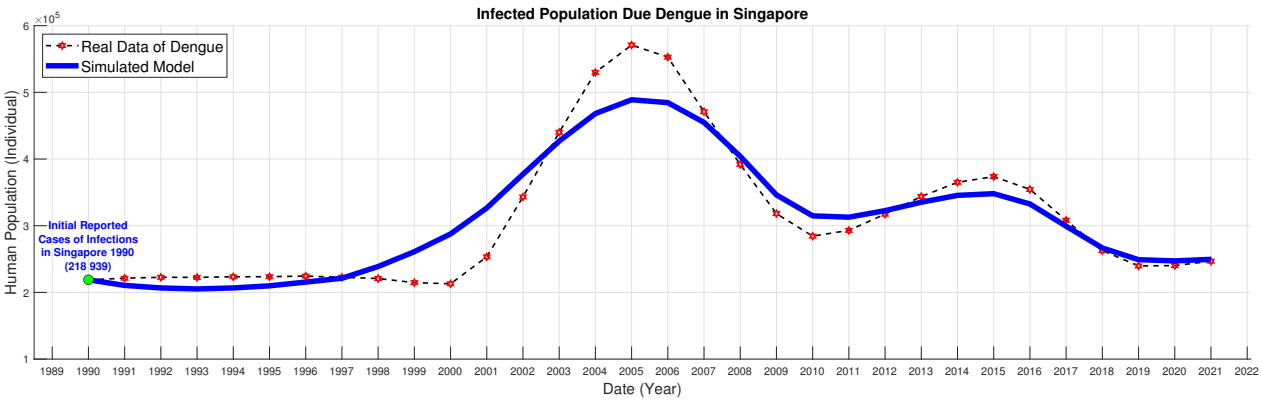

Figure 3.2: The reported cases of dengue in Singapore (shown with red markers) compared to the predicted cumulative infected cases provided by the proposed model (represented by blue line).

Figure 3.3 shows the trend of infected individuals and those hospitalized due to dengue in Singapore from 1990 to 2021. The curve representing infected individuals displays a fluctuating pattern, with noticeable peaks in certain years, indicating periods of increased infection rates. In contrast, the curve for hospitalized individuals follows the infection curve but remains at lower levels, indicating that only a portion of the infected population required hospitalization. Together, these curves illustrate the relationship between the total number of infections and severity of cases requiring medical care in hospitals over time.

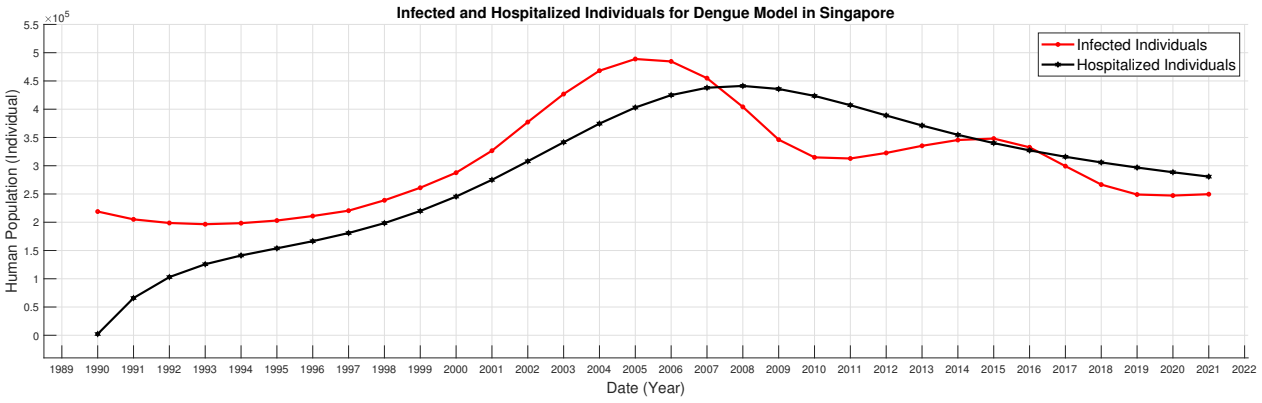

Figure 3.3: Infected and Hospitalized Individuals for Dengue Model in Singapore.

Figure 3.4 presents the trends of exposed and recovered individuals in Singapore within the dengue model from 1990 to 2021. The number of exposed individuals decreases over time as more people become infected and recover from the disease. In contrast, the number of recovered individuals shows a gradual increase, reflecting the cumulative number of

people who gained immunity after infection. The points at which these curves intersect indicate significant shifts in disease dynamics, such as periods when recovery rates surpass infection rates.

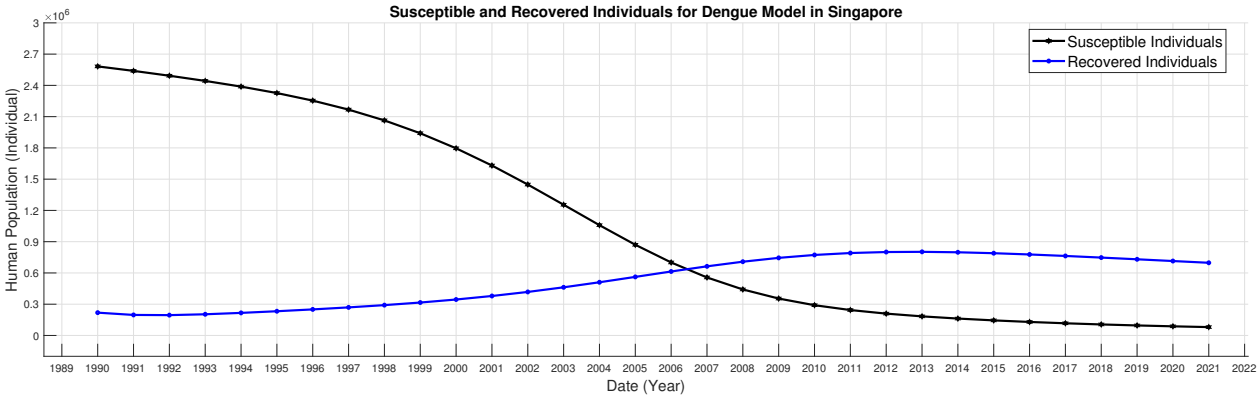

Figure 3.4: Susceptible and Recovered Individuals for Dengue Model in Singapore.

Figure 3.5 illustrates the impact of different transmission rate β values on the number of dengue-infected individuals in Singapore from 1990 to 2021. The colored lines represent different scenarios for changes in transmission rate values.

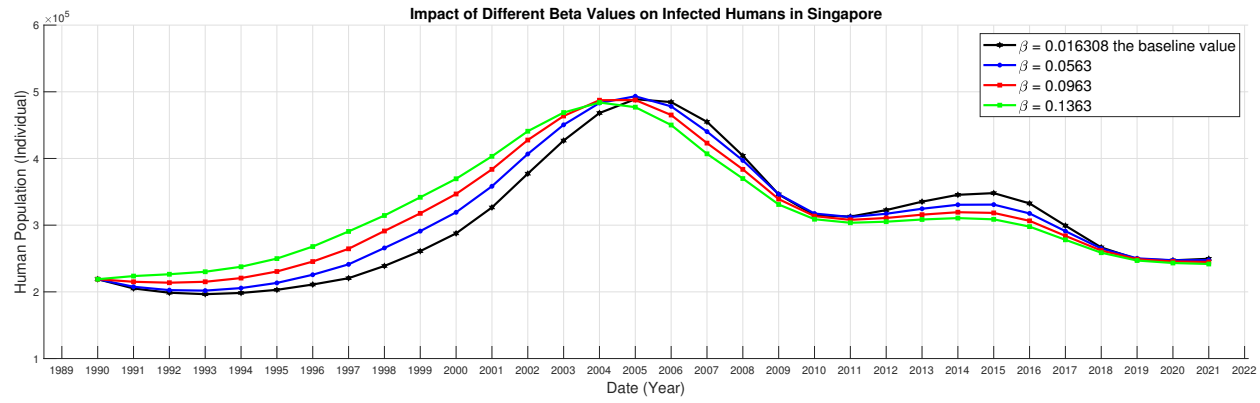

Figure 3.5: Impact of Different β Values on Infected Humans in Singapore.

The numerical simulation shows that as the β value increases, the number of infections rises significantly, especially during periods of peak infection. The graph demonstrates that altering the β value leads to substantial differences in infection numbers, with higher β values resulting in a larger number of infected individuals. This reflects the effect of increased transmission rates on the spread of the disease.

Singapore's Measures Against Dengue Fever and Their Impact on Disease Transmission

Singapore has implemented several preventive measures to combat dengue fever, which significantly affects the transmission rate β. These measures include controlling mosquito breeding sites by removing stagnant water, launching awareness campaigns to increase knowledge of mosquito bite prevention, using insecticides, and enhancing healthcare and patient follow-up. These actions have led to a reduction in mosquito numbers and cases of infection, contributing to a decrease in the transmission rate β, and limiting the spread of dengue fever.

Fitted Data Analysis of Dengue in Costa Rica

This section presents a numerical study to contribute to a comprehensive understanding and effective management of dengue in Costa Rica using data from reliable health sources. Statistical and graphical methods were employed to examine the key epidemiological indicators and provide insights into the dengue situation in the country.

Costa Ricas warm, humid climate, coupled with a rainy season spanning from May to November, creates ideal conditions for the breeding of mosquitoes responsible for transmitting the dengue virus, especially in densely populated urban areas. The spread of dengue is closely tied to the rainy season, because stagnant water provides breeding grounds for mosquitoes. Despite ongoing efforts by health authorities, controlling the spread of the disease remains a significant challenge, underscoring the need for robust strategies for mosquito control.

The total population of Costa Rica was $N = 3\,158\,253$ in 1990 [76]. Initial reported dengue cases $I_N(0) = 78\,620$ [73].

In our analysis, we assume that the total population N remains constant; however, a significant increase in population was observed from 1990 to 2021. Therefore, we cannot directly compare the infection rate in 1990, where there were $78\,620$ cases out of a population of $3\,158\,253$, to the infection rate in 2021, where there were $127\,337$ cases out of a population of $5\,153\,957$. To ensure accuracy, we will adjust the infection rate for each year based on the initial total population in 1990 (Table 3.2), enabling a precise comparison of infection rates over time. Based on these considerations, we will calculate the average recruitment and natural death rates for the entire period from 1990 to 2021 [77].

Interpretation	Ref.	1990	1991	⋯	2020	2021	Average
Population of Costa Rica	[76]	3 158 253	3 239 414	⋯	5 123 105	5 153 957	-
Initial dengue cases	[73]	78 620	79 644	⋯	12 2913	127 337	-
Adjusted dengue cases	-	78 620	77 649	⋯	75 772	78 030	-
Recruitment rate Λ	[77]	0.0274	0.0266	⋯	0.0122	0.0119	0.018096875
Natural death rate μ	[77]	0.0039	0.0039	⋯	0.0056	0.0072	0.004478125

Table 3.2: Adjusted parameters and initial data of infected population in Costa Rica from 1990 to 2021.

Lemma 3.1 ensures that the population remains within specified limits, maintaining the validity of our model by reflecting real-world population constraints. Then,

$$N_0 = N_{1990} = 3\,158\,253 \quad \text{and} \quad N(t) \leq N_{2021} = 5\,153\,957.$$

Subsequently, it must hold that:

$$\begin{aligned} N_{2021} &\leq N_{1990} \exp\left((\Lambda - \mu)\,\ell\right) \\ &\leq \min\left\{N_{1990} \times \exp\left((0.018096875 - 0.004478125)\,\ell\right)\right\}. \end{aligned}$$

The SIHR(N)–SEI(M) model admits a unique solution when $\ell < 0.7817$ (unit = 50 years). Thus, ℓ should not exceed 39 years, and N should not be greater than 5.3781×10^6, per Lemma 3.1's limitations.

The basic reproduction number in this case is:

$$\mathfrak{Rb} \simeq 0.592189356 < 1.$$

Figure 3.6 illustrates the development of dengue cases in Costa Rica over a span of 31 years starting in 1990. The curve reflects clear fluctuations in the number of reported cases, with periods marked by significant increases in infections followed by gradual declines. These variations indicate the influence of environmental and health factors as well as advancements in prevention and treatment methods. The data also highlight a gradual improvement in disease control in recent years despite continued fluctuations during certain periods.

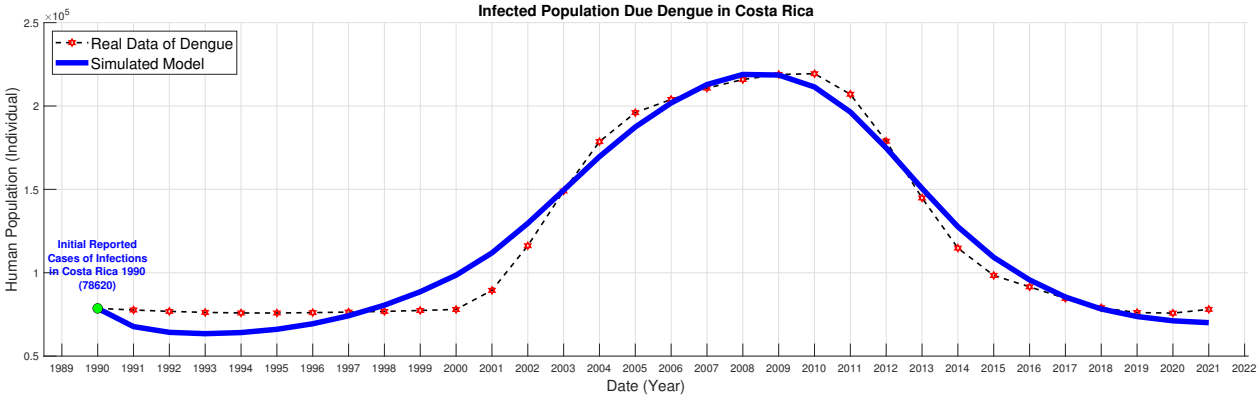

Figure 3.6: The reported cases of dengue in Costa Rica (shown with red markers) compared to the predicted cumulative infected cases provided by the proposed model (represented by blue line).

Figure 3.7 shows the trends of infected and recovered individuals in Costa Rica within the dengue model from 1990 to 2021. The curve representing infected individuals shows fluctuations in the number of cases, with significant peaks occurring during certain years, indicating periods of increased infection rates. The curve for recovered individuals shows a steady increase over time, reflecting the cumulative number of individuals who recovered and gained immunity. The divergence between these two curves highlights the progression of the epidemic and recovery dynamics in the population.

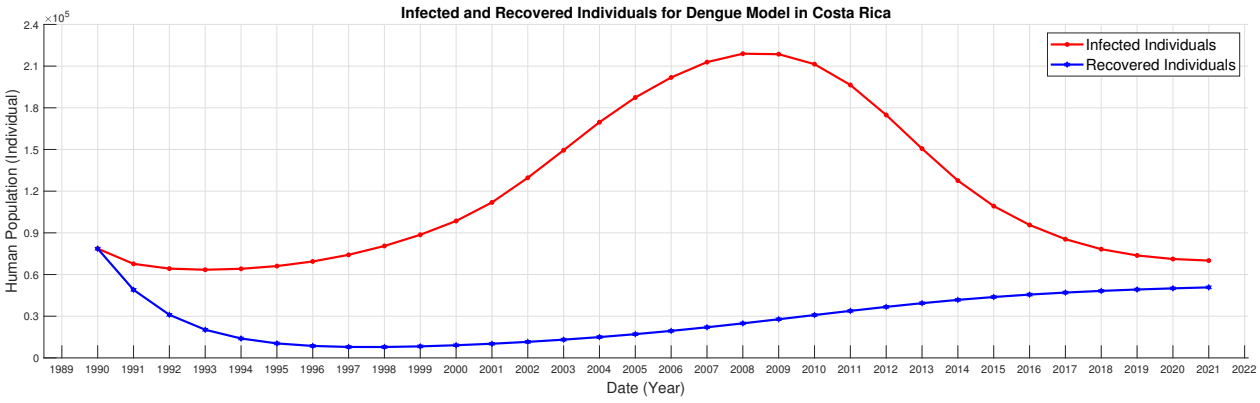

Figure 3.7: Infected and Recovered Individuals for Dengue Model in Costa Rica.

Figure 3.8 illustrates the trends in susceptible and hospitalized individuals in Costa Rica under the dengue model from 1990 to 2021. The curve for susceptible individuals initially starts at a high level, gradually decreasing over time as more individuals become infected and either recover or require hospitalization. In contrast, the curve for hospitalized

individuals remains significantly lower, following a pattern that mirrors the number of infections, but with fewer cases requiring hospitalization. This figure shows the relationship between susceptible individuals and those requiring medical attention in hospitals over a given timeframe.

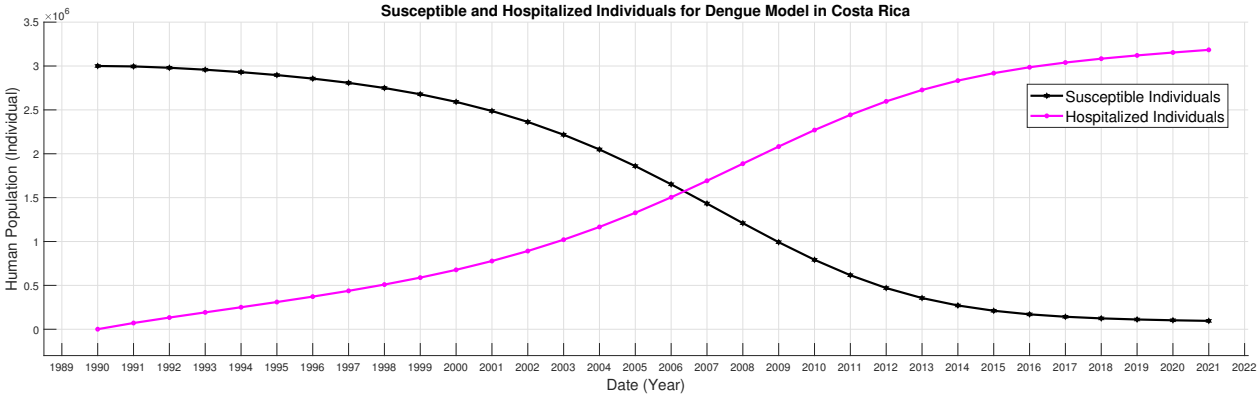

Figure 3.8: Susceptible and Hospitalized Individuals for Dengue Model in Costa Rica.

Figure 3.9 depicts the dynamics of mosquito populations in Costa Rica according to a dengue fever model. The curves represent the numbers of susceptible, exposed, and infected mosquitoes from 1990 to 2021. The number of susceptible mosquitoes remains relatively stable with minor fluctuations, while the populations of exposed and infected mosquitoes show a gradual increase over the years. Both the exposed and infected mosquito populations exhibit a steady growth trend, indicating an increase in the transmission potential of dengue fever over time. These trends highlight the importance of mosquito control to prevent the spread of dengue.

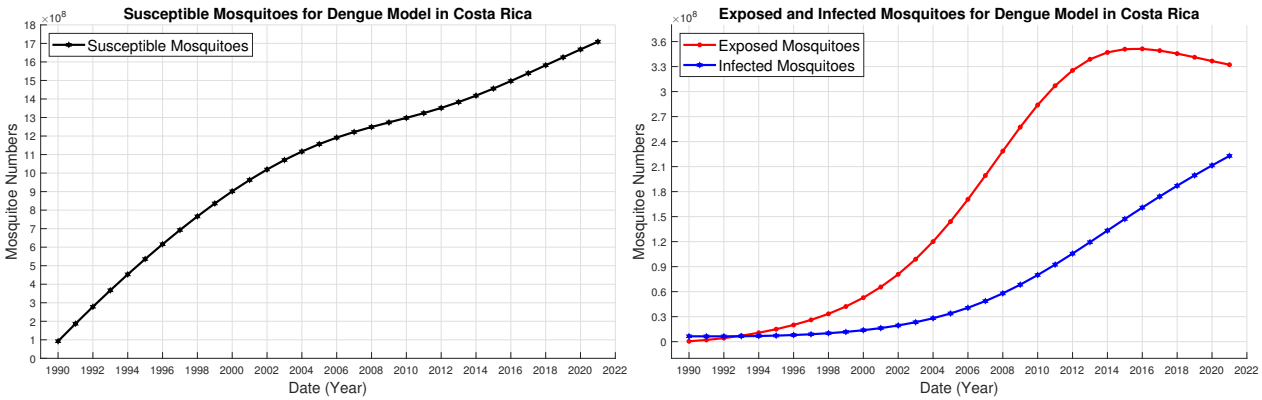

Figure 3.9: Susceptible, Exposed, and Infected Mosquitoes for Dengue Model in Costa Rica.

Figure 3.10 shows that higher β values increase dengue infections in Costa Rica, similar to Singapore, highlighting the need to control transmission rates.

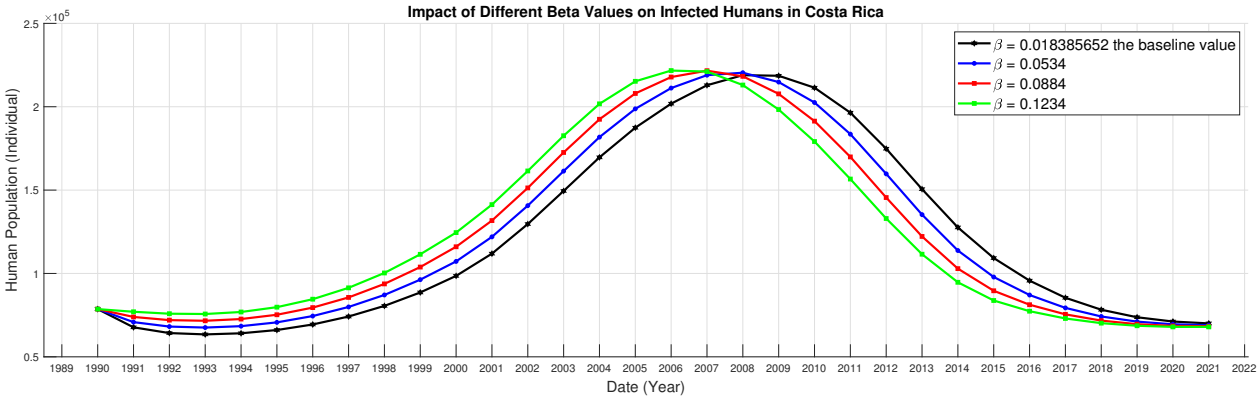

Figure 3.10: Impact of Different β Values on Infected Humans in Costa Rica.

Costa Rica's Dengue Strategies: Impact on Transmission and Infection Rates

Costa Rica has implemented several measures to combat dengue fever, aiming to reduce the spread of the disease and lower the number of infections. These measures include community awareness campaigns focused on the importance of eliminating mosquito breeding sites, such as stagnant water, which provides an ideal environment for the Aedes aegypti mosquito, the virus carrier. Health authorities also carried out insecticide spraying programs in areas most prone to dengue outbreaks, in addition to enhancing healthcare programs for the early detection and appropriate treatment of infections.

These measures have had a noticeable impact on reducing the transmission rate β, leading to a decrease in the spread of infections among the population. Furthermore, improvements in the healthcare system and increased community awareness have contributed to a significant reduction in the number of recorded cases in certain affected areas. However, Costa Rica continues to face seasonal challenges in controlling the spread of dengue due to environmental and climatic factors that promote mosquito breeding.

3.4.2 Assessing Dengue Challenges in High $\mathfrak{Rb}$ Countries

Fitted Data Analysis of Dengue in Yemen

This section presents a numerical study to contribute to a comprehensive understanding and effective management of dengue in Yemen using data from reliable health sources.

Yemen's climate is characterized by dry and sporadic rainy seasons, creating periodically suitable environments for mosquito breeding. The healthcare system in Yemen is severely weakened due to ongoing conflicts, making it difficult to manage dengue outbreaks. Additionally, environmental changes lead to increased mosquito populations, posing a major challenge to health authorities in controlling the spread of the disease.

The total population of Yemen was $N = 13\,375\,121$ in 1990 [78]. Initial reported dengue cases, $I_N(0) = 1\,851$ [73].

Due to population growth from 1990 to 2021, we adjusted the infection rates to ensure accurate comparisons (Table 3.3). In 1990, there were $1\,851$ cases out of a population of $13\,375\,121$, and in 2021, there were $8\,074$ cases out of a population of $32\,981\,641$ [79].

Interpretation	**Ref.**	1990	1991	$\cdots$	2020	2021	**Average**
Population of Yemen	[78]	13 375 121	13 895 851	$\cdots$	32 284 046	32 981 641	-
Initial dengue cases	[73]	1 851	1 986	$\cdots$	7 705	8 074	-
Adjusted dengue cases	-	1 851	1 912	$\cdots$	3 192	3 274	-
Recruitment rate Λ	[79]	0.0526	0.0517	$\cdots$	0.0313	0.0305	0.03850625
Natural death rate μ	[79]	0.0118	0.0115	$\cdots$	0.0065	0.0068	0.0079625

Table 3.3: Adjusted parameters and initial data of infected population in Yemen from 1990 to 2021.

Lemma 3.1 ensures that the population remains within specified limits, maintaining the validity of our model by reflecting real-world population constraints. Then,

$$N_0 = N_{1990} = 13\,375\,121 \quad \text{and} \quad N(t) \leq N_{2021} = 32\,981\,641.$$

Subsequently, it must hold that:

$$N_{2021} \leq N_{1990} \exp\left((\Lambda - \mu)\,\ell\right).$$

The SIHR(N)–SEI(M) model admits a unique solution when $\ell < 1.2358$ (unit = 50 years). Thus, ℓ should not exceed 62 years, and N should not be greater than 8.8299×10^7, per Lemma 3.1.

The basic reproduction number in this case is:

$$\mathfrak{Rb} \simeq 1.432852042 > 1.$$

Figure 3.11 shows a gradual increase in dengue cases in Yemen from 1990 to 2021, with a significant increase in the incidence rates reflecting the country's challenging health conditions. These data indicate an ongoing and growing spread of the disease, particularly in recent years.

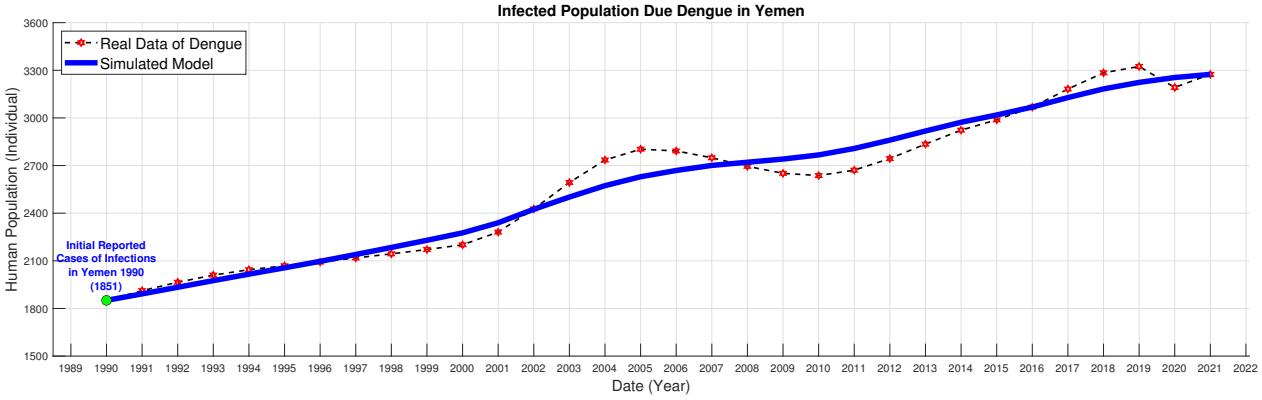

Figure 3.11: The reported cases of dengue in Yemen (shown with red markers) compared to the predicted cumulative infected cases provided by the proposed model (represented by blue line).

Figure 3.12 shows the numbers of exposed and infected mosquitoes in Yemen from 1990 to 2021. Exposed mosquitoes decrease continuously, indicating a rapid transition to infection or the impact of the interventions. Infected mosquitoes initially increase due to favorable conditions, followed by a decrease reflecting health interventions or depletion of susceptible mosquito populations.

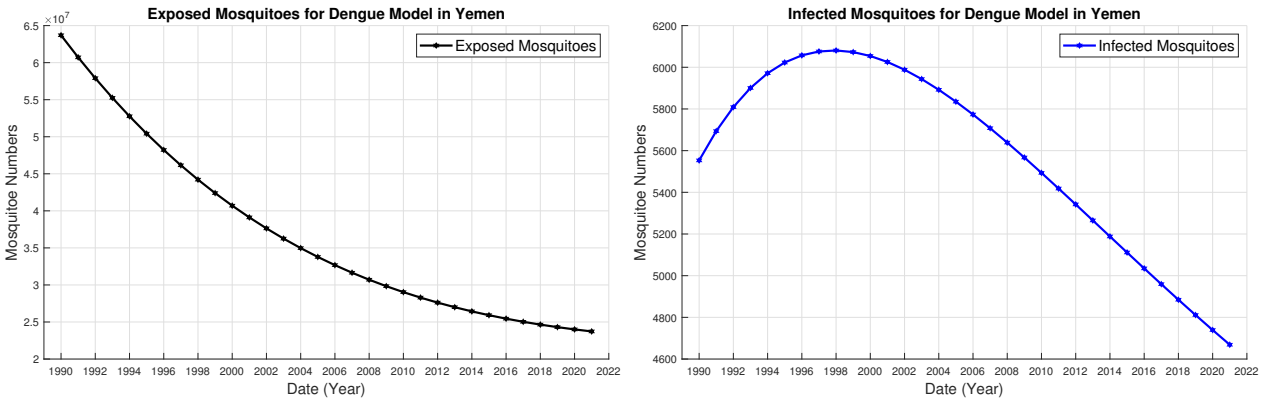

Figure 3.12: Exposed and Infected Mosquitoes for Dengue Model in Yemen.

Yemen's Dengue Efforts Amid Humanitarian Challenges

Yemen has undertaken various efforts to combat dengue fever, including extensive awareness campaigns, mosquito spraying operations in the most affected areas, and improvements in sanitation and elimination of mosquito breeding sites. Health programs

have been implemented to enhance the prevention and provision of medical care for infected individuals. However, the country has faced significant humanitarian challenges such as ongoing conflicts and resource shortages, which have limited the effectiveness of these measures. These challenges have impacted the ability of authorities to control the spread of the disease, increasing the transmission rate β and resulting in an increase in the number of infections.

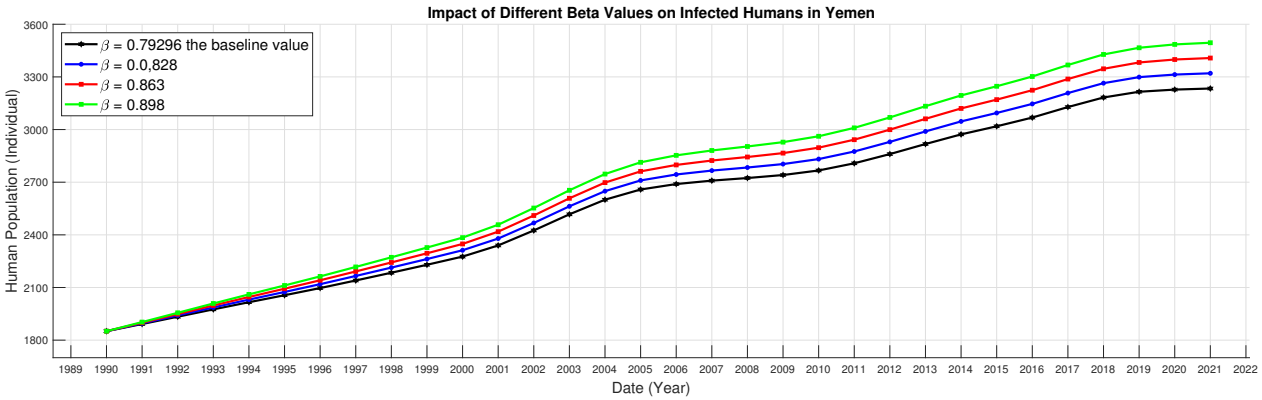

Figure 3.13: Impact of Different Beta Values on Infected Humans in Yemen.

Fitted Data Analysis of Dengue in India

This section presents a numerical study to enhance the understanding and management of dengue in India, using reliable health data. The Indian monsoon season from June to September leads to stagnant water accumulation, which is ideal for Aedes mosquito breeding. Densely populated urban areas with poor infrastructure exacerbate this problem. Improving environmental management and healthcare is essential for reducing the dengue spread in India.

The total population of India was $N = 870\,452\,165$ in 1990 [80]. Initial reported dengue cases, $I_N\,(0) = 11\,262\,313$ [73].

Due to population growth from 1990 to 2021, we adjusted the infection rates to ensure accurate comparisons (Table 3.4). In 1990, there were $11\,262\,313$ cases out of a population of $870\,452\,165$, and in 2021, there were $28\,205\,520$ cases out of a population of $1\,407\,563\,842$ [81].

Interpretation	Ref.	1990	1991	⋯	2020	2021	Average
Population of India	[80]	870 452 165	888 941 756	⋯	1 396 387 127	1 407 563 842	-
Initial dengue cases	[73]	11 262 313	11 570 731	⋯	28 379 898	28 205 520	-
Adjusted dengue cases	-	11 262 313	11 330 065	⋯	17 690 899	17 442 588	-
Recruitment rate Λ	[81]	0.0315	0.0309	⋯	0.0166	0.0164	0.023621875
Natural death rate μ	[81]	0.0109	0.0106	⋯	0.0074	0.0094	0.00829375

Table 3.4: Adjusted parameters and initial data of infected population in India from 1990 to 2021.

Lemma 3.1 ensures that the population remains within specified limits, maintaining the validity of our model by reflecting real-world population constraints. Then,

$$N_0 = N_{1990} = 870\,452\,165 \quad \text{and} \quad N(t) \leq N_{2021} = 1\,407\,563\,842.$$

Subsequently, it must hold that:

$$N_{2021} \leq N_{1990} \exp\left((\Lambda - \mu)\,\ell\right).$$

The SIHR(N)–SEI(M) model admits a unique solution when $\ell < 2.1568$ (unit = 50 years). Thus, ℓ should not exceed 108 years, and N should not be greater than 4.546×10^9, per Lemma 3.1.

The basic reproduction number in this case is:

$$\mathfrak{Rb} \simeq 1.157058336 > 1.$$

Figure 3.14 shows the evolution of confirmed dengue cases in India over a 31-year period starting in 1990. The graph illustrates a nearly constant increase in cases, reflecting an increasing spread of the disease. The simulated model (blue line) aligns well with the given data (red dots), highlighting the prediction accuracy. The data reveal a continuous rise in cases, with a notable increase toward the end of the last decade, influenced by factors such as climate change and environmental and health conditions.

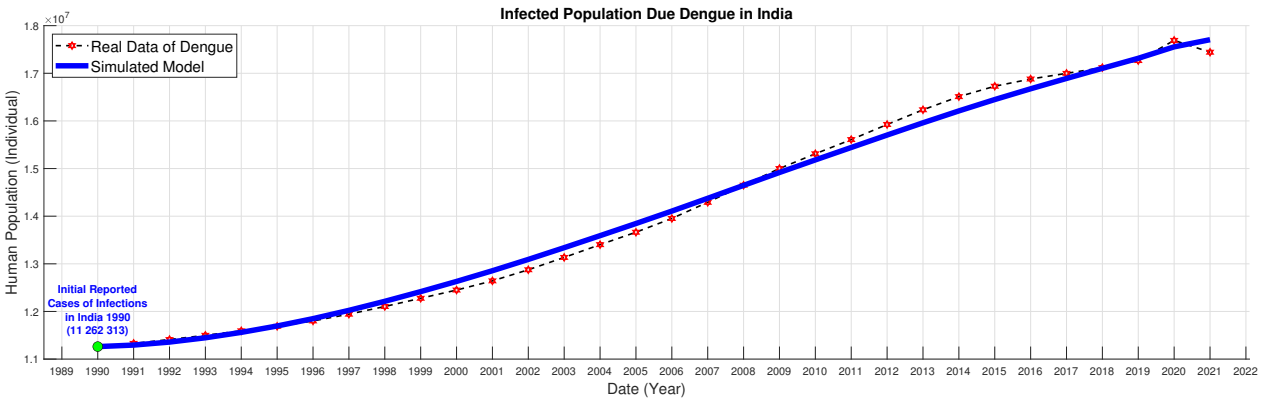

Figure 3.14: The reported cases of dengue in India (shown with red markers) compared to the predicted cumulative infected cases provided by the proposed model (represented by blue line).

The Impact of Preventive Measures and Challenges on the Spread of Dengue Fever in India

India has implemented several measures to combat infectious diseases such as dengue and malaria, including health awareness campaigns, mosquito control programs, improved sanitation systems, and the distribution of mosquito nets and medications. Improved sanitation helps eliminate stagnant water, which reduces mosquito breeding grounds, and promotes hygiene practices that decrease the chances of disease transmission. Despite these efforts, India continues to face significant challenges due to its high population density, which contributes to the rapid spread of diseases. Population density directly affects the transmission rate β, as it facilitates the transmission of infections among individuals due to proximity and overcrowding. This leads to a significant increase in the number of infections, making disease control efforts more difficult. Additionally, challenges related to providing healthcare in rural areas and poverty further complicate these efforts, making it more difficult to control the spread of diseases.

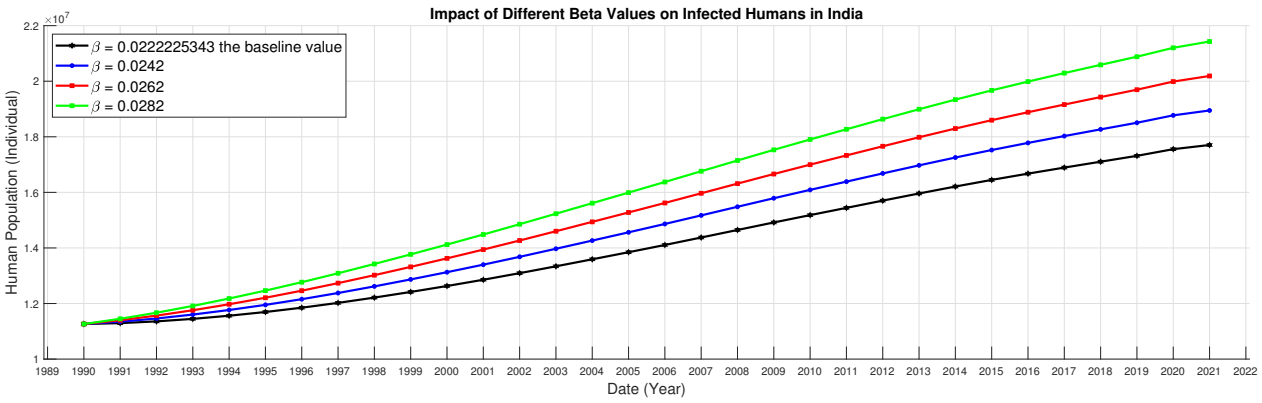

Figure 3.15: Impact of Different Beta Values on Infected Humans in India.

Appendix

The tables below provide a deeper understanding of the results presented in Figures 3.2, 3.6, 3.11, and 3.14. They provide the predicted parameter values used in the dengue model, along with biological descriptions that clarify the practical context of these values. The tables also include relevant references.

Parameter	Interpretation	Singapore	Costa Rica	Yemen	India	Reference
Λ	Recruitment rate of human	0.0117375	0.018096875	0.03850625	0.023621875	Estimated [75, 77, 79, 81]
$S_N(0)$	Initial number of S_N	2 582 164	3 000 235	13 371 400	847 816 042	Calculated
$I_N(0)$	Initial number of I_N	218 939	78 620	1 851	11 262 313	[73]
$H_N(0)$	Initial number of H_N	2 189	786	19	112 623	Assumed
$R_N(0)$	Initial number of R_N	218 917	78 612	1 851	11 261 187	Assumed
$S_M(0)$	Initial number of S_M	11 994 358	92 337 163	403 314 325	4 736 917 167	Fitted
$E_M(0)$	Initial number of E_M	26 272 680	9 434 400	63 696 193	4 553 926 611	Fitted
$I_M(0)$	Initial number of I_M	2 528 194	6 461 939	5 553	337 886 302	Fitted
θ	Death rate of I_N	0.260679388	0.283002815	0.024439245	0.004446672	Fitted
β	Rate of transmission from I_M to S_N	0.016307937	0.018385652	0.792959268	0.022222534	Fitted
γ	Rate of transmission from I_N to S_M	0.018519329	0.026267211	0.760276407	0.017184335	Fitted
κ	Immunity loss rate of humans	0.168569916	0.473613608	0.167072631	0.455354374	Fitted
p	Rate of transfer from I_N to H_N	0.348741437	0.909090909	0.006459612	0.006998654	Fitted
q	Recovery rate from I_N	0.031703767	0.082644628	0.014138738	0.038188419	Fitted
τ	Recovery rate from H_N	0.370708911	0.007829356	0.001654441	0.072030928	Fitted
δ	Rate of infectiousness of mosquitoes	0.001918616	0.003487147	6.6862×10^{-6}	0.004643516	Fitted
λ	Recruitment rate of mosquito	0.869565217	0.869565217	0.65276169	0.305173	Fitted
υ	Natural death rate of mosquitoes	0.023501763	0.022521412	0.048898988	0.025624351	Fitted
μ	Natural death rate of humans	0.00465	0.004478125	0.0079625	0.00829375	Estimated [75, 77, 79, 81]

Table 3.5: Parameters and initial data of the SIHR(N)–SEI(M) model.

CHAPTER 4

MATHEMATICAL INSIGHTS INTO CUTANEOUS LEISHMANIASIS DYNAMICS

This chapter discusses the transmission of cutaneous leishmaniasis using a mathematical system that describes the interaction between humans and the infected mosquito, considering the factors influencing disease spread.

4.1 Introduction

Cutaneous leishmaniasis is one of the most prevalent parasitic diseases worldwide, posing a significant public health challenge in numerous countries, particularly in the Middle East, North Africa, and parts of South America. The disease is primarily transmitted through the bite of infected female Phlebotomus sandflies, which thrive in semi-arid and rural environments. Cutaneous leishmaniasis is characterized by the appearance of skin ulcers or lesions, which, although not fatal, can cause permanent scars. In some cases, the disease can progress to more severe forms if left untreated [82].

Cutaneous leishmaniasis represents an increasing burden, with the World Health Organization (WHO) estimating over $700\,000$ to 1 million new cases annually, primarily in endemic regions [82]. The disease is transmitted through the bite of infected female Phlebotomus sandflies, which inject Leishmania parasites into the host's skin. These parasites then multiply within macrophages, leading to skin ulcers or lesions. The spread of this disease is driven by several factors, including urbanization, environmental changes, population displacement, and socioeconomic challenges that hinder access to healthcare. Developing effective strategies for prevention, treatment, and control of cutaneous leishmaniasis is essential to reduce its impact on affected communities [83].

By incorporating real epidemiological data from affected regions, mathematical models can accurately identify the factors contributing to outbreaks and highlight critical areas for intervention to reduce disease spread.

In this chapter, the dynamics of the epidemic are modeled by dividing the total human population (denoted as N) into five distinct classes:

- S_N: Susceptible individuals.
- E_N: Exposed individuals.
- I_N: Symptomatic infectious individuals.
- A_N: Asymptomatic infectious individuals.
- R_N: Recovered individuals.

Additionally, the sandfly population surrounding the human population (denoted as M) is divided into:

- S_M: Susceptible sandflies.
- I_M: Infected sandflies.

The parameters of the SEIAR(N)–SI(M) model are defined as follows:

- Λ indicates the rate of increase in the susceptible individuals.
- λ represents the rate of increase in the susceptible sandflies.
- $\mu < \Lambda$ expresses the natural death rate for humans.
- $\upsilon < \lambda$ presents the natural death rate of sandflies.
- β is the probability rate of disease transmission from infected sandflies to susceptible humans.
- γ is the probability rate of disease transmission from infected humans to susceptible sandflies.
- κ represents the proportion of recovered individuals who lose temporary immunity and become susceptible again.
- $\theta < 1$ probability that an exposed human develops symptomatic cutaneous leishmaniasis infection after leaving the incubation period.
- δ is the rate at which the treated population leave the class E_N
- q and p are the recovery rates from infectious populations I_N and A_N respectively.

Motivated by the above-mentioned works, we propose the following system of ordinary

differential equations for $0 \leq t \leq \ell < \infty$:

$$\begin{cases} \frac{dS_N(t)}{dt} &= \Lambda N(t) + \kappa R_N(t) - \left(\frac{\beta I_M(t)}{M(t)} + \mu\right) S_N(t) \\ \frac{dE_N(t)}{dt} &= \frac{\beta I_M(t)}{M(t)} S_N(t) - (\delta + \mu) E_N(t) \\ \frac{dI_N(t)}{dt} &= \theta\delta E_N(t) - (p + \mu) I_N(t) \\ \frac{dA_N(t)}{dt} &= (1-\theta)\delta E_N(t) - (q + \mu) A_N(t) \\ \frac{dR_N(t)}{dt} &= pI_N(t) + qA_N(t) - (\kappa + \mu) R_N(t) \\ \frac{dS_M(t)}{dt} &= \lambda M(t) - \left(\frac{\gamma(I_N(t) + A_N(t))}{N(t)} + \upsilon\right) S_M(t) \\ \frac{dI_M(t)}{dt}) &= \frac{\gamma(I_N(t) + A_N(t))}{N(t)} S_M(t) - \upsilon I_M(t). \end{cases} \tag{4.1}$$

In system (4.1), the first five equations represent the dynamics of the human population, whereas the last two equations describe the dynamics of the sandfly population.

To better understand the transmission dynamics of infectious diseases between humans and sandflies in the SEIAR(N)–SI(M) model outlined in system (4.1), we refer to the following chart:

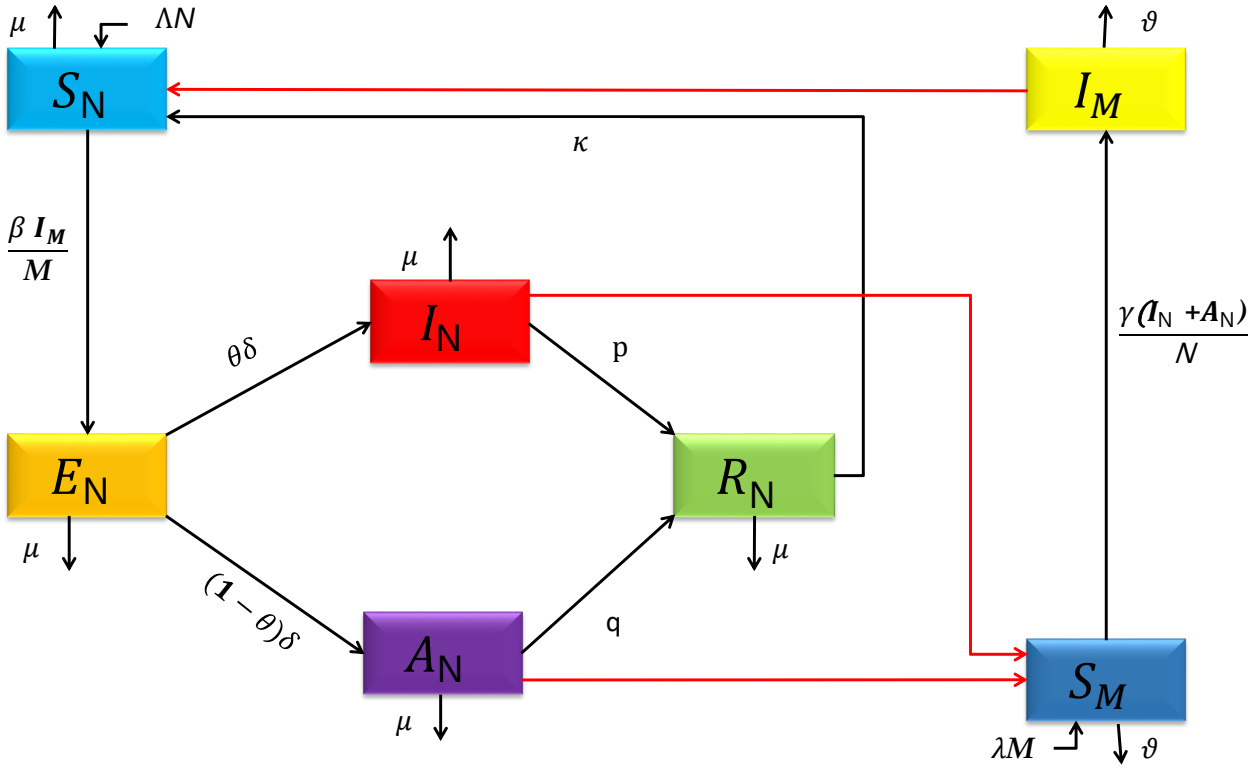

Figure 4.1: Flowchart of SEIAR(N)–SI(M).

This chapter aims to provide a comprehensive understanding of the dynamics involved in the transmission of cutaneous leishmaniasis and the factors that influence it. We begin by analyzing the behavior of the SEIAR(N)–SI(M) mathematical model, examining its solutions' existence, uniqueness, and stability, ensuring that the model's solutions are applicable and sustainable in various contexts. Additionally, we determine the basic reproduction number, explore the equilibrium points within the model, and analyze their stability to guide disease control strategies and predict future trends.

We validate the accuracy of our model using real data from Algeria, focusing on M'Sila province, because it has recently recorded a high incidence of the disease in the country. By doing so, we aim to identify local factors contributing to the spread of cutaneous leishmaniasis. This validation process enhances the model's precision and helps develop targeted and effective strategies for disease control.

4.2 Dynamic Analysis of the Feasible Region

4.2.1 Positivity and Boundedness of the Model

The SEIAR(N)–SI(M) model (4.1) is investigated within a biologically feasible region in $\mathbb{R}^7_+$, as defined in the subsequent lemma.

Lemma 4.1. *Assume that M_0 represents the initial total sandfly population, let N_0 be the initial total human population at $t = 0$, where $0 \leq t \leq \ell < \infty$. Consequently, the solution to the considered model is confined to the feasible region, given by*

$$\Omega = \left\{(S_N, E_N, I_N, A_N, R_N, S_M, I_M) \in \mathbb{R}^7_+ : 0 \leq N(t) \leq N_0 \exp(\Lambda \ell),\ 0 \leq M(t) \leq M_0 \exp(\lambda \ell)\right\}$$

with

$$N(t) = S_N(t) + E_N(t) + I_N(t) + A_N(t) + R_N(t), \qquad M(t) = S_M(t) + I_M(t).$$

Proof. Let

$$N(t) = S_N(t) + E_N(t) + I_N(t) + A_N(t) + R_N(t),$$

then

$$\frac{dN(t)}{dt} = \frac{dS_N(t)}{dt} + \frac{dE_N(t)}{dt} + \frac{dI_N(t)}{dt} + \frac{dA_N(t)}{dt} + \frac{dR_N(t)}{dt}.$$

Now, summing all the human equations of (4.1), we get

$$\begin{aligned} \frac{dN(t)}{dt} &= (\Lambda - \mu) N(t) \\ &\leq \Lambda N(t). \end{aligned}$$

Consequently,

$$N(t) \leq N_0 + \int_0^t \Lambda N(\tau)\, d\tau.$$

Applying Gronwall lemma [23], we obtain

$$N(t) \leq N_0 \exp(\Lambda \ell),$$

where N_0 is the total human population at $t = 0$.
In another way, let

$$M(t) = S_M(t) + I_M(t),$$

then

$$\frac{dM(t)}{dt} = \frac{dS_M(t)}{dt} + \frac{dI_M(t)}{dt}.$$

Now, summing all the sandfly equations of (4.1), we obtain

$$\begin{aligned} \frac{dM(t)}{dt} &= (\lambda - \upsilon) M(t) \\ &\leq \lambda M(t). \end{aligned}$$

Or

$$M(t) \leq M_0 + \int_0^t \lambda M(\tau)\, d\tau.$$

Therefore,

$$M(t) \leq M_0 \exp(\lambda \ell),$$

where M_0 is the total sandfly population at $t = 0$. □

In subsequent sections of this chapter, we assume the existence of two positive constants:

$$\mathcal{N} \leq N_0 \exp(\Lambda \ell), \qquad \mathcal{M} \leq M_0 \exp(\lambda \ell),$$

where the total human population N and sandfly population M remained fixed throughout the chapter period and can be expressed as $N(t) = \mathcal{N}$ and $M(t) = \mathcal{M}$. This assumption was made to normalize the SEIAR(N)–SI(M) model (4.1). Therefore, we put:

$$\begin{aligned} &\mathcal{S}(t) = \tfrac{S_N(t)}{\mathcal{N}}, \quad \mathcal{E}(t) = \tfrac{E_N(t)}{\mathcal{N}}, \quad \mathcal{I}(t) = \tfrac{I_N(t)}{\mathcal{N}}, \quad \mathcal{A}(t) = \tfrac{A_N(t)}{\mathcal{N}}, \\ &\mathcal{R}(t) = \tfrac{\mathcal{R}_N(t)}{\mathcal{N}}, \quad \mathcal{V}(t) = \tfrac{S_M(t)}{\mathcal{M}}, \quad \mathcal{F}(t) = \tfrac{I_M(t)}{\mathcal{M}}, \end{aligned} \tag{4.2}$$

then we obtain

$$\begin{cases} \frac{d\mathcal{S}(t)}{dt} &= \Lambda + \kappa\mathcal{R}(t) - (\beta\mathcal{F}(t) + \mu)\mathcal{S}(t), \\ \frac{d\mathcal{E}(t)}{dt} &= \beta\mathcal{F}(t)\mathcal{S}(t) - (\delta + \mu)\mathcal{E}(t), \\ \frac{d\mathcal{I}(t)}{dt} &= \theta\delta\mathcal{E}(t) - (p + \mu)\mathcal{I}(t), \\ \frac{d\mathcal{A}(t)}{dt} &= (1-\theta)\delta\mathcal{E}(t) - (q + \mu)\mathcal{A}(t), \\ \frac{d\mathcal{R}(t)}{dt} &= p\mathcal{I}(t) + q\mathcal{A}(t) - (\kappa + \mu)\mathcal{R}(t), \\ \frac{d\mathcal{V}(t)}{dt} &= \lambda - (\gamma(\mathcal{I}(t) + \mathcal{A}(t)) + \upsilon)\mathcal{V}(t), \\ \frac{d\mathcal{F}(t)}{dt} &= \gamma(\mathcal{I}(t) + \mathcal{A}(t))\mathcal{V}(t) - \upsilon\mathcal{F}(t), \end{cases} \tag{4.3}$$

along with the positive initial conditions

$$\mathcal{S}(0) = \varphi_1,\ \mathcal{E}(0) = \varphi_2,\ \mathcal{I}(0) = \varphi_3,\ \mathcal{A}(0) = \varphi_4,\ \mathcal{R}(0) = \varphi_5,\ \mathcal{V}(0) = \varphi_6,\ \mathcal{F}(0) = \varphi_7. \tag{4.4}$$

4.2.2 Existence Results of Solutions for the Normalized Model

In this section, we explore the existence and uniqueness of solutions to problem (4.6)–(4.7) using Banach's fixed-point theorem.

Let $\varphi = (\mathcal{S}, \mathcal{E}, \mathcal{I}, \mathcal{A}, \mathcal{R}, \mathcal{V}, \mathcal{F}) \in \Omega$, where $\Omega = [C([0, \ell], [0, 1])]^7$ is a Banach space with

$$\|\varphi\|_\Omega = \max\{\|\mathcal{S}\|_\infty, \|\mathcal{E}\|_\infty, \|\mathcal{I}\|_\infty, \|\mathcal{A}\|_\infty, \|\mathcal{R}\|_\infty, \|\mathcal{V}\|_\infty, \|\mathcal{F}\|_\infty\}$$

and let $\psi = (\psi_1, \psi_2, \psi_3, \psi_4, \psi_5, \psi_6, \psi_7)$, be such that

$$\begin{cases} \psi_1(t, \varphi(t)) &= \Lambda - (\beta\mathcal{F}(t) + \mu)\mathcal{S}(t) + \kappa\mathcal{R}(t), \\ \psi_2(t, \varphi(t)) &= \beta\mathcal{F}(t)\mathcal{S}(t) - (\delta + \mu)\mathcal{E}(t), \\ \psi_3(t, \varphi(t)) &= \theta\delta\mathcal{E}(t) - (p + \mu)\mathcal{I}(t), \\ \psi_4(t, \varphi(t)) &= (1-\theta)\delta\mathcal{E}(t) - (q + \mu)\mathcal{A}(t), \\ \psi_5(t, \varphi(t)) &= p\mathcal{I}(t) + q\mathcal{A}(t) - (\kappa + \mu)\mathcal{R}(t), \\ \psi_6(t, \varphi(t)) &= \lambda - (\gamma(\mathcal{I}(t) + \mathcal{A}(t)) + \upsilon)\mathcal{V}(t), \\ \psi_7(t, \varphi(t)) &= \gamma(\mathcal{I}(t) + \mathcal{A}(t))\mathcal{V}(t) - \upsilon\mathcal{F}(t). \end{cases} \tag{4.5}$$

It is evident that ψ is a continuous function.

Applying an integral to both sides of the system yields

$$\frac{d\varphi(t)}{dt} = \psi(t, \varphi(t)), \tag{4.6}$$

taking into account the conditions

$$\varphi(0) = \varphi_0 = (\varphi_1, \varphi_2, \varphi_3, \varphi_4, \varphi_5, \varphi_6, \varphi_7), \tag{4.7}$$

we obtain the following system of integral equations

$$\varphi(t) = \varphi_0 + \int_0^t \psi(\tau, \varphi(\tau))\, d\tau,$$

which is equivalent to the original problem (4.6)–(4.7).

Theorem 4.1. *Let $\beta, \delta, \theta, \kappa, \gamma, q, p, \upsilon, \mu, \ell \in \mathbb{R}_+$, be such that*

$$\eta = \max\{\beta + \mu, \delta + \mu, p + \mu, q + \mu, \kappa + \mu, \gamma + \upsilon\}.$$

If

$$\eta\ell < 1, \tag{4.8}$$

thus, there is a unique solution to the problem (4.6)–(4.7) on $[0, \ell]$.

Proof. The proof begins with transformation of problem (4.6)–(4.7) into a fixed-point problem $\mathcal{T}\varphi(t) = \varphi(t)$, with

$$\mathcal{T}\varphi(t) = (\mathcal{T}_1\varphi(t), \mathcal{T}_2\varphi(t), \mathcal{T}_3\varphi(t), \mathcal{T}_4\varphi(t), \mathcal{T}_5\varphi(t), \mathcal{T}_6\varphi(t), \mathcal{T}_7\varphi(t))$$

and

$$\mathcal{T}\varphi(t) = \varphi_0 + \int_0^t \psi(\tau, \varphi(\tau))\, d\tau. \tag{4.9}$$

Observing that for $\varphi \in \Omega$, the operators $\mathcal{T}_i\varphi$ for $1 \leq i \leq 7$ are continuous. Consequently, $\mathcal{T}\varphi$ is an element of Ω, with

$$\|\mathcal{T}\varphi\|_\Omega = \max_{1\leq i\leq 7} \|\mathcal{T}_i\varphi\|_\infty .$$

The equivalence between problems (4.6)–(4.7) and (4.9) implies that $\mathcal{T}$ includes fixed points for solving the aforementioned problem.
Let $\varphi, \omega \in \Omega$, then

$$|\mathcal{T}_i\varphi(t) - \mathcal{T}_i\omega(t)| \leq \int_0^t |\psi_i(\tau, \varphi(\tau)) - \psi_i(\tau, \omega(\tau))|\, d\tau, \ \forall i \in \overline{1,7}, \tag{4.10}$$

where ψ_i satisfies (4.5) for each $1 \leq i \leq 7$. We have

$$\begin{aligned}
|\psi_1(t, \varphi(t)) - \psi_1(t, \omega(t))| &= |\kappa(\mathcal{R}_\varphi(t) - \mathcal{R}_\omega(t)) - [(\beta\mathcal{F}_\varphi(t) + \mu)\mathcal{S}_\varphi(t) \\
&\quad - (\beta\mathcal{F}_\omega(t) + \mu)\mathcal{S}_\omega(t)]| \\
&\leq \kappa|\mathcal{R}_\varphi(t) - \mathcal{R}_\omega(t)| + \mu|\mathcal{S}_\varphi(t) - \mathcal{S}_\omega(t)| \\
&\quad + |\beta\mathcal{F}_\varphi(t)\mathcal{S}_\varphi(t) - \beta\mathcal{F}_\omega(t)\mathcal{S}_\omega(t)| \\
&\leq \kappa|\mathcal{R}_\varphi(t) - \mathcal{R}_\omega(t)| + (\beta + \mu)|\mathcal{S}_\varphi(t) - \mathcal{S}_\omega(t)| \\
&\quad + \beta|\mathcal{F}_\varphi(t) - \mathcal{F}_\omega(t)| \\
&\leq \max\{\kappa, \beta + \mu\}\|\varphi - \omega\|_\Omega .
\end{aligned} \tag{4.11}$$

Similarly, we obtain for all $t \in [0, \ell]$,

$$\begin{aligned}
|\psi_2(t, \varphi(t)) - \psi_2(t, \omega(t))| &\leq \max\{\beta, \delta + \mu\} \|\varphi - \omega\|_\Omega, \\
|\psi_3(t, \varphi(t)) - \psi_3(t, \omega(t))| &\leq \max\{\theta\delta, p + \mu\} \|\varphi - \omega\|_\Omega, \\
|\psi_4(t, \varphi(t)) - \psi_4(t, \omega(t))| &\leq \max\{(1-\theta)\delta, q + \mu\} \|\varphi - \omega\|_\Omega, \\
|\psi_5(t, \varphi(t)) - \psi_5(t, \omega(t))| &\leq \max\{p, q, \kappa + \mu\} \|\varphi - \omega\|_\Omega, \\
|\psi_6(t, \varphi(t)) - \psi_6(t, \omega(t))| &\leq (\gamma + \upsilon) \|\varphi - \omega\|_\Omega, \\
|\psi_7(t, \varphi(t)) - \psi_7(t, \omega(t))| &\leq \max\{\gamma, \upsilon\} \|\varphi - \omega\|_\Omega.
\end{aligned}$$

Then

$$|\psi_i(t, \varphi(t)) - \psi_i(t, \omega(t))| \leq \eta \|\varphi - \omega\|_\Omega, \ \forall i \in \overline{1,7}. \tag{4.12}$$

From (4.10), we find

$$\|\mathcal{T}_i\varphi - \mathcal{T}_i\omega\|_\infty \leq \eta\ell \|\varphi - \omega\|_\Omega, \ \forall i \in \overline{1,7}.$$

and

$$\|\mathcal{T}\varphi - \mathcal{T}\omega\|_\Omega \leq \eta\ell \|\varphi - \omega\|_\Omega.$$

Referring to (4.8), $\mathcal{T}$ is considered as a contraction operator. By employing Banach's Contraction Principle, it can be deduced that $\mathcal{T}$ possesses a unique fixed point, which corresponds to the unique solution of the problem (4.6)–(4.7) on $[0, \ell]$. □

4.2.3 Ulam-Hyers Stability for the Normalized Model

Definition 4.1. *The system of differential equations (4.6) is Ulam-Hyers stable if there exists a real number $c > 0$ such that for each $\varepsilon = \max\{\varepsilon_1, \ldots, \varepsilon_7\}$ with $\varepsilon_i > 0$, $i \in \overline{1,7}$, and for each solution $\omega \in \Omega$ of the inequality*

$$\left| \frac{d}{dt}\omega_i(t) - \psi_i(t, \omega(t)) \right| \leq \varepsilon_i, \quad t \in [0, \ell], \ i \in \overline{1,7}, \tag{4.13}$$

there exists $\varphi \in \Omega$ a solution of (4.6) with

$$\|\omega - \varphi\|_\Omega \leq c\varepsilon.$$

Definition 4.2. *The system of differential equations (4.6) is generalized Ulam-Hyers stable if there exists $\xi \in C(\mathbb{R}_+, \mathbb{R}_+)$, $\xi(0) = 0$, such that for each solution $\omega \in \Omega$ of inequality (4.13), there exists a solution $\varphi \in \Omega$ of (4.6) with*

$$\|\omega - \varphi\|_\Omega \leq \xi(\varepsilon).$$

Remark 4.1 ([24, 21]). *If $\omega \in \Omega$ is a solution of inequality (4.13), then there exist $(\varepsilon_i)_{i\in\overline{1,7}} > 0$ and $\phi \in \Omega$, such that*

1. $\frac{d}{dt}\omega_i(t) = \psi_i(t, \omega(t)) + \phi_i(t), t \in [0, \ell], \ i \in \overline{1,7}$,
2. $|\phi_i(t)| \leq \varepsilon_i$, *for all* $t \in [0, \ell]$, *and each* $i \in \overline{1,7}$.

The subsequent lemma aids in establishing the stability of system (4.6).

Lemma 4.2. *If $\omega \in \Omega$ is the solution of inequality (4.13), then there exist $(\varepsilon_i)_{i\in\overline{1,7}} > 0$ such that ω will be the solution of the inequality*

$$\left|\omega_i(t) - \omega_i(0) - \int_0^t \psi_i(\tau, \omega(\tau))\, d\tau\right| \leq \ell\varepsilon_i,$$

for each $i \in \overline{1,7}$.

Proof. If ω is a solution of (4.13), we have from Remark 4.1

$$\begin{cases} \frac{d}{dt}\omega_i(t) = \psi_i(t, \omega(t)) + \phi_i(t), & t \in [0, \ell], \ i \in \overline{1,7}, \\ |\phi_i(t)| \leq \varepsilon_i, & (\varepsilon_i)_{i\in\overline{1,7}} > 0, \end{cases}$$

hence

$$\omega_i(t) = \omega_i(0) + \int_0^t [\psi_i(\tau, \omega(\tau)) + \phi_i(\tau)]\, d\tau.$$

Also,

$$\begin{aligned} \left|\omega_i(t) - \omega_i(0) - \int_0^t \psi_i(\tau, \omega(\tau))\, d\tau\right| &= \left|\omega_i(0) + \int_0^t [\psi_i(\tau, \omega(\tau)) + \phi_i(\tau)]\, d\tau \right. \\ &\quad \left. - \omega_i(0) - \int_0^t \psi_i(\tau, \omega(\tau))\, d\tau\right| \\ &\leq \int_0^t |\phi_i(\tau)|\, d\tau \leq \ell\varepsilon_i, \quad \forall i \in \overline{1,7}. \end{aligned}$$

That establishes the lemma. □

Theorem 4.2. *Assuming that (4.8) holds, system (4.6) is Ulam-Hyers stable. Furthermore, it can also be asserted that (4.6) is a generalized Ulam-Hyers stable system.*

Proof. Let $(\varepsilon_i)_{i\in\overline{1,7}} > 0$, we define $\omega \in \Omega$ as a solution of the inequality

$$\left|\frac{d}{dt}\omega_i(t) - \psi_i(t, \omega(t))\right| \leq \varepsilon_i, \quad t \in [0, \ell], \ i \in \overline{1,7},$$

and $\varphi \in \Omega$ is the unique solution of system (4.6) with the conditions

$$\varphi_i(0) = \omega_i(0), \quad \forall i \in \overline{1,7}.$$

Then

$$\varphi_i(t) = \omega_i(0) + \int_0^t \psi_i(\tau, \varphi(\tau))\, d\tau,$$

and

$$\begin{aligned} |\omega_i(t) - \varphi_i(t)| &= \left|\omega_i(t) - \omega_i(0) - \int_0^t \psi_i(\tau, \varphi(\tau))\, d\tau\right| \\ &\leq \left|\omega_i(t) - \omega_i(0) - \int_0^t \psi_i(\tau, \omega(\tau))\, d\tau\right| \\ &\quad + \int_0^t |\psi_i(\tau, \omega(\tau)) - \psi_i(\tau, \varphi(\tau))|\, d\tau. \end{aligned}$$

Using (4.12), and Lemma 4.2, we get

$$|\omega_i(t) - \varphi_i(t)| \leq \ell(\varepsilon_i + \eta \|\varphi - \omega\|_\Omega), \quad \forall t \in [0, \ell], \ \forall i \in \overline{1,7}.$$

Taking the maximum from both sides, we obtain

$$\|\varphi - \omega\|_\Omega \leq \ell(\varepsilon + \eta \|\varphi - \omega\|_\Omega).$$

Thus

$$\|\varphi - \omega\|_\Omega \leq c\varepsilon,$$

where $c = \frac{\ell}{1-\eta\ell}$. This implies that system (4.6) is stable in the Ulam-Hyers sense and is consequently generalized Ulam-Hyers stable if we set $\xi(t) = ct$. □

4.3 Analysis for the SEIAR(N)–SI(M) Model

4.3.1 Basic Reproduction Number and Equilibrium Points

Theorem 4.3. *The basic reproduction number of system (4.3) is determined by*

$$\mathfrak{Rb} = \sqrt{\frac{\beta\gamma\lambda\Lambda}{\upsilon^2\mu(\delta+\mu)}\left(\frac{\theta\delta}{p+\mu} + \frac{(1-\theta)\delta}{q+\mu}\right)}. \tag{4.14}$$

Proof. Because the SEIAR(N)–SI(M) model is composed of infection components $\mathcal{E}$, $\mathcal{I}$, $\mathcal{A}$, and $\mathcal{F}$, we obtain:

$$y_i - z_i = \begin{pmatrix} \beta\mathcal{F}(t)\mathcal{S}(t) - (\delta+\mu)\mathcal{E}(t) \\ \theta\delta\mathcal{E}(t) - (p+\mu)\mathcal{I}(t) \\ (1-\theta)\delta\mathcal{E}(t) - (q+\mu)\mathcal{A}(t) \\ \gamma(\mathcal{I}(t)+\mathcal{A}(t))\mathcal{V}(t) - \upsilon\mathcal{F}(t) \end{pmatrix}.$$

Accordingly,

$$y_i = \begin{pmatrix} \beta\mathcal{F}(t)\mathcal{S}(t) \\ 0 \\ 0 \\ \gamma(\mathcal{I}(t)+\mathcal{A}(t))\mathcal{V}(t) \end{pmatrix}, \; z_i = \begin{pmatrix} (\delta+\mu)\mathcal{E}(t) \\ -\theta\delta\mathcal{E}(t) + (p+\mu)\mathcal{I}(t) \\ -(1-\theta)\delta\mathcal{E}(t) + (q+\mu)\mathcal{A}(t) \\ \upsilon\mathcal{F}(t) \end{pmatrix}.$$

Here, y_i denotes the rate of new infections appearing in compartment i, and z_i denotes the rate of transitions between compartment i and other infected compartments for each $i \in \{1,2,3,4\}$.

The new infection matrix $\mathcal{Y}$ and transition matrix $\mathcal{Z}$ are assessed at the disease-free equilibrium point $\mathfrak{Dfp}$ (Theorem 4.4), as follows:

$$\mathcal{Y} = \begin{pmatrix} 0 & 0 & 0 & \beta\bar{\mathcal{S}} \\ 0 & 0 & 0 & 0 \\ 0 & 0 & 0 & 0 \\ 0 & \gamma\bar{\mathcal{V}} & \gamma\bar{\mathcal{V}} & 0 \end{pmatrix}, \; \mathcal{Z} = \begin{pmatrix} \delta+\mu & 0 & 0 & 0 \\ -\theta\delta & p+\mu & 0 & 0 \\ -(1-\theta)\delta & 0 & q+\mu & 0 \\ 0 & 0 & 0 & \upsilon \end{pmatrix}.$$

Following the next-generation matrix principle, the basic reproduction number is defined as the spectral radius of matrix $\mathcal{Y}\mathcal{Z}^{-1}$ and is given by (4.14). □

The initial step in comprehending a differential equation is to identify equilibrium points. In epidemiology, we are concerned with two types of equilibrium point:

- Disease-free equilibrium is defined as the point at which no disease (or death from disease) is introduced into the population and is depicted in the model as $\mathcal{E} = \mathcal{I} = \mathcal{A} = \mathcal{F} = 0$.
- Other equilibrium points, where $\mathcal{I} \neq 0$, $\mathcal{A} \neq 0$ and $\mathcal{F} \neq 0$, are indicated as endemic equilibrium points (or outbreak equilibrium points).

We define the positive real values

$$\lambda_1 = \delta + \mu, \qquad \lambda_2 = p + \mu,$$
$$\lambda_3 = q + \mu, \qquad \lambda_4 = \kappa + \mu,$$

to facilitate the calculations and establish the following theorem.

Theorem 4.4. *The system (4.3) has two types of equilibrium points*

1. *Disease-free equilibrium*

$$\mathfrak{Dfp} = \left(\bar{\mathcal{S}}, \bar{\mathcal{E}}, \bar{\mathcal{I}}, \bar{\mathcal{A}}, \bar{\mathcal{R}}, \bar{\mathcal{V}}, \bar{\mathcal{F}}\right) = \left(\frac{\Lambda}{\mu}, 0, 0, 0, 0, \frac{\lambda}{\upsilon}, 0\right).$$

2. *Endemic equilibrium point* $\mathfrak{Eqp} = (\mathcal{S}^*, \mathcal{E}^*, \mathcal{I}^*, \mathcal{A}^*, \mathcal{R}^*, \mathcal{V}^*, \mathcal{F}^*)$ *which is*

$$\mathfrak{Eqp} = \left(\mathcal{S}^*, \mathcal{E}^*, \frac{\theta\delta}{\lambda_2}\mathcal{E}^*, \frac{(1-\theta)\,\delta}{\lambda_3}\mathcal{E}^*, \left(\frac{p\theta\delta}{\lambda_2\lambda_4} + \frac{q\,(1-\theta)\,\delta}{\lambda_3\lambda_4}\right)\mathcal{E}^*, \frac{\lambda}{\gamma\lambda_5\mathcal{E}^* + \upsilon}, \frac{\gamma\lambda\lambda_5\mathcal{E}^*}{\upsilon\left(\gamma\lambda_5\mathcal{E}^* + \upsilon\right)}\right),$$

where

$$\mathcal{S}^* = \bar{\mathcal{S}} - \frac{\lambda_2\lambda_3\left(\lambda_1 + \kappa\right) + \kappa\delta\left(\theta\lambda_3 + (1-\theta)\,\lambda_2\right)}{\lambda_2\lambda_3\lambda_4}\mathcal{E}^*,$$

also

$$\mathcal{E}^* = \frac{\upsilon^2\lambda_1\lambda_2\lambda_3\lambda_4}{\gamma\lambda_5\left[\upsilon\lambda_1\lambda_2\lambda_3\lambda_4 + \beta\lambda\left[\lambda_2\lambda_3\left(\lambda_1 + \kappa\right) + \kappa\delta\left(\theta\lambda_3 + (1-\theta)\,\lambda_2\right)\right]\right]}\left(\mathfrak{Rb}^2 - 1\right),$$

with

$$\lambda_5 = \frac{\theta\delta}{\lambda_2} + \frac{(1-\theta)\,\delta}{\lambda_3},$$

The existence of the endemic equilibrium point depends on $\mathfrak{Rb} > 1$.

Proof. To determine the equilibrium points for system (4.3), we set $\frac{d\varphi\,(t)}{dt} = \vec{0}$, with $\varphi = (\mathcal{S}, \mathcal{E}, \mathcal{I}, \mathcal{A}, \mathcal{R}, \mathcal{V}, \mathcal{F})$. Therefore

$$\begin{cases} 0 &= \Lambda + \kappa\mathcal{R}\,(t) - \left(\beta\mathcal{F}\,(t) + \mu\right)\mathcal{S}\,(t)\,, & (eq1)\\ 0 &= \beta\mathcal{F}\,(t)\,\mathcal{S}\,(t) - \lambda_1\mathcal{E}\,(t)\,, & (eq2)\\ 0 &= \theta\delta\mathcal{E}\,(t) - \lambda_2\mathcal{I}\,(t)\,, & (eq3)\\ 0 &= (1-\theta)\,\delta\mathcal{E}\,(t) - \lambda_3\mathcal{A}\,(t)\,, & (eq4)\\ 0 &= p\mathcal{I}\,(t) + q\mathcal{A}\,(t) - \lambda_4\mathcal{R}\,(t)\,, & (eq5)\\ 0 &= \lambda - \left(\gamma\left(\mathcal{I}\,(t) + \mathcal{A}\,(t)\right) + \upsilon\right)\mathcal{V}\,(t)\,, & (eq6)\\ 0 &= \gamma\left(\mathcal{I}\,(t) + \mathcal{A}\,(t)\right)\mathcal{V}\,(t) - \upsilon\mathcal{F}\,(t)\,, & (eq7) \end{cases}$$

From equations $(eq3)$ and $(eq4)$, we have

$$\mathcal{I}(t)=\frac{\theta\delta}{\lambda_2}\mathcal{E}(t) \quad \text{and} \quad \mathcal{A}(t)=\frac{(1-\theta)\,\delta}{\lambda_3}\mathcal{E}(t).$$

then we replace it in $(eq5)$, $(eq6)$, and $(eq7)$, to get

$$\mathcal{R}(t)=\left(\frac{p\theta\delta}{\lambda_2\lambda_4}+\frac{q(1-\theta)\,\delta}{\lambda_3}\right)\mathcal{E}(t), \qquad \mathcal{V}(t)=\frac{\lambda}{\gamma\lambda_5\mathcal{E}(t)+\upsilon}, \qquad \mathcal{F}(t)=\frac{\gamma\lambda\lambda_5\mathcal{E}(t)}{\upsilon(\gamma\lambda_5\mathcal{E}(t)+\upsilon)}.$$

If we add $(eq1)$ to $(eq2)$ we obtain

$$\mathcal{S}(t)=\bar{\mathcal{S}}-\frac{\lambda_2\lambda_3(\lambda_1+\kappa)+\kappa\delta(\theta\lambda_3+(1-\theta)\lambda_2)}{\lambda_2\lambda_3\lambda_4}\mathcal{E}(t),$$

1. If $\mathcal{E}=0$, we can easily obtain the first disease-free equilibrium point $\mathfrak{Dfp}$.

2. When $\mathcal{E}\neq 0$, equation $(eq2)$ gives us

$$\mathcal{E}^*=\frac{\upsilon^2\lambda_1\lambda_2\lambda_3\lambda_4}{\gamma\lambda_5[\upsilon\lambda_1\lambda_2\lambda_3\lambda_4+\beta\lambda[\lambda_2\lambda_3(\lambda_1+\kappa)+\kappa\delta(\theta\lambda_3+(1-\theta)\lambda_2)]]}\left(\mathfrak{Rb}^2-1\right).$$

Consequently, we obtain the required endemic equilibrium point $\mathfrak{Eqp}$, which exists for $\mathfrak{Rb}>1$.

Hence, the theorem is proved. □

4.3.2 Stability Study of Disease-Free Equilibrium Point

Local Stability Analysis of $\mathfrak{Dfp}$

Theorem 4.5. *Suppose that*

$$\beta\gamma\delta\bar{\mathcal{V}}\bar{\mathcal{S}}<\lambda_1\lambda_2\lambda_3+\lambda_1\lambda_2\upsilon+\lambda_1\lambda_3\upsilon+\lambda_2\lambda_3\upsilon,$$

then, $\mathfrak{Dfp}$ of the system (4.3) achieves local asymptotic stability when $\mathfrak{Rb}<1$.

Proof. The Jacobian matrix for system (4.3) is expressed as follows

$$J=\begin{pmatrix}
\frac{\partial\psi_1}{\partial\mathcal{S}} & \frac{\partial\psi_1}{\partial\mathcal{E}} & \frac{\partial\psi_1}{\partial\mathcal{I}} & \frac{\partial\psi_1}{\partial\mathcal{A}} & \frac{\partial\psi_1}{\partial\mathcal{R}} & \frac{\partial\psi_1}{\partial\mathcal{V}} & \frac{\partial\psi_1}{\partial\mathcal{F}}\\
\frac{\partial\psi_2}{\partial\mathcal{S}} & \frac{\partial\psi_2}{\partial\mathcal{E}} & \frac{\partial\psi_2}{\partial\mathcal{I}} & \frac{\partial\psi_2}{\partial\mathcal{A}} & \frac{\partial\psi_2}{\partial\mathcal{R}} & \frac{\partial\psi_2}{\partial\mathcal{V}} & \frac{\partial\psi_2}{\partial\mathcal{F}}\\
\frac{\partial\psi_3}{\partial\mathcal{S}} & \frac{\partial\psi_3}{\partial\mathcal{E}} & \frac{\partial\psi_3}{\partial\mathcal{I}} & \frac{\partial\psi_3}{\partial\mathcal{A}} & \frac{\partial\psi_3}{\partial\mathcal{R}} & \frac{\partial\psi_3}{\partial\mathcal{V}} & \frac{\partial\psi_3}{\partial\mathcal{F}}\\
\frac{\partial\psi_4}{\partial\mathcal{S}} & \frac{\partial\psi_4}{\partial\mathcal{E}} & \frac{\partial\psi_4}{\partial\mathcal{I}} & \frac{\partial\psi_4}{\partial\mathcal{A}} & \frac{\partial\psi_4}{\partial\mathcal{R}} & \frac{\partial\psi_4}{\partial\mathcal{V}} & \frac{\partial\psi_4}{\partial\mathcal{F}}\\
\frac{\partial\psi_5}{\partial\mathcal{S}} & \frac{\partial\psi_5}{\partial\mathcal{E}} & \frac{\partial\psi_5}{\partial\mathcal{I}} & \frac{\partial\psi_5}{\partial\mathcal{A}} & \frac{\partial\psi_5}{\partial\mathcal{R}} & \frac{\partial\psi_5}{\partial\mathcal{V}} & \frac{\partial\psi_5}{\partial\mathcal{F}}\\
\frac{\partial\psi_6}{\partial\mathcal{S}} & \frac{\partial\psi_6}{\partial\mathcal{E}} & \frac{\partial\psi_6}{\partial\mathcal{I}} & \frac{\partial\psi_6}{\partial\mathcal{A}} & \frac{\partial\psi_6}{\partial\mathcal{R}} & \frac{\partial\psi_6}{\partial\mathcal{V}} & \frac{\partial\psi_6}{\partial\mathcal{F}}\\
\frac{\partial\psi_7}{\partial\mathcal{S}} & \frac{\partial\psi_7}{\partial\mathcal{E}} & \frac{\partial\psi_7}{\partial\mathcal{I}} & \frac{\partial\psi_7}{\partial\mathcal{A}} & \frac{\partial\psi_7}{\partial\mathcal{R}} & \frac{\partial\psi_7}{\partial\mathcal{V}} & \frac{\partial\psi_7}{\partial\mathcal{F}}
\end{pmatrix}$$

where $\psi_{1\leq i\leq 7}\left(t,\varphi\left(t\right)\right)$ represents the right-hand side of (4.3). Then

$$J=\begin{pmatrix}
-\left(\beta\mathcal{F}+\mu\right) & 0 & 0 & 0 & \kappa & 0 & -\beta\mathcal{S}\\
\beta\mathcal{F} & -\lambda_1 & 0 & 0 & 0 & 0 & \beta\mathcal{S}\\
0 & \theta\delta & -\lambda_2 & 0 & 0 & 0 & 0\\
0 & \left(1-\theta\right)\delta & 0 & -\lambda_3 & 0 & 0 & 0\\
0 & 0 & p & q & -\lambda_4 & 0 & 0\\
0 & 0 & -\gamma\mathcal{V} & -\gamma\mathcal{V} & 0 & -\left(\gamma\left(\mathcal{I}+\mathcal{A}\right)+\upsilon\right) & 0\\
0 & 0 & \gamma\mathcal{V} & \gamma\mathcal{V} & 0 & \gamma\left(\mathcal{I}+\mathcal{A}\right) & -\upsilon
\end{pmatrix}.$$

The eigenvalues of $J\left(\mathfrak{Dfp}\right)$ are given as the roots of the following characteristic polynomial

$$P_1\left(X\right)=-\left(\mu+X\right)\left(\upsilon+X\right)\left(\lambda_4+X\right)\left(X^4+a_3X^3+a_2X^2+a_1X+a_0\right),$$

with

$$\begin{aligned}
a_0 &= \upsilon\lambda_1\lambda_2\lambda_3\left(1-\mathfrak{Rb}^2\right),\\
a_1 &= \lambda_1\lambda_2\lambda_3+\lambda_1\lambda_2\upsilon+\lambda_1\lambda_3\upsilon+\lambda_2\lambda_3\upsilon-\beta\gamma\delta\bar{\mathcal{S}}\bar{\mathcal{V}},\\
a_2 &= \lambda_1\lambda_2+\lambda_1\lambda_3+\lambda_2\lambda_3+\lambda_1\upsilon+\lambda_2\upsilon+\lambda_3\upsilon,\\
a_3 &= \lambda_1+\lambda_2+\lambda_3+\upsilon.
\end{aligned}$$

As $\beta\gamma\delta\bar{\mathcal{V}}\bar{\mathcal{S}}<\lambda_1\lambda_2\lambda_3+\lambda_1\lambda_2\upsilon+\lambda_1\lambda_3\upsilon+\lambda_2\lambda_3\upsilon$, we find a_0,a_1,a_2 and a_3 are nonnegative coefficients when $\mathfrak{Rb}<1$. According to Descartes's rule, the roots of $P_1\left(X\right)$ are negative reals or complexes of negative real parts and that makes $\mathfrak{Dfp}$ is locally asymptotically stable. □

Global Stability Analysis of $\mathfrak{Dfp}$

Theorem 4.6. *The disease-free equilibrium point $\mathfrak{Dfp}$ of system (4.3) is globally asymptotically stable if $\mathfrak{Rb}<1$.*

Proof. To prove the theorem, we examine the following Lyapunov function

$$W\left(\mathcal{S},\mathcal{E},\mathcal{I},\mathcal{A},\mathcal{R},\mathcal{V},\mathcal{F}\right)=c_1\mathcal{E}+c_2\mathcal{I}+c_3\mathcal{A}+c_4\mathcal{F}.$$

We consider c_i to be positive constants for $i\in\{1,2,3,4\}$, which will be determined later.

The derivative of W along with the solution of system (4.3) is calculated as follows

$$\begin{aligned}
\frac{dW}{dt} &= c_1\frac{d\mathcal{E}}{dt} + c_2\frac{d\mathcal{I}}{dt} + c_3\frac{d\mathcal{A}}{dt} + c_4\frac{d\mathcal{F}}{dt} \\
&= c_1\left[\beta\mathcal{F}\mathcal{S} - \lambda_1\mathcal{E}\right] + c_2\left[\theta\delta\mathcal{E} - \lambda_2\mathcal{I}\right] + c_3\left[(1-\theta)\,\delta\mathcal{E} - \lambda_3\mathcal{A}\right] \\
&+ c_4\left[\gamma\left(\mathcal{I}+\mathcal{A}\right)\mathcal{V} - \upsilon\mathcal{F}\right] \\
&\leq c_1\left[\frac{\beta\Lambda}{\mu}\mathcal{F} - \lambda_1\mathcal{E}\right] + c_2\left[\theta\delta\mathcal{E} - \lambda_2\mathcal{I}\right] + c_3\left[(1-\theta)\,\delta\mathcal{E} - \lambda_3\mathcal{A}\right] \\
&+ c_4\left[\gamma\left(\mathcal{I}+\mathcal{A}\right)\frac{\lambda}{\upsilon} - \upsilon\mathcal{F}\right] \\
&= \left[-c_1\lambda_1 + c_2\theta\delta + c_3\left(1-\theta\right)\delta\right]\mathcal{E} + \left[-c_2\lambda_2 + c_4\frac{\gamma\lambda}{\upsilon}\right]\mathcal{I} \\
&+ \left[-c_3\lambda_3 + c_4\frac{\gamma\lambda}{\upsilon}\right]\mathcal{A} + \left[c_1\frac{\beta\Lambda}{\mu} - c_4\upsilon\right]\mathcal{F}.
\end{aligned}$$

By choosing $c_1 = \frac{\mu\upsilon}{\beta\Lambda}\lambda_2\lambda_3$, $c_2 = \frac{\gamma\lambda}{\upsilon}\lambda_3$, $c_3 = \frac{\gamma\lambda}{\upsilon}\lambda_2$, and $c_4 = \lambda_2\lambda_3$, we obtain

$$\frac{dW}{dt} \leq \frac{\mu\upsilon}{\beta\Lambda}\lambda_1\lambda_2\lambda_3\left(\mathfrak{Rb}^2 - 1\right)\mathcal{E}.$$

Thus, if $\mathfrak{Rb} < 1$, then $\frac{dW}{dt} < 0$. According to LaSalle's invariance principle [58], this implies that $\mathfrak{Dfp}$ is globally asymptotically stable. □

4.3.3 Stability Study of Endemic Equilibrium Point

Local Stability Analysis of $\mathfrak{Eqp}$

Let g_0, g_1, g_2, and g_3 be such that

$$\begin{aligned}
g_0 &= \frac{\left(\gamma\left(\mathcal{I}^*+\mathcal{A}^*\right)+\upsilon\right)\left[\lambda_1\lambda_2\lambda_3\lambda_4 + \beta\mathcal{F}^*\left(\lambda_2\lambda_3\left(\lambda_1+\kappa\right) + \delta\kappa\left(\theta\lambda_3 + \left(1-\theta\right)\lambda_2\right)\right)\right]}{\delta\lambda_4\left(\theta\lambda_3 + \left(1-\theta\right)\lambda_2\right)}, \\
g_1 &= \frac{\beta\mathcal{F}^*\kappa\left[\mu\lambda_2\lambda_3\left(\lambda_1+\kappa\right) + \mu\kappa\delta\left(\theta\lambda_3 + \left(1-\theta\right)\lambda_2\right) + \left(\gamma\left(\mathcal{I}^*+\mathcal{A}^*\right)+\upsilon\right)\left(\lambda_9 + \kappa\delta\left(p\theta + q\left(1-\theta\right)\right)\right)\right]}{\mu\lambda_4 + \left(\lambda_4+\mu\right)\left(\theta\lambda_3 + \left(1-\theta\right)\lambda_2\right)} \\
&+ \frac{\mu\lambda_1\lambda_2\lambda_3\lambda_4 + \left(\mu\lambda_8 + \lambda_1\lambda_2\lambda_3\lambda_4\right)\left(\gamma\left(\mathcal{I}^*+\mathcal{A}^*\right)+\upsilon\right)}{\mu\lambda_4 + \left(\lambda_4+\mu\right)\left(\theta\lambda_3 + \left(1-\theta\right)\lambda_2\right)}, \\
g_2 &= \frac{\lambda_1\lambda_2\lambda_3\lambda_4 + \lambda_8\left(\gamma\left(\mathcal{I}^*+\mathcal{A}^*\right)+\upsilon+\mu\right) + \lambda_7\left(\beta\mathcal{F}^*+\mu\right)\left(\gamma\left(\mathcal{I}^*+\mathcal{A}^*\right)+\upsilon\right)}{\theta\lambda_3 + \left(1-\theta\right)\lambda_2 + \lambda_4 + \mu} \\
&+ \frac{\beta\mathcal{F}^*\left[\lambda_9 + \kappa\delta\left(\theta\lambda_3 + \left(1-\theta\right)\lambda_2 + \mu\right)\right]}{\theta\lambda_3 + \left(1-\theta\right)\lambda_2 + \lambda_4 + \mu}, \\
g_3 &= \lambda_8 + \lambda_6\left(\beta\mathcal{F}^*+\mu\right)\left(\gamma\left(\mathcal{I}^*+\mathcal{A}^*\right)+\upsilon\right) + \lambda_7\left(\gamma\left(\mathcal{I}^*+\mathcal{A}^*\right) + \beta\mathcal{F}^* + \upsilon + \mu\right),
\end{aligned}$$

where

$$\begin{aligned}
\lambda_6 &= \lambda_1+\lambda_2+\lambda_3+\lambda_4, \\
\lambda_7 &= \lambda_1\lambda_2 + \lambda_1\lambda_3 + \lambda_1\lambda_4 + \lambda_2\lambda_3 + \lambda_2\lambda_4 + \lambda_3\lambda_4, \\
\lambda_8 &= \lambda_1\lambda_2\lambda_3 + \lambda_1\lambda_2\lambda_4 + \lambda_1\lambda_3\lambda_4 + \lambda_2\lambda_3\lambda_4, \\
\lambda_9 &= \mu\lambda_2\lambda_3 + \left(\lambda_1+\kappa\right)\left(\mu\lambda_2 + \mu\lambda_3 + \lambda_2\lambda_3\right).
\end{aligned}$$

Theorem 4.7. *If we put*

$$\beta\gamma\delta\mathcal{V}^*\mathcal{S}^* < \min\left\{g_0, g_1, g_2, g_3\right\},$$

then the endemic equilibrium point $\mathfrak{Eqp}$ *of system (4.3) is locally asymptotically stable if* $\mathfrak{Rb} > 1$.

Proof. As shown in the previous section, the Jacobian matrix $J\left(\mathfrak{Eqp}\right)$ for (4.3) is

$$J_{\mathfrak{Eqp}} = \begin{pmatrix} -\left(\beta\mathcal{F}^* + \mu\right) & 0 & 0 & 0 & \kappa & 0 & -\beta\mathcal{S}^* \\ \beta\mathcal{F}^* & -\lambda_1 & 0 & 0 & 0 & 0 & \beta\mathcal{S}^* \\ 0 & \theta\delta & -\lambda_2 & 0 & 0 & 0 & 0 \\ 0 & (1-\theta)\,\delta & 0 & -\lambda_3 & 0 & 0 & 0 \\ 0 & 0 & p & q & -\lambda_4 & 0 & 0 \\ 0 & 0 & -\gamma\mathcal{V}^* & -\gamma\mathcal{V}^* & 0 & -\left(\gamma\left(\mathcal{I}^* + \mathcal{A}^*\right) + \upsilon\right) & 0 \\ 0 & 0 & \gamma\mathcal{V}^* & \gamma\mathcal{V}^* & 0 & \gamma\left(\mathcal{I}^* + \mathcal{A}^*\right) & -\upsilon \end{pmatrix}.$$

The characteristic polynomial is given by

$$P_2\left(X\right) = -\left(\upsilon + X\right)\left(X^6 + a_5X^5 + a_4X^4 + a_3X^3 + a_2X^2 + a_1X + a_0\right),$$

where

$$\begin{aligned} a_0 &= \mu\lambda_2\left(\theta\delta\lambda_3 + (1-\theta)\,\delta\lambda_2\right)\left(g_0 - \beta\gamma\delta\mathcal{V}^*\mathcal{S}^*\right), \\ a_1 &= \left(\mu\lambda_4 + (\lambda_4+\mu)\left(\theta\lambda_3 + (1-\theta)\,\lambda_2\right)\right)\left(g_1 - \beta\gamma\delta\mathcal{V}^*\mathcal{S}^*\right), \\ a_2 &= \left(\theta\lambda_3 + (1-\theta)\,\lambda_2 + \lambda_4 + \mu\right)\left(g_2 - \beta\gamma\delta\mathcal{V}^*\mathcal{S}^*\right), \\ a_3 &= g_3 - \beta\gamma\delta\mathcal{V}^*\mathcal{S}^*, \\ a_4 &= \lambda_7 + \lambda_6\left(\gamma\left(\mathcal{I}^* + \mathcal{A}^*\right) + \beta\mathcal{F}^* + \upsilon + \mu\right) + \left(\gamma\left(\mathcal{I}^* + \mathcal{A}^*\right) + \upsilon\right)\left(\beta\mathcal{F}^* + \mu\right), \\ a_5 &= \lambda_6 + \gamma\left(\mathcal{I}^* + \mathcal{A}^*\right) + \beta\mathcal{F}^* + \upsilon + \mu. \end{aligned}$$

According to Descartes' rule, the roots of $P_2\left(X\right)$ are negative reals or complexes of negative real parts. Therefore, the required result is obtained. □

Global Stability Analysis of $\mathfrak{Eqp}$

From system (4.3), we obtain

$$\begin{cases} \Lambda = \left(\beta\mathcal{F}^* + \mu\right)\mathcal{S}^* - \kappa\mathcal{R}^*, \\ \lambda_1\mathcal{E}^* = \beta\mathcal{F}^*\mathcal{S}^*, \\ \theta\delta\mathcal{E}^* = \lambda_2\mathcal{I}^*, \\ (1-\theta)\,\delta\mathcal{E}^* = \lambda_3\mathcal{A}^*, \\ \lambda_4\mathcal{R}^* = p\mathcal{I}^* + q\mathcal{A}^*, \\ \lambda = \left(\gamma\left(\mathcal{I}^* + \mathcal{A}^*\right) + \upsilon\right)\mathcal{V}^*, \\ \upsilon\mathcal{F}^* = \gamma\left(\mathcal{I}^* + \mathcal{A}^*\right)\mathcal{V}^*. \end{cases}$$

Now, let us define

$$\begin{cases} \mathcal{Z}_1 = \frac{\lambda_1 \mathcal{E}^*}{\mathcal{S}\mathcal{E}} \left(\mathcal{E}^* - \mathcal{E}\right) + \beta \left(\mathcal{F} - \mathcal{F}^*\right) + \frac{\kappa}{\mathcal{S}} \left(\mathcal{R}^* - \mathcal{R}\right), \\ \mathcal{Z}_2 = \frac{\theta\delta}{\mathcal{I}} \left(\mathcal{E}^* - \mathcal{E}\right) + \gamma \left(\mathcal{V} - \mathcal{V}^*\right) + \frac{\gamma\mathcal{V}}{\mathcal{F}} \left(\mathcal{F}^* - \mathcal{F}\right) + \frac{p}{\mathcal{R}} \left(\mathcal{R}^* - \mathcal{R}\right), \\ \mathcal{Z}_3 = \frac{(1-\theta)\delta}{\mathcal{A}} \left(\mathcal{E}^* - \mathcal{E}\right) + \gamma \left(\mathcal{V} - \mathcal{V}^*\right) + \frac{\gamma\mathcal{V}}{\mathcal{F}} \left(\mathcal{F}^* - \mathcal{F}\right) + \frac{q}{\mathcal{R}} \left(\mathcal{R}^* - \mathcal{R}\right), \\ \mathcal{Z}_4 = \frac{\beta\mathcal{S}}{\mathcal{E}} \left(\mathcal{E}^* - \mathcal{E}\right) + \frac{\upsilon\mathcal{F}^*}{\mathcal{V}^*\mathcal{F}} \left(\mathcal{V}^* - \mathcal{V}\right). \end{cases}$$

To prove the theorem concerning global stability, we propose the following hypothesis.

Hyp. There exist three nonnegative functions $\mathcal{X}_1$, $\mathcal{X}_2$, $\mathcal{X}_3$, and $\mathcal{X}_4$ such that

$$\begin{cases} \mathcal{Z}_1 = \left(\mathcal{X}_1 - \frac{\lambda_1 \mathcal{E}^*}{\mathcal{S}^*} - \mu\right) \frac{\mathcal{S}-\mathcal{S}^*}{\mathcal{S}}, \\ \mathcal{Z}_2 = \left(\mathcal{X}_2 - \lambda_2\right) \frac{\mathcal{I}-\mathcal{I}^*}{\mathcal{I}}, \\ \mathcal{Z}_3 = \left(\mathcal{X}_3 - \lambda_3\right) \frac{\mathcal{A}-\mathcal{A}^*}{\mathcal{A}}, \\ \mathcal{Z}_4 = \left(\mathcal{X}_4 - \upsilon\right) \frac{\mathcal{F}-\mathcal{F}^*}{\mathcal{F}}. \end{cases}$$

Theorem 4.8. *Assume that hypothesis (**Hyp**) holds. Then, the endemic equilibrium point* $\mathfrak{Eqp}$ *of system (4.3) is globally asymptotically stable if* $\mathfrak{Rb} > 1$.

Proof. We analyze the following nonlinear Lyapunov function of the Goh-Volterra form:

$$\begin{aligned} W\left(\mathcal{S},\mathcal{E},\mathcal{I},\mathcal{A},\mathcal{R},\mathcal{V},\mathcal{F}\right) &= \left[\mathcal{S}\left(t\right) - \mathcal{S}^* - \mathcal{S}^* \log \tfrac{\mathcal{S}(t)}{\mathcal{S}^*}\right] + \left[\mathcal{E}\left(t\right) - \mathcal{E}^* - \mathcal{E}^* \log \tfrac{\mathcal{E}(t)}{\mathcal{E}^*}\right] \\ &+ \left[\mathcal{I}\left(t\right) - \mathcal{I}^* - \mathcal{I}^* \log \tfrac{\mathcal{I}(t)}{\mathcal{I}^*}\right] + \left[\mathcal{A}\left(t\right) - \mathcal{A}^* - \mathcal{A}^* \log \tfrac{\mathcal{A}(t)}{\mathcal{A}^*}\right] \\ &+ \left[\mathcal{R}\left(t\right) - \mathcal{R}^* - \mathcal{R}^* \log \tfrac{\mathcal{R}(t)}{\mathcal{R}^*}\right] + \left[\mathcal{V}\left(t\right) - \mathcal{V}^* - \mathcal{V}^* \log \tfrac{\mathcal{V}(t)}{\mathcal{V}^*}\right] \\ &+ \left[\mathcal{F}\left(t\right) - \mathcal{F}^* - \mathcal{F}^* \log \tfrac{\mathcal{F}(t)}{\mathcal{F}^*}\right]. \end{aligned}$$

By calculating the derivative of W with respect to time along the solutions of system (4.3), we obtain

$$\begin{aligned} \frac{dW}{dt} \leq &\left(1 - \frac{\mathcal{S}^*}{\mathcal{S}}\right) \frac{d\mathcal{S}}{dt} + \left(1 - \frac{\mathcal{E}^*}{\mathcal{E}}\right) \frac{d\mathcal{E}}{dt} + \left(1 - \frac{\mathcal{I}^*}{\mathcal{I}}\right) \frac{d\mathcal{I}}{dt} \\ &+ \left(1 - \frac{\mathcal{A}^*}{\mathcal{A}}\right) \frac{d\mathcal{A}}{dt} + \left(1 - \frac{\mathcal{R}^*}{\mathcal{R}}\right) \frac{d\mathcal{R}}{dt} + \left(1 - \frac{\mathcal{V}^*}{\mathcal{V}}\right) \frac{d\mathcal{V}}{dt} \\ &+ \left(1 - \frac{\mathcal{F}^*}{\mathcal{F}}\right) \frac{d\mathcal{F}}{dt}. \end{aligned}$$

A simple calculation provides the following result

$$\begin{aligned} \left(1 - \frac{\mathcal{S}^*}{\mathcal{S}}\right) \frac{d\mathcal{S}}{dt} &= \left(1 - \frac{\mathcal{S}^*}{\mathcal{S}}\right) \left[\Lambda + \kappa\mathcal{R} - \left(\beta\mathcal{F} + \mu\right)\mathcal{S}\right] \\ &= \left(1 - \frac{\mathcal{S}^*}{\mathcal{S}}\right) \left[-\kappa\mathcal{R}^* + \left(\beta\mathcal{F}^* + \mu\right)\mathcal{S}^* + \kappa\mathcal{R} - \left(\beta\mathcal{F} + \mu\right)\mathcal{S}\right] \\ &= \frac{\mathcal{S} - \mathcal{S}^*}{\mathcal{S}} \left[-\mu\left(\mathcal{S} - \mathcal{S}^*\right) - \kappa\left(\mathcal{R}^* - \mathcal{R}\right) - \beta\mathcal{F}\mathcal{S} + \beta\mathcal{F}^*\mathcal{S}^*\right]. \end{aligned}$$

As

$$\begin{aligned} \beta\mathcal{F}^*\mathcal{S}^* - \beta\mathcal{F}\mathcal{S} &= \beta\mathcal{F}^*\mathcal{S}^* - \beta\mathcal{F}^*\mathcal{S} + \beta\mathcal{F}^*\mathcal{S} - \beta\mathcal{F}\mathcal{S} \\ &= -\beta\mathcal{S}\left(\mathcal{F} - \mathcal{F}^*\right) - \frac{\lambda_1\mathcal{E}^*}{\mathcal{S}^*}\left(\mathcal{S} - \mathcal{S}^*\right), \end{aligned} \tag{4.15}$$

then

$$\left(1-\frac{\mathcal{S}^*}{\mathcal{S}}\right)\frac{d\mathcal{S}}{dt}=-\left(\frac{\lambda_1\mathcal{E}^*}{\mathcal{S}^*}+\mu\right)\frac{(\mathcal{S}-\mathcal{S}^*)}{\mathcal{S}}-(\mathcal{S}-\mathcal{S}^*)\left[\beta\left(\mathcal{F}-\mathcal{F}^*\right)+\frac{\kappa}{\mathcal{S}}\left(\mathcal{R}^*-\mathcal{R}\right)\right].$$

In same way, we find

$$\begin{aligned}\left(1-\frac{\mathcal{E}^*}{\mathcal{E}}\right)\frac{d\mathcal{E}}{dt} &= \left(1-\frac{\mathcal{E}^*}{\mathcal{E}}\right)\left[\beta\mathcal{F}\mathcal{S}-\lambda_1\mathcal{E}\right]\\ &= \frac{\mathcal{E}-\mathcal{E}^*}{\mathcal{E}}\left[\beta\mathcal{F}\mathcal{S}-\lambda_1\left(\mathcal{E}-\mathcal{E}^*\right)-\lambda_1\mathcal{E}^*\right]\\ &= -\lambda_1\frac{\left(\mathcal{E}-\mathcal{E}^*\right)^2}{\mathcal{E}}-\frac{\mathcal{E}^*-\mathcal{E}}{\mathcal{E}}\left[\beta\mathcal{F}\mathcal{S}-\beta\mathcal{F}^*\mathcal{S}^*\right].\end{aligned}$$

Using (4.15) gives us

$$\left(1-\frac{\mathcal{E}^*}{\mathcal{E}}\right)\frac{d\mathcal{E}}{dt}=-\lambda_1\frac{\left(\mathcal{E}-\mathcal{E}^*\right)^2}{\mathcal{E}}-\frac{\lambda_1\mathcal{E}^*}{\mathcal{S}^*\mathcal{E}}\left(\mathcal{E}^*-\mathcal{E}\right)\left(\mathcal{S}-\mathcal{S}^*\right)-\frac{\beta\mathcal{S}}{\mathcal{E}}\left(\mathcal{E}^*-\mathcal{E}\right)\left(\mathcal{F}-\mathcal{F}^*\right).$$

Next

$$\begin{aligned}\left(1-\frac{\mathcal{I}^*}{\mathcal{I}}\right)\frac{d\mathcal{I}}{dt} &= \left(\frac{\mathcal{I}-\mathcal{I}^*}{\mathcal{I}}\right)\left[\theta\delta\mathcal{E}-\lambda_2\mathcal{I}\right]\\ &= \left(\frac{\mathcal{I}-\mathcal{I}^*}{\mathcal{I}}\right)\left[\theta\delta\mathcal{E}-\lambda_2\left(\mathcal{I}-\mathcal{I}^*\right)-\lambda_2\mathcal{I}^*\right]\\ &= -\lambda_2\frac{\left(\mathcal{I}-\mathcal{I}^*\right)^2}{\mathcal{I}}-\frac{\theta\delta}{\mathcal{I}}\left(\mathcal{I}-\mathcal{I}^*\right)\left(\mathcal{E}^*-\mathcal{E}\right).\end{aligned}$$

Also

$$\begin{aligned}\left(1-\frac{\mathcal{A}^*}{\mathcal{A}}\right)\frac{d\mathcal{A}}{dt} &= \left(1-\frac{\mathcal{A}^*}{\mathcal{A}}\right)\left[\left(1-\theta\right)\delta\mathcal{E}-\lambda_3\mathcal{A}\right]\\ &= \left(\frac{\mathcal{A}-\mathcal{A}^*}{\mathcal{A}}\right)\left[\left(1-\theta\right)\delta\mathcal{E}-\lambda_3\left(\mathcal{A}-\mathcal{A}^*\right)-\lambda_3\mathcal{A}^*\right]\\ &= -\lambda_3\frac{\left(\mathcal{A}-\mathcal{A}^*\right)^2}{\mathcal{A}}-\frac{\left(1-\theta\right)\delta}{\mathcal{A}}\left(\mathcal{A}-\mathcal{A}^*\right)\left(\mathcal{E}^*-\mathcal{E}\right).\end{aligned}$$

and

$$\left(1-\frac{\mathcal{R}^*}{\mathcal{R}}\right)\frac{d\mathcal{R}}{dt}=-\lambda_4\frac{\left(\mathcal{R}-\mathcal{R}^*\right)^2}{\mathcal{R}}-\left(\mathcal{R}^*-\mathcal{R}\right)\left[\frac{p}{\mathcal{R}}\left(\mathcal{I}-\mathcal{I}^*\right)+\frac{q}{\mathcal{R}}\left(\mathcal{A}-\mathcal{A}^*\right)\right].$$

Next

$$\begin{aligned}\left(1-\frac{\mathcal{V}^*}{\mathcal{V}}\right)\frac{d\mathcal{V}}{dt} &= \left(1-\frac{\mathcal{V}^*}{\mathcal{V}}\right)\left[\lambda-\left(\gamma\left(\mathcal{I}+\mathcal{A}\right)+\upsilon\right)\mathcal{V}\right]\\ &= \left(1-\frac{\mathcal{V}^*}{\mathcal{V}}\right)\left[\left(\gamma\left(\mathcal{I}^*+\mathcal{A}^*\right)+\upsilon\right)\mathcal{V}^*-\left(\gamma\left(\mathcal{I}+\mathcal{A}\right)+\upsilon\right)\mathcal{V}\right]\\ &= -\upsilon\frac{\left(\mathcal{V}-\mathcal{V}^*\right)^2}{\mathcal{V}}+\frac{\mathcal{V}-\mathcal{V}^*}{\mathcal{V}}\left[\gamma\left(\mathcal{I}^*+\mathcal{A}^*\right)\mathcal{V}^*-\gamma\left(\mathcal{I}+\mathcal{A}\right)\mathcal{V}\right].\end{aligned}$$

As

$$\begin{aligned}\gamma\left(\mathcal{I}^*+\mathcal{A}^*\right)\mathcal{V}^*-\gamma\left(\mathcal{I}+\mathcal{A}\right)\mathcal{V} &= \gamma\left(\mathcal{I}^*+\mathcal{A}^*\right)\mathcal{V}^*+\gamma\left(\mathcal{I}^*+\mathcal{A}^*\right)\mathcal{V}\\ &- \gamma\left(\mathcal{I}^*+\mathcal{A}^*\right)\mathcal{V}-\gamma\left(\mathcal{I}+\mathcal{A}\right)\mathcal{V}\\ &= -\gamma\mathcal{V}\left[\left(\mathcal{I}-\mathcal{I}^*\right)+\left(\mathcal{A}-\mathcal{A}^*\right)\right]-\frac{\upsilon\mathcal{F}^*}{\mathcal{V}^*}\left(\mathcal{V}-\mathcal{V}^*\right), \qquad (4.16)\end{aligned}$$

then

$$\left(1-\frac{\mathcal{V}^*}{\mathcal{V}}\right)\frac{d\mathcal{V}}{dt}=-\left(\frac{\upsilon\mathcal{F}^*}{\mathcal{V}^*}+\upsilon\right)\frac{(\mathcal{V}-\mathcal{V}^*)^2}{\mathcal{V}}-\gamma\left(\mathcal{V}-\mathcal{V}^*\right)\left[(\mathcal{I}-\mathcal{I}^*)+(\mathcal{A}-\mathcal{A}^*)\right].$$

Also

$$\begin{aligned}\left(1-\frac{\mathcal{F}^*}{\mathcal{F}}\right)\frac{d\mathcal{F}}{dt} &= \left(1-\frac{\mathcal{F}^*}{\mathcal{F}}\right)\left[\gamma\left(\mathcal{I}+\mathcal{A}\right)\mathcal{V}-\upsilon\mathcal{F}\right]\\ &= \frac{\mathcal{F}-\mathcal{F}^*}{\mathcal{F}}\left[\gamma\left(\mathcal{I}+\mathcal{A}\right)\mathcal{V}-\upsilon\left(\mathcal{F}-\mathcal{F}^*\right)-\upsilon\mathcal{F}^*\right]\\ &= -\upsilon\frac{(\mathcal{V}-\mathcal{V}^*)^2}{\mathcal{V}}-\frac{\mathcal{F}^*-\mathcal{F}}{\mathcal{F}}\left[\gamma\left(\mathcal{I}^*+\mathcal{A}^*\right)\mathcal{V}^*-\gamma\left(\mathcal{I}+\mathcal{A}\right)\mathcal{V}\right].\end{aligned}$$

Using (4.16) gives us

$$\begin{aligned}\left(1-\frac{\mathcal{F}^*}{\mathcal{F}}\right)\frac{d\mathcal{F}}{dt} &= -\upsilon\frac{(\mathcal{V}-\mathcal{V}^*)^2}{\mathcal{V}}-\frac{\upsilon\mathcal{F}^*}{\mathcal{V}^*\mathcal{F}}\left(\mathcal{F}^*-\mathcal{F}\right)\left(\mathcal{V}-\mathcal{V}^*\right)\\ &\quad -\frac{\gamma\mathcal{V}}{\mathcal{F}}\left(\mathcal{F}^*-\mathcal{F}\right)\left[(\mathcal{I}-\mathcal{I}^*)+(\mathcal{A}-\mathcal{A}^*)\right].\end{aligned}$$

Then

$$\begin{aligned}\frac{dW}{dt}\leq &-\left(\frac{\lambda_1\mathcal{E}^*}{\mathcal{S}^*}+\mu\right)\frac{(\mathcal{S}-\mathcal{S}^*)^2}{\mathcal{S}}-\lambda_1\frac{(\mathcal{E}-\mathcal{E}^*)^2}{\mathcal{E}}-\lambda_2\frac{(\mathcal{I}-\mathcal{I}^*)^2}{\mathcal{I}}-\lambda_3\frac{(\mathcal{A}-\mathcal{A}^*)^2}{\mathcal{A}}\\ &-\lambda_4\frac{(\mathcal{R}-\mathcal{R}^*)^2}{\mathcal{R}}-\left(\frac{\upsilon\mathcal{F}^*}{\mathcal{V}^*}+\upsilon\right)\frac{(\mathcal{V}-\mathcal{V}^*)^2}{\mathcal{V}}-\upsilon\frac{(\mathcal{F}-\mathcal{F}^*)^2}{\mathcal{F}}\\ &-\mathcal{H}_1\left(\mathcal{S}-\mathcal{S}^*\right)-\mathcal{H}_2\left(\mathcal{I}-\mathcal{I}^*\right)-\mathcal{H}_3\left(\mathcal{A}-\mathcal{A}^*\right)-\mathcal{H}_4\left(\mathcal{F}-\mathcal{F}^*\right).\end{aligned}$$

By employing (**Hyp**), we get

$$\begin{aligned}\frac{dW}{dt} \leq &-\mathcal{X}_1\frac{(\mathcal{S}-\mathcal{S}^*)^2}{\mathcal{S}}-\lambda_1\frac{(\mathcal{E}-\mathcal{E}^*)^2}{\mathcal{E}}-\mathcal{X}_2\frac{(\mathcal{I}-\mathcal{I}^*)^2}{\mathcal{I}}-\mathcal{X}_3\frac{(\mathcal{A}-\mathcal{A}^*)^2}{\mathcal{A}}\\ &-\lambda_4\frac{(\mathcal{R}-\mathcal{R}^*)^2}{\mathcal{R}}-\left(\frac{\upsilon\mathcal{F}^*}{\mathcal{V}^*}+\upsilon\right)\frac{(\mathcal{V}-\mathcal{V}^*)^2}{\mathcal{V}}-\mathcal{X}_4\frac{(\mathcal{F}-\mathcal{F}^*)^2}{\mathcal{F}}.\end{aligned}$$

Because all parameters are nonnegative, we obtain $\frac{dW}{dt}\leq 0$ when $\mathfrak{Rb}>1$. According to LaSalle's invariance principle [58], $(\mathcal{S},\mathcal{E},\mathcal{I},\mathcal{A},\mathcal{R},\mathcal{V},\mathcal{F})\to(\mathcal{S}^*,\mathcal{E}^*,\mathcal{I}^*,\mathcal{A}^*,\mathcal{R}^*,\mathcal{V}^*,\mathcal{F}^*)$ as $t\to\infty$. □

4.4 Data Fitting Analysis through Numerical Simulation

In this section, we validate our analytical results by specifying particular parameter values and applying a numerical solution method to the model. The parameters, as detailed in Table 4.2, are based on consistent scaling to ensure alignment with the correct physical dimensions. For clarity, all model parameters are adjusted to conform to the time dimension, ensuring consistency with the model requirements.

4.4.1 Fitted Data Analysis of Cutaneous Leishmaniasis in Algeria

This section presents a numerical study that comprehensively understands and effectively manages cutaneous leishmaniasis in Algeria, utilizing data from reliable health sources. Statistical and graphical methods were employed to examine key epidemiological indicators and offer insights into the cutaneous leishmaniasis situation in the country.

Algeria's warm and humid climate significantly contributes to the spread of cutaneous leishmaniasis by providing an ideal environment for sandfly vectors. Its geographical location, bordered by Morocco, Tunisia, and Libya–countries with high disease incidences (Figure 4.2)–facilitates easier transmission due to the constant movement of people and goods across these borders. Furthermore, rural populations living near domestic animals, which serve as reservoirs for the parasite, contribute to the disease's prevalence throughout the region.

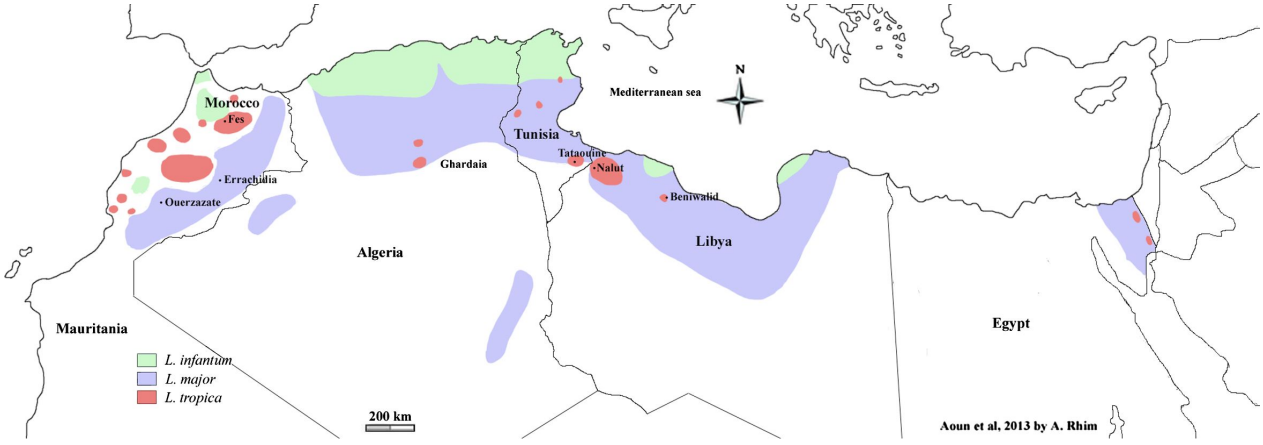

Figure 4.2: Geographical distribution of cutaneous leishmaniasis cases due to L. infantum, L. major, and L. tropica in North African countries [85].

The total population of Algeria was $N = 32\,956\,690$ in 2005 [70]. Initial reported cutaneous leishmaniasis cases $I_N(0) = 30\,227$, according to the World Health Organization [86].

In our analysis, we assume that the total population N remains constant. However, a significant increase in population was observed from 2005 to 2023. Therefore, we cannot directly compare the infection rate in 2005, where there were $30\,227$ cases out of a population of $32\,956\,690$, to the infection rate in 2023, where there were $7\,557$ cases out of a population of $45\,606\,480$.

To ensure accuracy, we adjust the infection rate for each year based on the initial total population in 2005, enabling a precise comparison of infection rates over time, (see Table 4.1, we use the abbreviation Cu. Le. instead of Cutaneous Leishmaniasis).

Based on these considerations, we calculate the average recruitment and natural death rates for the entire period from 2005 to 2023 [72].

Interpretation	**Ref.**	2005	2006	$\cdots$	2022	2023	**Average**
Population of Algeria	[70]	32 956 690	33 435 080	$\cdots$	44 903 225	45 606 480	-
Initial Cu. Le. cases	[86]	30 227	14 379	$\cdots$	5 744	7 557	-
Adjusted Cu. Le. cases	-	30 227	14 173	$\cdots$	4 216	5 461	-
Recruitment rate Λ	[72]	0.0208	0.0216	$\cdots$	-	-	0.023770588
Natural death rate μ	[72]	0.0047	0.0047	$\cdots$	0.0043	-	0.004616667

Table 4.1: Adjusted parameters and initial data of infected population in Algeria from 2005 to 2023.

Lemma 4.1 ensures that the population remains within specified limits, maintaining the validity of our model by reflecting real-world population constraints. Then,

$$N_0 = N_{2005} = 32\,956\,690 \quad \text{and} \quad N(t) \leq N_{2023} = 45\,606\,480.$$

Subsequently, it must hold that:

$$\begin{aligned} N_{2023} &\leq N_{2005} \exp(\Lambda \ell) \\ &\leq \min\left\{N_{2005} \times \exp(0.023770588\ell)\right\}. \end{aligned}$$

Based on the predicted parameter values listed in Table 4.2, the SEIAR(N)-SI(M) model admits a unique solution when $\ell < 1.2552$ (unit = 20 years). Thus, ℓ should not exceed 25 years, and N should not be greater than 59 707 579, according to Lemma 4.1's limitations.

Parameter	Interpretation	Baseline Value	Reference
Λ	Recruitment rate of human	0.023770588	Estimated [72]
$S_N(0)$	Initial number of S_N	32 926 463	Calculated
$E_N(0)$	Initial number of E_N	0	Assumed
$I_N(0)$	Initial number of I_N	30 227	[86]
$A_N(0)$	Initial number of A_N	0	Assumed
$R_N(0)$	Initial number of R_N	0	Assumed
$S_M(0)$	Initial number of S_M	28 114 166	Fitted
$I_M(0)$	Initial number of I_M	3 658 164	Fitted
β	Rate of transmission from I_M to S_N	0.0523401	Fitted
δ	Rate of individuals exiting class E_H	0.032663	Fitted
κ	Rate of transfer from R_N to S_N	0.6732704	Fitted
θ	Symptomatic Cu. Le. probability	0.5911227	Fitted
p	Recovery rate from I_N	0.7921	Fitted
q	Recovery rate from A_N	0.5954292	Fitted
λ	Recruitment rate of sandflies	0.8796	Fitted
γ	Transmission rate from I_N and A_N to S_M	0.0292525	Fitted
υ	Natural death rate of sandflies	0.4847334	Fitted
μ	Natural death rate of humans	0.004616667	Estimated [72]

Table 4.2: Parameters and initial data of the SEIAR(N)–SI(M) model.

The basic reproduction number in this case is:

$$\mathfrak{Rb} \simeq 0.1918 < 1.$$

Figure 4.3 displays the progression of reported cutaneous leishmaniasis cases in Algeria from 2005 to 2023. The curve reveals an initial high number of infections in 2005, recorded at 30 227 cases. This was followed by a rapid decline over subsequent years, reaching a relatively low and stable infection level by 2017. The graph also shows minor fluctuations in infection rates in the later years, reflecting periodic increases and decreases due to environmental or epidemiological factors. The simulated model, represented by the blue curve, closely aligns with the real data, suggesting the model's effectiveness in capturing the dynamics of the disease spread. This trend indicates overall improvement in controlling the disease, likely due to enhanced public health interventions and prevention measures.

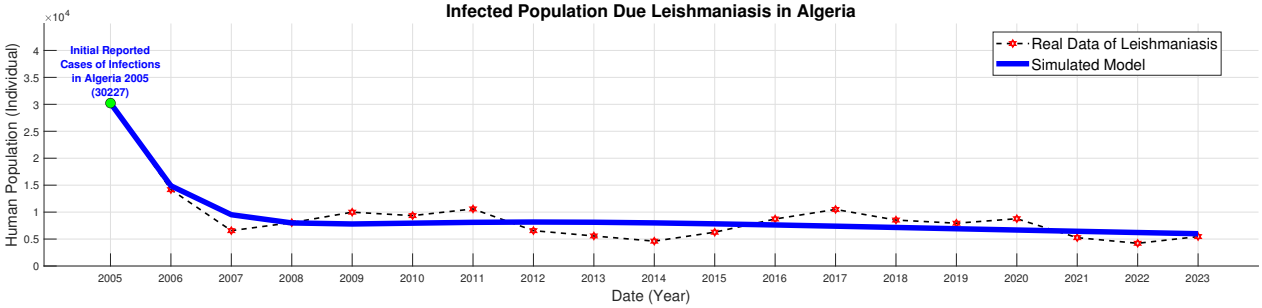

Figure 4.3: The reported cases of Cu. Le. in Algeria (shown with red markers) compared to the predicted cumulative infected cases provided by the proposed model (represented by blue line).

Figure 4.4 illustrates the trends of susceptible individuals for cutaneous leishmaniasis in Algeria from 2005 to 2023. The curve for susceptible individuals starts at a certain level and gradually increases over time as more individuals become vulnerable to the disease. This increase reflects the growing number of individuals who have not yet been infected but are at risk of contracting the disease. The figure highlights the relationship between the number of susceptible individuals and the rising risk of infection over the given period.

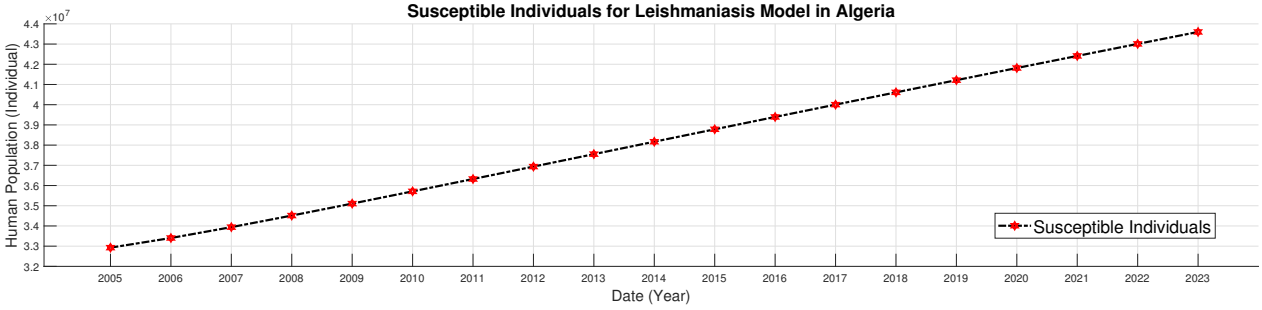

Figure 4.4: Susceptible individuals for cutaneous leishmaniasis model in Algeria.

Figure 4.5 demonstrates the dynamics of cutaneous leishmaniasis in Algeria between 2005 and 2023 through three categories: symptomatic infectious individuals, asymptomatic infectious individuals, and recovered individuals. The red curve shows a sharp decline in the number of symptomatic infections after 2005, reflecting the impact of effective health interventions in reducing the spread of symptomatic cases. In contrast, the black curve demonstrates a gradual increase in asymptomatic infections followed by stabilization, indicating challenges in detecting silent cases that may contribute to disease transmission. The blue curve reflects a continuous increase in the number of recovered individuals, highlighting significant improvements in recovery rates due to advancements in treatment and preventive measures. Overall, the figure indicates improved disease control while emphasizing the need for enhanced efforts to detect asymptomatic infections.

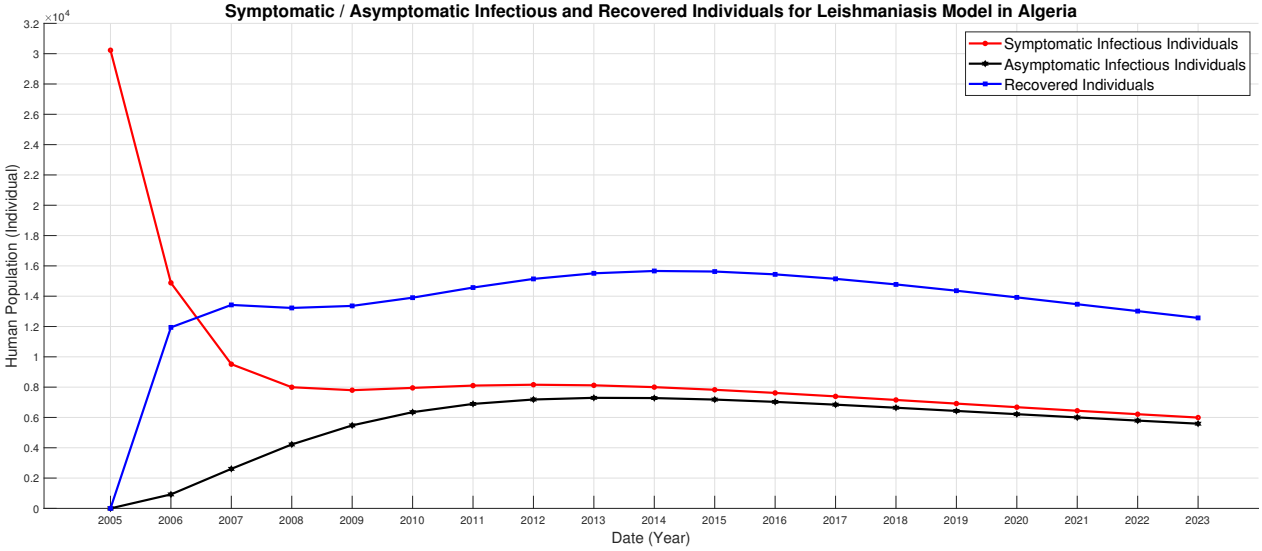

Figure 4.5: Symptomatic, asymptomatic infectious, and recovered individuals for cutaneous leishmaniasis model in Algeria.

Figure 4.6 illustrates the impact of different transmission rate β values on the number of individuals infected with cutaneous leishmaniasis in Algeria from 2005 to 2023. The colored lines represent different scenarios for changes in transmission rate values.

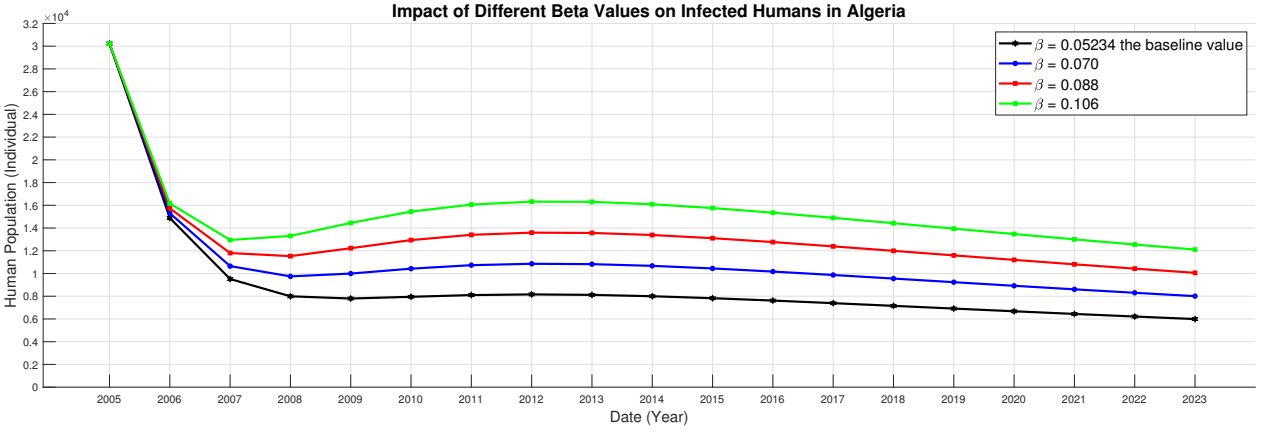

Figure 4.6: Impact of Different Beta Values on Symptomatic Infectious Individuals in Algeria.

The numerical simulation shows that as the β value increases, the number of infections rises significantly, especially during peak infection periods. The graph demonstrates that altering the β value leads to substantial differences in the number of infections, with higher β values resulting in a larger number of infected individuals. This reflects the effect of increased transmission rates on the spread of the disease.

4.4.2 Fitted Data Analysis of Cutaneous Leishmaniasis in M'Sila

This section presents a numerical study aimed at providing a comprehensive understanding and effective management of cutaneous leishmaniasis in M'Sila, utilizing data from reliable health sources [87]. Statistical and graphical methods were employed to examine key epidemiological indicators and offer insights into the cutaneous leishmaniasis situation in the region.

M'Sila province is characterized by a semi-arid climate with high summer temperatures and low winter rainfall, creating favorable conditions for the breeding of sandflies, the primary vector of cutaneous leishmaniasis. These natural conditions, combined with unplanned urbanization, poor sanitation infrastructure, and a lack of preventive awareness, significantly contribute to the spread of the disease in the region. Figure 4.7 illustrates the geographical location of M'Sila province on the map of Algeria, providing spatial context for the study and linking the findings to the targeted area.

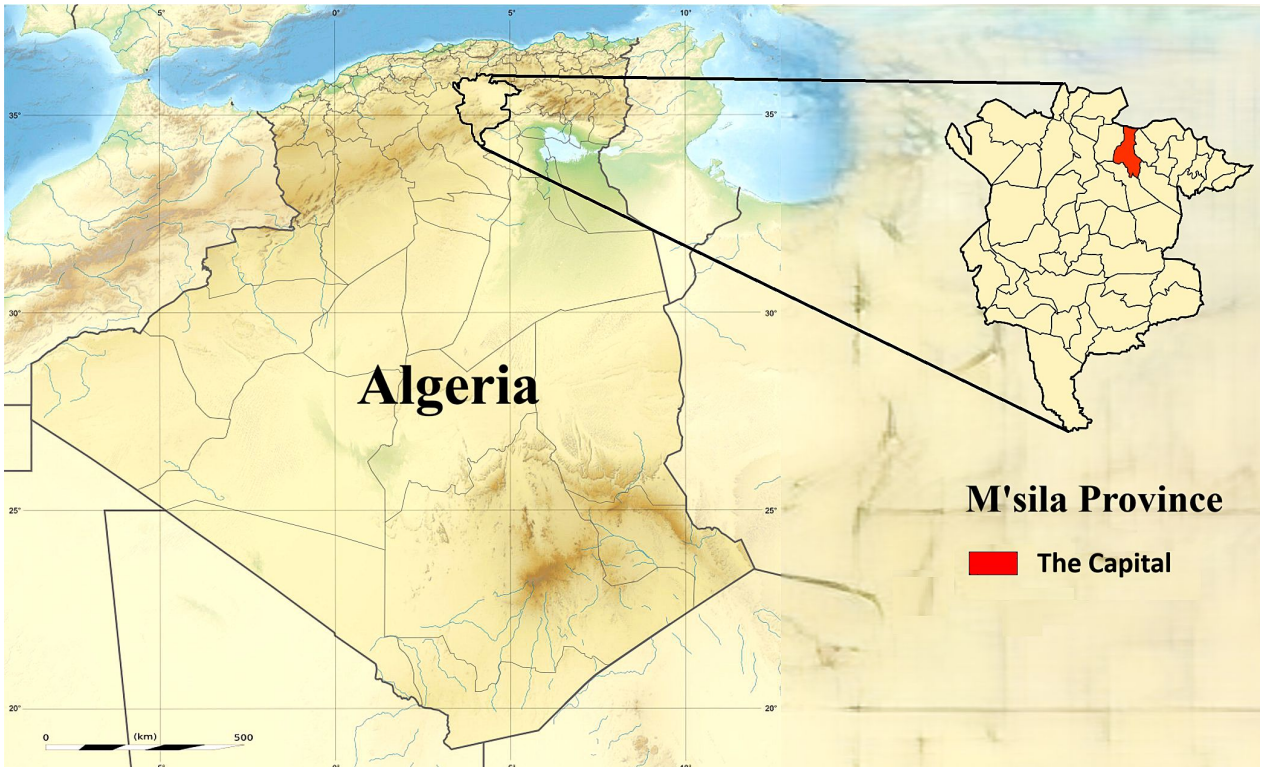

Figure 4.7: Location of M'Sila province in Algeria.

The curves presented in Figure 4.8 provide an accurate comparison between the recorded real data of cutaneous leishmaniasis cases in M'Sila province from 2018 to 2023 (red dots) and the simulated results of the mathematical model (blue line). This comparison reveals distinct patterns in the dynamics of disease spread throughout the year.

Generally, a decline in the number of infected cases is observed during the early months of each year. This decline is often linked to climatic factors such as low temperatures, which hinder the

activity of the sandflies, the primary vector of the disease. However, a notable exception is observed in December, where the data consistently show a significant increase in cases. This December surge may be attributed to a combination of factors, including:

- The delayed appearance of symptoms from infections acquired in preceding months.
- Local environmental and agricultural activities that may extend the favorable conditions for sandfly activity.

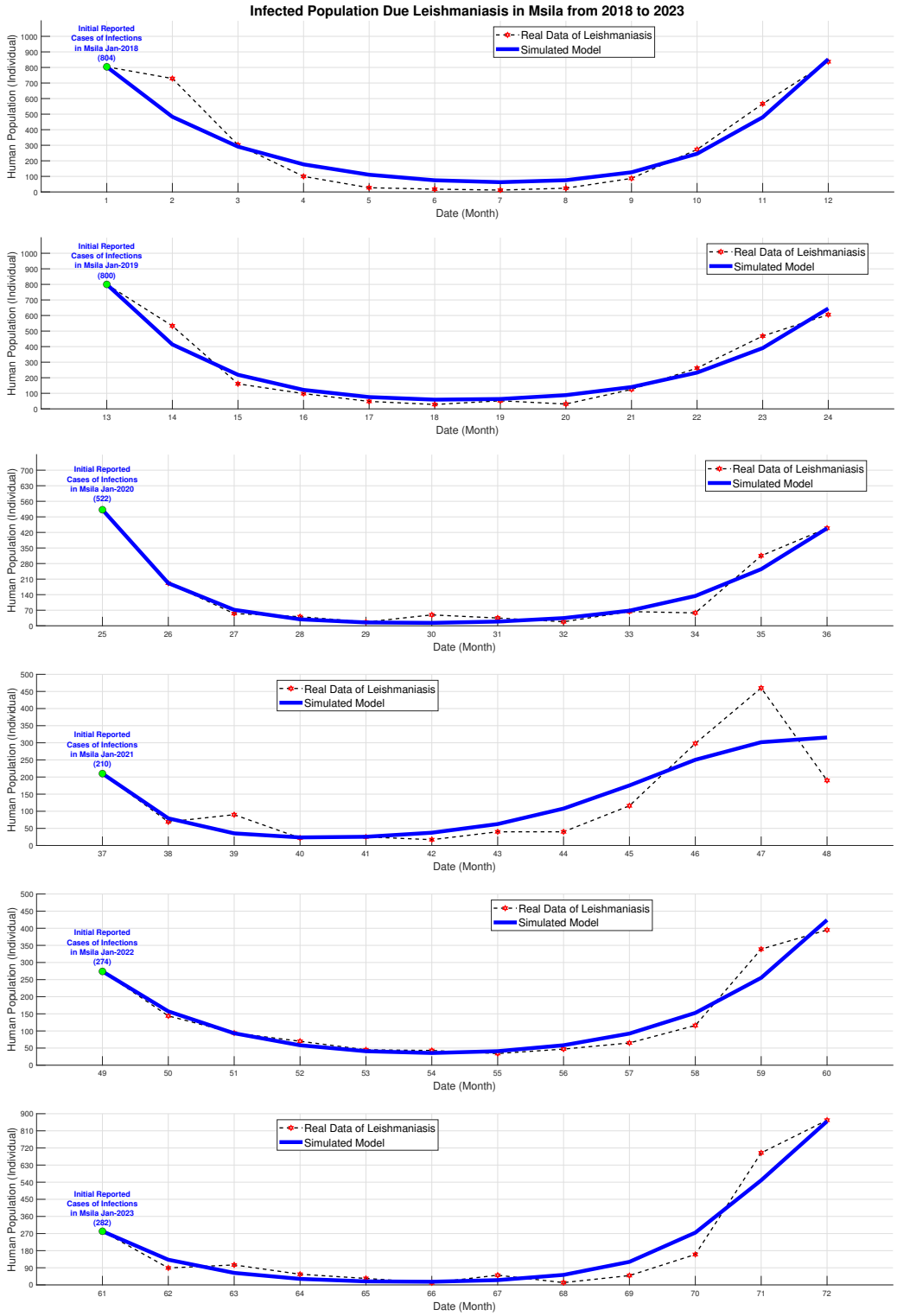

Figure 4.8: Comparison between real data and mathematical model of cutaneous leishmaniasis dynamics in M'Sila (2018-2023).

4.5 Significance and Closing Remarks on Numerical Simulation

Cutaneous leishmaniasis is a parasitic disease transmitted to humans by biting infected female sandflies. Environmental conditions, such as high humidity and vegetation, poor infrastructure, inadequate waste management, population displacement, migration, and human activities that disturb sandfly habitats contribute to the spread. Climate change also plays a significant role in expanding sandfly populations to new areas.

Preventive measures include improving waste management, using insecticides, wearing long sleeves, applying insect repellents, and using insecticide-treated bed nets. Public health awareness campaigns are essential for educating communities on these preventive measures.

Treatment involves early diagnosis and appropriate medical care to prevent severe disfigurement or other complications. Treatment options typically include antileishmanial drugs and supportive care such as wound management to facilitate healing and minimize scarring.

These measures reduce the contact rate between humans and sandflies, significantly lowering disease transmission. Prompt and effective treatment also helps reduce the reservoir of infection, curbing the spread. Implementing integrated prevention and control strategies is essential to mitigate the impact on affected communities.

Conclusion

In this thesis, we have presented a comprehensive analysis of the dynamics of malaria, dengue fever, and cutaneous leishmaniasis transmission using advanced mathematical models. Our research aimed to investigate the factors influencing the spread of these diseases and to propose effective strategies for their prevention and control. Both traditional and fractional mathematical models were employed to ,explore the impact of environmental and behavioral factors on disease transmission emphasizing the significance of mathematical modeling as a tool for guiding public health policies.

For malaria, we used the SIP(N)–SI(M) model, incorporating fractional calculus to assess the impact of memory effects on disease dynamics. One of the key findings of this research is that fractional calculus provides higher accuracy in predicting disease progression compared to traditional models. Through stability and uniqueness analysis, we identified a suitable and feasible region for the models solutions from both epidemiological and mathematical perspectives. The model was applied to real-world data from Algeria, and numerical simulations demonstrated the impact of transmission rates on the number of infected individuals. The results confirmed that reducing the basic reproduction number below one is essential for controlling malaria. Consequently, we concluded that preventive measures such as insecticide-treated bed nets and the use of effective medications are crucial in limiting the disease's spread.

For dengue fever, we utilized the SIHR(N)–SEI(M) mathematical model to analyze disease transmission in different environments. Our analysis highlighted the role of environmental factors, such as temperature, rainfall, and poor urban planning, in the disease's spread. Numerical simulations demonstrated that transmission rates directly influence the number of infected individuals, underscoring the need for swift action during outbreaks. Based on our findings, we emphasized that reducing the basic reproduction number below one can be achieved through public health measures such as mosquito control, insecticide spraying, and the widespread use of treated bed nets, along with community health education. These targeted interventions are essential for mitigating the diseases impact and ensuring community safety.

For cutaneous leishmaniasis, we developed a mathematical SEIAR(N)–SI(M) model to describe disease transmission dynamics between humans and the sandfly vector. This model, highlighted

the influence of environmental and behavioral factors on disease spread serving as a valuable tool for understanding how human interaction with the environment affects transmission. Through this modeling approach, we explored the role of environmental conditions in either promoting or mitigating the disease's spread. Our findings identified effective prevention strategies, such as reducing stagnant water and controlling the sandfly population.

The results of this thesis have underscored the importance of mathematical modeling in understanding infectious disease dynamics. The application of fractional calculus in malaria modeling has enhanced prediction accuracy and provided deeper ,insights into the complex interactions between humans and mosquitoes. Meanwhile the traditional models used for dengue fever and leishmaniasis have highlighted the critical role of local and early interventions. Our findings confirm that mathematical models are essential tools for predicting disease behavior, guiding public health strategies, and ultimately reducing the burden of infectious diseases.

Based on our findings, several recommendations can be made to mitigate the spread of these diseases and improve prevention and treatment strategies. First, reducing the basic reproduction number below one in all studied cases is crucial, which requires the implementation of effective preventive measures such as insecticide ,spraying, the use of treated bed nets, and timely medical treatment. Second increasing community awareness of personal and environmental preventive methods is key to controlling disease spread. Third, improving health data collection and epidemic surveillance is essential to ensuring rapid and effective responses during outbreaks.

In conclusion, this thesis emphasizes the vital role of mathematical modeling in enhancing our understanding of infectious disease dynamics and guiding public health policies. By employing both traditional and fractional models, our research has provided accurate insights that contribute to the development of improved prevention and control strategies for malaria, dengue fever, and cutaneous leishmaniasis. The practical application of these models has demonstrated their potential in significantly reducing the health and economic burden of these diseases on society.

Bibliography

[1] P .A. Naik, M. Farman, A. Zehra, K. S. Nisar, E. Hincal, *Analysis and modeling with fractal-fractional operator for an epidemic model with reference to COVID-19 modeling*, Partial Differentiaf Equations in Applied Mathematics, **10**, (2024) 100663.

[2] P. A. Naik, A. Zehra, M. Farman, A. Shehzad, S. Shahzeen, Z. Huang, *Forecasting and dynamical modeling of reversible enzymatic reactions with a hybrid propotional fractional derivative*, Front. Phys., **11**, (2023) 1307307.

[3] S.Jamil, P. A. Naik, M. Farman, M. U. Sleem, A. H. Ganie, *Stability and complex dynamical analysis of COVID-19 epidemic model with non-singular kernel of Mittag-Leffer law*, j. Appl. Math. Comput., **70**, (2024) 3441–3476.

[4] P. A. Naik, B. M. Yeolekar, S. Qureshi, M. Yeolekar, A. Madzvamuse, *Modeling and analysis of the fractional-order epidemic model to investigate mutual influence in HIV/HCV co-infection*, Nonliner Dyn, **112**, (2024) 11679–11710.

[5] P. A. Naik, M. Yavuz, S. Qureshi, M. Naik, K. M. Owolabi, A. Soomro, A. H.Ganie, *Memory impacts in hepatitis C: Aglobal analysis of a fractional-order model with an effective treatment*, Computer Methods and Programs in Biomedicine, **254**, (2024) 108306.

[6] M. Farman, A. Shehzad, K. S. Nisar, E. Hincal, A. Akgul, *A mathematical fractal-fractional model to control tuberculosis prevalence with sensitivity, stability, and simulation under feasible circumstances*, Computers in Biology Medicine, **178**, (2024) 108756.

[7] K. S. Nisar, M. Farman , *Analysis of a mathematical model with hybrid fractional derivatives under different kernel for hearing loss due to mumps virus*, International Journal of Modelling and Simulation, (2024) 1–27.

[8] M. Farman, N. Gokbulut, U. Hurdoganoglu, E. Hincal,K. Suer, *Fractional order model of MRSA bacterial infection with real data fitting: Computational Analysis and Modeling*, Computers in Biology and Medicine, **173**, (2024) 108367.

[9] K. S. Nisar, M. Farman, A. Zehra, E. Hincal, *Numerical and analytical study of fractional order tumor model through modeling with treatment of chemotherapy*, International Journal of Modelling and Simulation, (2024) 1–14.

[10] K. S. Nisar, M. Farman, M. Abdel-Aty, C. Ravichandran, *A review of fractional order epidemic models for life sciences problems: Past, present and future*, Alexandria Engineering Journal, **95**, (2024) 283–305.

[11] J. Li, *Malaria model with stage-structured mosquitoes*. Math Biosci Eng 2011;8(3):753–68.

[12] S. Olaniyi, OS. Obabiyi, *Mathematical model for malaria transmission dynamics in human and mosquito populations with nonlinear forces of infection*. Int. J. Pure Appl. Math. 2013;88(1):125–56.

[13] Osman MA-RE-N, Adu IK, C. A. Yang, *simple SEIR mathematical model of malaria transmission*. Asian Res J Math 2017;7(3):1–22.

[14] J. Djordjevic, C. J. Silva, D. F. M. Torres, *A stochastic SICA epidemic model for HIV transmission*, Appl. Math. Lett., 84 (2018), 168–175.

[15] F. Ndaïrou, I. Area, J. J. Nieto, C. J. Silva and D. F. M. Torres, *Mathematical modeling of Zika disease in pregnant women and newborns with microcephaly in Brazil*, Math. Methods. Appl. Sci., 41(18) (2018), 8929–8941.

[16] A. Rachah and D. F. M. Torres, *Dynamics and optimal control of Ebola transmission*, Math. Comput. Sci., 10(3)(2016), 331–342.

[17] A. Ullah, T. Abdeljawad, S. Ahmad and K. Shah, *Study of a fractional-order epidemic model of Childhood diseases*,Journal of Function Spaces, vol. 2020.

[18] H. Ouedraoga and A. Guiro, *Analysis of dengue disease transmission model with general incidence functions*, Nonlinear Dyn. Syst., **23**(1) (2023), 79–94

[19] S. A. Carvalho, S. O. Da Silva, and I. D. C. Charret, *Mathematical modeling of Dengue epidemic: control methods and vaccination strategies*, Theory Biosci., **138** (2019), 223–239.

[20] B. Z. Naaly, T. Marijani, A. Isdory, and J. Z. Ndendya, *Mathematical modeling of the effects of vector control, treatment and mass awareness on the transmission dynamics of dengue fever*. Computer Methods and Programs in Biomedicine Update, **6** (2024), 100159.

[21] S. Bounouiga, B. Basti, and N. Benhamidouche, *Mathematical exploration of Malaria transmission dynamics: Insights from fractional models and numerical simulation*, Adv. Theory Simul., **2**(8)(2024), 2400630.

[22] A. O. Atede, A. Omame, and S. C. Inyama, *A fractional order vaccination model for COVID-19 incorporating environmental transmission: a case study using Nigerian data*, Bulletin of Biomathematics, **1**(1) (2023), 78–110.

[23] B. Basti, Y. Arioua and N. Benhamidouche, *Existence results for nonlinear Katugampola fractional differential equations with an integral condition*, Acta Math. Univ. Comenian., **89**(2) (2020), 243–260.

[24] B. Basti, B. Chennaf, M. A. Boubekeur, and S. Bounouiga, *Fractional mathematical model for exploring the influence of infectious diseases on population with chronic conditions*, Adv. Theory Simul., **7** (2024), 2301285.

[25] B. Basti, N. Hammami, I. Berrabah, F. Nouioua, R. Djemiat, and N. Benhamidouche, *Stability analysis and existence of solutions for a modified SIRD model of COVID-19 with fractional derivatives*, Symmetry, **13**(8) (2021), 1431.

[26] M. D. Ortigueira and J. A. Tenreiro Machado, *What is a fractional derivative*?, J. Comput. Phys. 293 (2015), 4–13.

[27] U. K. Nwajeri, A. Omame, and C. P. Onyenegecha, *Analysis of a fractional order model for HPV and CT co-infection*, Results in Physics, **28** (2021), 104643.

[28] R. Toledo-Hernandez, V. Rico-Ramirez, G. A. Iglesias-Silva and U. M. Diwekar, *A fractional calculus approach to the dynamic optimization of biological reactive systems. Part I: Fractional models for biological reactions*, Chem. Eng. Sci., 117 (2014), 217–228.

[29] B. Basti and N. Benhamidouche, *Existence results of self-similar solutions to the Caputo-type's space-fractional heat equation*, Surv. Math. Appl., **15** (2020), 153–168.

[30] B. Basti, R. Djemiat, and N. Benhamidouche, *Theoretical studies on the existence and uniqueness of solutions for a multidimensional nonlinear time and space-fractional reaction-diffusion/wave equation*, Mem. Differ. Equ. Math. Phys., **89** (2023), 1–16.

[31] R. Djemiat, B. Basti, and N. Benhamidouche, *Analytical studies on the global existence and blow-up of solutions for a free boundary problem of two-dimensional diffusion equations of moving fractional order*, Adv. Theory Nonlinear Anal. Appl. **6**(8) (2022), 287–299.

[32] R. Djemiat, B. Basti, and N. Benhamidouche, *Existence of traveling wave solutions for a free boundary problem of a higher-order space-fractional wave equation*, Appl. Math. E-Notes, **22** (2022), 427–436.

[33] R. Djemiat, B. Basti, and N. Benhamidouche, *Cauchy problem for Jordan-Moore-Gibson-Thompson equations of nonlinear acoustics with fractional operators*, An. Stiint. Univ. Al. I. Cuza Iasi. Mat., **69**(2) (2023), 143–161.

[34] R. L. Magin, *Fractional calculus in bioengineering*, Begell House, 2006.

[35] F. Nouioua and B. Basti, *Global existence and blow-up of generalized self-similar solutions for a space-fractional diffusion equation with mixed conditions*, Ann. Univ. Paedag. Crac. Stud. Math. **20** (2021), 43–56.

[36] R. Toledo-Hernandez, V. Rico-Ramirez, G. A. Iglesias-Silva, and U. M. Diwekar, *A fractional calculus approach to the dynamic optimization of biological reactive systems. Part I: Fractional models for biological reactions*, Chem. Eng. Sci., **117** (2014), 217–228.

[37] S. Annas, M. I. Pratama, M. Rifandi, W. Sanusi, and S. Side, *Stability analysis and numerical simulation of SEIR model for pandemic COVID-19 spread in Indonesia*, Chaos, Solit. Fract., **139** (2020), 110072.

[38] A. A. Gebremeskel, H. E. Krogstad, *Mathematical Modelling of Endemic Malaria Transmission*, American Journal of Applied Mathematics, Vol. 3, No. 2, 2015, pp. 36–46.

[39] C. Xu, W. Zhang, C. Aouiti, Z. Liu, and L. Yao, *Bifurcation insight for a fractional-order stage-structured predator–prey system incorporating mixed time delays*, Mathematical Methods in the Applied Sciences, (2023).

[40] M. Sinan, K. J. Ansari, A. Kanwala, K. Shah, T. Abdeljawad, Zakirullah, B. Abdalla, *Analysis of the mathematical model of cutaneous Leishmaniasis disease*, Alexandria Engineering Journal, **72** (2023), 117–134.

[41] K. Khan, R. Zarin, A. Khan, A. Yusuf, M. Al-Shomrani, and A. Ullah, *Stability analysis of five-grade Leishmania epidemic model with harmonic mean-type incidence rate*, Adv. Differ. Equ., **2021**(1) (2021), 86.

[42] M. Safan and A. Altheyabi , *Mathematical analysis of an anthroponotic cutaneous leishmaniasis model with asymptomatic infection*, Mathematics, **11**(2023), 2388.

[43] M. Alqhtani, K. M. Saad, R. Zarin, Amir Khan, and W. M. Hamanah, *Qualitative behavior of a highly non-linear cutaneous Leishmania epidemic model under convex incidence rate with real data*, Mathematical Biosciences and Engineering, **21**(2)(2024), 2084–2120.

[44] A. Mubayi, M. Paredes, and J. Ospina, *A comparative assessment of epidemiologically different cutaneous leishmaniasis outbreaks in Madrid, Spain and Tolima, Colombia: An estimation of the reproduction number via a mathematical model*, Mathematical Biosciences and Engineering, Trop. Med. Infect. Dis., **3**(2018), 43.

[45] E. R. Scheinerman, *Invitation to Dynamical Systems*, Courier Corporation, 2013.

[46] S. Wiggins, *Texts In Applied Mathematics. Introduction to Applied Nonliear Dynamical Systems and Chaos*,. Second Edition. Spriner, New York. 2000.

[47] S. Wiggins, *Introduction to applied Nonlinear Dynamical Systems and Chaos*. Springer,(2003).

[48] R. Chill, *Equations différentielles et stabilité*. Université de Metz, (2006).

[49] J. J. Anagnost, and C. A. Desoer, *An elementary proof of the routh-hurwitz stability criterion*. Circuits, Systems and Signal Processing, **10**(1):5974, 1991.

[50] L. J. Allen, *An Introduction to Mathematical Biology*. Pearson, 2007

[51] Z. Ma, and J. Li, *Dynamical Modeling and Analysis of Epidemics*. World Scientifi, 2009.

[52] A. GRANAS, and J. DUGUNDJI, *Fixed Point Theory*, Springer-Verlag, New York, 2003.

[53] Y. Arioua, B. Basti, and N. Benhamidouche, *Initial value problem for nonlinear implicit fractional differential equations with Katugampola derivative*, Appl. Math. E-Notes, **19** (2019), 397–412.

[54] B. Basti, Y. Arioua, and N. Benhamidouche, *Existence and uniqueness of solutions for nonlinear Katugampola fractional differential equations*, J. Math. Appl., **42** (2019), 35–61.

[55] B. Basti and N. Benhamidouche, *Global existence and blow-up of generalized self-similar solutions to nonlinear degenerate diffusion equation not in divergence form*, Appl. Math. E-Notes, **20** (2020), 367–387.

[56] B. Basti and Y. Arioua, *Existence study of solutions for a system of n-nonlinear fractional differential equations with integral conditions*, J. Math. Phys. Anal. Geom., **18**(3) (2022), 350–367.

[57] A. Zeeshan, Z. Akbar, and S. Kamal, *Ulam stability results for the solutions of nonlinear implicit fractional order differential equations*, **48**(4), (2018), 1092–1109.

[58] J. P. LaSalle, *Some extensions of Liapunov's second method. IRE Trans*. Circuit Theory 1960, 7, 520–527.

[59] C. Vargas-De-Leon, *Volterra-type Lyapunov functions for fractional-order epidemic systems*, Commun. Nonlinear Sci. Numer. Simul., **24**(1–3) (2015), 75–85.

[60] K. Diethelm, N. J. Ford, and A. D. Freed, *A predictor-corrector approach for the numerical solution of fractional differential equations*, Nonlinear Dyn.29 (2002), 3–22.

[61] K. Diethelm, N. J. Ford, and A. D. Freed, *Detailed error analysis for a fractional Adams method*, Numer. Algorithms, **36** (2004), 31–52.

[62] P. Roman, *Application of the Adams-Bashfort-Mowlton Method to the Numerical Study of Linear Fractional Oscillators Models*, In AIP Conference Proceedings; AIP Publishing LLC. Melville, NY, USA, 2021.

[63] R. Garrappa, *On linear stability of predictor-corrector algorithms for fractional differential equations*, Int. J. Comput. Math., **87**(10) (2010), 2281–90.

[64] Dengue and severe dengue, World Health Organization, https://www.who.int/news-room/fact-sheets/detail/dengue-and-severe-dengue

[65] A. Kolimenakis, S. Heinz, M. L. Wilson, V. Winkler, L. Yakob, A. Michaelakis, D. Papachristos, C. Richardson, and O. Horstick, *The role of urbanisation in the spread of Aedes mosquitoes and the diseases they transmit-A systematic review*. PLoS Negl Trop Dis., **15**(9) (2021). Doi: 10.1371/journal.pntd.0009631.

[66] M. Gómez, D. Martinez, M. Muñoz, J. D. Ramírez, *Aedes aegypti and Ae. albopictus microbiome/virome: new strategies for controlling arboviral transmission?*, Parasit Vectors, **15** (2022), 287.

[67] Dr. Rahul Singh, *Dengue fever: Symptoms, Causes, Prevention and Homeopathic Treatment*, October 21, 2021, https://www.doctorrahulsingh.com/dengue-fever-symptoms-causes-prevention-and-homeopathic-treatment/

[68] A. I. K. Butt, M. Imran, B. A. McKinney, S. Batool, and H. Aftab, *Mathematical and Stability Analysis of DengueMalaria Co-Infection with Disease Control Strategies*, Mathematics, **11**(22) (2023), 4600.

[69] A. Abidemi and N. A. Bazilah Aziz, *Analysis of deterministic models for dengue disease transmission dynamics with vaccination perspective in Johor, Malaysia*, Int. J. Appl. Comput. Math. **8**(1) (2022), 45.

[70] Algeria Population 1950-2024, https://www.macrotrends.net/countries/DZA/algeria/population

[71] Number of confirmed malaria cases, World Health Organization, https://www.who.int/data/gho/data/indicators/indicator-details/GHO/number-confirmed-malaria-cases

[72] Population growth in Algeria, https://www.donneesmondiales.com/afrique/algerie/croiss-ppl.php

[73] Dengue fever infections, Our World in Data, https://ourworldindata.org/grapher/dengue-incidence?tab=tabletime=earliest.2017

[74] Singapore Population 1950-2024, https://www.macrotrends.net/global-metrics/countries/sgp/singapore/population

[75] Population growth in Singapore, https://www.worlddata.info/asia/singapora/populatingrowth.php

[76] Costa Rica Population 1950-2024, https://www.macrotrends.net/global-metrics/countries/CRI/costa-rica/population

[77] Population growth in Costa Rica, https://www.worlddata.info/america/costa-rica/populatingrowth.php

[78] Yemen Population 1950-2024, https://www.macrotrends.net/global-metrics/countries/YEM/yemen/population

[79] Population growth in Yemen, https://www.worlddata.info/asia/yemen/populatingrowth.php

[80] India Population 1950-2024, https://www.macrotrends.net/global-metrics/countries/IND/india/population

[81] Population growth in India, https://www.worlddata.info/asia/india/populatingrowth.php

[82] World Health Organization, Leishmaniasis, https://www.who.int/news-room/fact-sheets/detail/leishmaniasis

[83] CDC Yellow Book 2024, Leishmaniasis, Cutaneous, https://wwwnc.cdc.gov/travel/yellowbook/2024/infections-diseases/leishmaniasis-cutaneous

[84] A. Hailu, A. M. Musa, C. Royce, and M. Wasunna, *Visceral leishmaniasis: new health tools are needed*, PLoS Med., **2**(7) (2005), e211. 10.1371/journal.pmed.0020211

[85] K. Aoun and A. Bouratbine, *Cutaneous leishmaniasis in north Africa: a review*, Parasite, **21** (2014), 14. 10.1051/parasite/2014014

[86] Number of cases of cutaneous leishmaniasis reported, World Health Organization, https://www.who.int/data/gho/data/indicators/indicator-details/GHO/number-of-cases-of-cutaneous-leishmaniasis-reported

[87] Pasteur Institute of Algeria. https://www.insp.dz/index.php/Non-categorise/rem.html

[88] T. Karimi, I. Sharifi, M. R. Aflatoonian et al., *A long-lasting emerging epidemic of anthroponotic cutaneous leishmaniasis in southeastern Iran: population movement and peri-urban settlements as a major risk factor*, Parasites Vectors, **14** (2021), 122. 10.1186/s13071-021-04619-3

[89] E. Montaner-Angoiti, L. Llobat, *Is leishmaniasis the new emerging zoonosis in the world?*, Vet. Res. Commun., 47(2023), 1777–1799. 10.1007/s11259-023-10171-5

[90] H. Agoune, H. Khemais, D. Said, *Sig, Por La Gestion Forestire Aplication A La Wilaya De M'Sila*, [Professional master thesis], M'Sila, Mohamed Boudiaf University of M'Sila, 2022. theses-algerie.com/2349067345800431

الملخص:

تقدم هذه الأطروحة وتبحث في العديد من النماذج المبتكرة لتحليل وفهم ديناميكيات انتقال الأمراض المعدية التي ينقلها البعوض، مثل الملاريا وحمى الضنك وداء الليشمانيات الجلدي. كما تقدم تحليلاً شاملاً لانتشار هذه الأمراض من خلال المحاكاة العددية، باستخدام بيانات صحية من بلدان مختلفة. علاوة على ذلك، فهي تدرس وجود الحلول، وحدانيتها، واستقرارها، إلى جانب استكشاف رقم التكاثر الأساسي ونقاط التوازن وخصائص استقرارها. تكشف المحاكاة العددية عن وجود علاقة مباشرة بين معدلات الانتقال وعدد الأفراد المصابين، مما يؤكد الحاجة الملحة إلى تنفيذ بروتوكولات علاج فعالة.

كلمات مفتاحية: النمذجة الرياضية، الأمراض المعدية، ديناميكيات السكان، الملاريا، حمى الضنك، داء الليشمانيات الجلدي، الوجود والوحدانية، رقم التكاثر الأساسي، نقاط التوازن، تحليل الاستقرار، المحاكاة العددية، معلمات التقدير، تحليل البيانات الصحية، وبروتوكولات العلاج.

Résumé :

Cette thèse présente et étudie plusieurs modèles innovants pour analyser et comprendre la dynamique de transmission des maladies infectieuses transmises par les moustiques, notamment le paludisme, la dengue et la leishmaniose cutanée. Elle fournit une analyse complète de la propagation de ces maladies grâce à des simulations numériques, en utilisant des données sanitaires récentes de plusieurs pays. En outre, l'étude examine l'existence, l'unicité et la stabilité des solutions, ainsi qu'une exploration du nombre de reproduction de base, des points d'équilibre et de leurs propriétés de stabilité. Les simulations numériques révèlent une corrélation directe entre les taux de transmission et le nombre d'individus infectés, soulignant le besoin urgent de mettre en œuvre des protocoles de traitement efficaces.

Mots clés : *Modélisation mathématique, maladies infectieuses, dynamique des populations, paludisme, dengue, leishmaniose cutanée, existence et unicité, taux de reproduction de base, points d'équilibre, analyse de stabilité, simulations numériques, paramètres d'estimation, analyse des données de santé et protocoles de traitement.*

Abstract:

This thesis introduces and investigates several innovative models to analyze and comprehend the transmission dynamics of mosquito-borne infectious diseases, including malaria, dengue fever, and cutaneous leishmaniasis. It provides a comprehensive analysis of the spread of these diseases through numerical simulations, utilizing recent health data from multiple countries. Furthermore, the study examines solutions' existence, uniqueness, and stability, alongside an exploration of the basic reproduction number, equilibrium points, and their stability properties. The numerical simulations reveal a direct correlation between transmission rates and the number of infected individuals, underscoring the urgent need to implement effective treatment protocols.

Key words: *Mathematical modeling, infectious diseases, population dynamics, malaria, dengue fever, cutaneous leishmaniasis, existence, uniqueness, basic reproduction number, equilibrium points, stability analysis, numerical simulations, estimation parameters, health data analysis, and treatment protocols.*

A.M.S Classifications: *34A08; 62P10; 92-10; 92B05; 93-10.*